Elaboration of a laser doped selective emitter for crystalline silicon solar cells.

Fabian Felipe Suarez Peinado

Thesis submitted in partial fullfiment of the requirements
for the degree of

Master in Physics.

Department of physics
Faculty of Mathematics and Natural Sciences
University of Oslo

2013

Abstract

A study of the laser doping technique from a phosohorus glass layer as a dopant source was carried out. This was done with the purpose of implementing a selective emitter in a crystal silicon solar cell. The main laser parameters studied were the average power output and the pulse repetition frequency. This led us to conclusions regarding the influence of the laser pulse shape on the produced doping concentration profiles, as well as quality of the recrystallized irradiated area. With this, optimal laser parameters are chosen for the elaboration of the selective emitter solar cell.

Regarding the implementation of the selective emitter solar cell the whole process was carried out. The laser parameters developed from the laser doping study were used and it was found out that the selective emitter does improve the blue response of the solar cell. Based on the results obtained various optimization steps are sugested for the improvement of the selective emitter solar cell. It is shown that the elaboration of a selective emitter by a laser doping technique, is a very adaptable process which if correctly implented can lead to a considerable increase in the performace of the cells.

Acknowledgement

Contents

1 Introduction

Solar cells is a very fast growing and active field of research, both because it constitutes one of the most promising solutions to many of the world's energy and environmental problems, and because it is a direct application of some of the major achievements in physics and technology during the twentieth century. During the first decade of the 21st century an increasing awareness on the problems related to the disponibility and use of fossil energy resources led to a considerable expansion of renewable energy usage. In particular the photovoltaic (PV) sector experienced an amazing increase in energy production that went from a total world capacity of less than 4 GW in 2002, to more than 100 Gw at the end of 2012 [1] (Figure 1). This increase in PV capacity went hand in hand with a decrease in solar modules prices and an increase in commercial solar cells' efficiency, which led to a decrease in the PV produced kilowatt hour price.
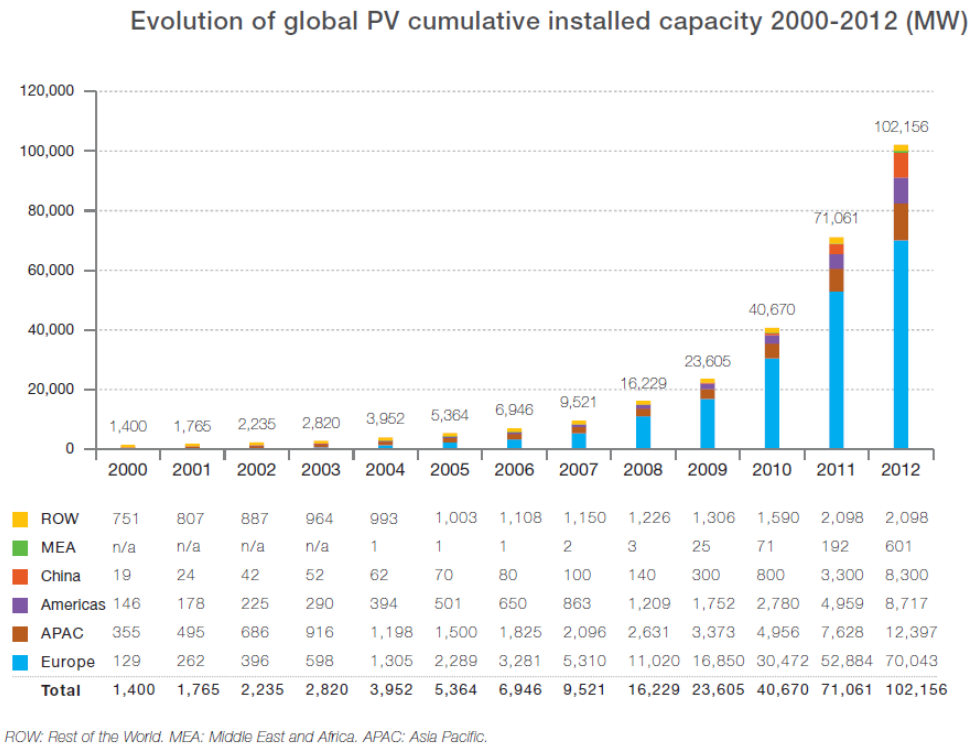
Figure 1: Taken from [1]

Nevertheless, in spite of great technological advances, in many countries PV energy production still relies on economical goverment incentives , this is because PV has not yet been able to reach the point where obtaining energy from it will cost less or equal than buying it from the electricity grid, which is called grid parity. Thus in order for PV to reach this point it is necessary to develop it's technology so that further increase in efficiency at low cost is attained. Being silicon the second most abundant element on the surface of the earth and a semiconductor with suitable physical and electronic properties for the conversion of light into electricity, it is very

natural that nowadays production and research of solar cells is mainly based on this material. For this reason the objective of the present thesis work is the study and implementation of an improving efficiency technique for silicon solar cells, which is the elaboration of a selective emitter by means of a laser doping process.

In a selective emitter solar cell the front thin N type zone which conforms one of the two main zones of the PN structure of the solar cell, is not homogenously doped but instead has a higher doping concentration in the region underneath the metal contacts. This eliminates the trade off that appears when choosing the optimal emitter concentration, between high minority carrier lifetimes in the bulk of the emitter and good charge transportation through the metal contacts, this allows to further increase the efficiency of the solar cell.

Laser doping from a phosphorus glass source is a functional technique whose applications extend over a wide range of semiconductor technologies. It is a very interesting field of research whose studies emcompass knowledge of photonics, semiconductor physics and thermodynamics. It was chosen for the development of the present thesis project because of its versatility and easyness of implementation over most of the solar cells baseline production processes. Therefore one of the main objectives of this thesis is to develop through experimentation an understanding of the laser doping process, that will allow us to establish methods to find optimal laser parameters for the elaboration of the selective emitter solar cells. The conclusions obtained on this topic will not only be useful for the development of the selective emitter solar cell but will rather extent to any field that require the implementation of this useful technique.

1.1 Thesis Outline.

The following is the summary of the chapters of the present thesis.

Chapter 2 is a review of the basic working principles of solar cells necessary to understand the central issued problem in the present thesis. A small review of various of the limiting factors of solar cells will be presented as well as an explanation on why selective emitters are a good choice for improving the efficiency of solar cells. Though an explanation on the problem of the optimization of the emitter doping concentration will be given in this chapter, a full physical description on the issues of lifetimes in semiconductors and transport in metal semiconductor interfaces will not be given until appendix B.

Chapter 3 is a brief presentation of the main manufacturing steps in the elaboration of the selective emitter solar cell, as well as the techniques used for it's characterization.

Chapter 4 is one of the main chapters. It begins with a review on the laser doping technique, based on previous studies from different authors. The experiments and results are presented. Finally and interpretation of the results is given

Chapter 5 is the one concerning the elaboration and characterization of the selective emitter solar cells. A small comparison with homogeneous emitter cells is given. Some possible improvements for the selective emitter cell are presented.

Chapter 6 is finally a summary of the main conclusions arrived in this thesis.

Apendix B is a short review of the theoretical background necessary to understand the underlying physical process giving rise to the recombination and generation mechanisms as well as the nature of the metal-semiconductor interface. Concepts which are central in the understanding of the concept of the selective emitter solar cell.

2 Solar cell operation review and selective emitter principles.

2.1 Basic solar cell operation principles.

Most of the commonly used solar cells are semiconductor electronic devices whose function is to convert solar light into electric energy. This is done by means of three basic steps: light trapping, charge separation and charge transport.

The common mechanism by which light is trapped in semiconductor solar cells is the photoelectric effect. This is a phenomena first described by Albert Einstein in which incoming light photons incident on a material's surface excite some electrons to a higher energy level. In the case of metal materials the electrons acquire enough energy to be removed from the metal's surface while in semiconductor materials the excited electrons jump from the static valence band to the conduction band. Since photons come in quantized amounts of energy when they get absorbed by the material they transfer all of its energy to the electrons, therefore the main requirement for an absorption event to take place is that the photon is energetic enough so that it can induce the electrons' energy transition. This means that photons with energy less than the semiconductors badgap will not be absorbed and will just go through the material. The main reason why semiconductors are such a good choice for photovoltaic converters, is that by having an energy band gap they are able to maintain the electrochemical energy potential produced by the light photons. Generally the amount of electric energy that can be trapped and stored for use in semiconductors is described by the Gibbs free energy given by $N\triangle\mu$, where N is the number of electrons and μ the chemical potential difference between electrons across the band gap.

Once the absorption process has taken place in the semiconductor two conducting charges are produced; an electron in the conduction band and a hole in the valence band. In order to take advantage of the energy arising from the absorbed photons, the conducting charges should quickly be spatially separated to avoid their recombination. This charge separation is usually accomplished by having a PN diode structure, which provides an electrostatic potential difference driving away the charges to two difference zones of the solar cell. The current passing through the junction of a diode under external Bias voltage and no illumination is given by the ideal diode equation [6]:

$$J_d = J_0(e^{qV/k_bT-1}). \tag{1}$$

where V is the external Bias voltage and J_0 is a material dependent constant that depends on the diffusion length of holes and electrons in the junction. The built in voltage across the junction is given by

$$V_{bi} = \frac{K_bT}{q}\ln\frac{N_dN_a}{n_i}. \tag{2}$$

Where N_a and N_d are the acceptor and donnor concentration of the P and N region respectively. The width of the depletion region is given by :

$$w = \left[\frac{N_a + N_d}{N_a N_d} \frac{2\epsilon(V_{bi})}{e} \right], \tag{3}$$

thus it is seen in equation 3 and 2 that the width of the depletion region decreases with doping concentration while V_{bi} increases.

Under equilibrium conditions the drift and diffusion current that control the behavior of the PN junctions cancel out and no net current is present. In a solar cell under illumination electron hole pairs are generated, this breaks the equilibrium concentration, thus the electron and hole Quasi Fermi levels separate. This creates a drift current composed of minority carriers across the band gap which accomplishes the charge separation in a semiconductor solar cell.

Then when the electric charges are in different zones of the cell, they are carried out from the semiconductor through some metal contacts, usually present in the front and back surface of the cell. Later it will be seen that this contacts are formed by metal-semiconductor junctions that can be made from different materials, depending on the optimization of the cell.

The transport of electric charge carriers in semiconductors is in general described by the following set of equations:

$$
\begin{aligned}
\frac{d^2\phi}{dx^2} &= \frac{q}{\varepsilon}(p - n + N_d - N_a) \\
J_e &= q\mu_e n \frac{d\phi}{dx} + qD_e \frac{dn}{dx} \\
J_h &= q\mu_h p \frac{d\phi}{dx} - qD_h \frac{dp}{dx} \\
\frac{1}{q}\frac{dJ_e}{dx} &= U - G \\
\frac{1}{q}\frac{dJ_h}{dx} &= -(U - G)
\end{aligned}
\tag{4}
$$

where ϕ is the electrical potential, p and n the conducting holes and electrons concentration, and G and U the generation and recombination rates. The first equation is the classical Poisson equation used in electromagnetic theory [2]. The second and third equations tell us that the motion of the charge carriers is determined by the electromagnetic fields and chemical potentials, arising from gradients in the relative electromagnetic energies of the energy bands and the gradients in charge concentration. The last two equations account for charge conservation and come from an specific form of the continuity equations. The specific nature of the generation and recombination mechanisms present in these equations will be studied on section B.1 Globally the effect of light absorption is to produce current as well as voltage, which causes the generation of electric power. Under illumination and at short circuit the cell produces a photocurrent described by the current short circuit density given by:

$$J_{sc} = q \int b_s(E)QE(E)dE, \tag{5}$$

where q is the electric charge, b_s is the photon flux density at a certain wavelength and QE is the quantum efficiency, i.e the probability that one striking photon on the cell generate one electron that gets transported out of the cell. Since solar cells are composed of a diode structure, when the contacts are connected to an external load, the voltage will generate a dark drift current J_{dark} which opposes the illumination current and is approximately equal to the ideal diode given in equation (1). Therefore in an ideal solar cell the total current density is given by:

$$J = J_{sc} - J_0(e^{qV/k_bT-1}).$$ (6)

When the contacts of the cell are isolated there is no net current flowing, and the voltage drop across the terminals of the cell is maximum and this is called the open circuit voltage. From equation 6 it can be seen that it is given by :

$$V_{oc} = \frac{k_bT}{q} \ln \left(\frac{J_{sc}}{J_0} + 1 \right)$$ (7)

The power density delivered by the solar cell is given by the product of the voltage across its terminals with the total current density produced . $P = JV$. The solar cell produces power only for a range of voltages from 0 to V_{oc} and for some especial voltage V_m in this range it will produce its maximum power P_m, with a certain current J_m. The efficiency the solar cell is the ratio between the maximum delivered power and the incoming light power, thus it is given by :

$$\eta = \frac{P_{out}}{P_{in}} = \frac{P_m}{P_{sun}} = \frac{J_mV_m}{P_{sun}} = \frac{FFJ_{sc}V_{oc}}{P_{sun}}$$ (8)

where FF is called the fill factor, which is a quantity that describes how square is the $J - V$ curve.

2.2 Solar cells' efficiency limiting factors

Altough the light coming from the sun is a very powerful source of energy, not all of it can be extracted to use as electricity . Even for a perfect semiconductor solar cell, there are fundamental efficiency limits that cannot be overcomed. In 1961 Shockley and Queisser published a paper in which they calculated the ultimate maximum efficiency for a perfect single bandgap solar cell [3].

The first fundamental factor that limits the cells' efficiency is the second law of thermodynamics and the blackbody radiation. A perfect cell that could absorb all the incoming energy from sun would eventually heat up and emit back some radiation, this reduces already the maximum efficiency to around 86%.

The next fundamental solar cells' limiting factor are the spectral losses. This comes from the fact that light photons with lower energy than the band gap will not be absorbed, while the ones with higher energy will be absorbed but the energy exceeding the band gap will be lost mainly as heat. In general solar cells made of semiconductor materials with smaller bandgap, will produce higher short circuit current because

more photons can be absorbed, but at the same a bigger diode saturation current will lead to a lower open circuit voltage V_{oc} .Taking into account the solar spectrum irradiation of the sun it is calculated that the ideal solar cell should have a bandgap of around $1.34eV$, which would give a maximum efficiency of 33.7%, while for a silicon solar cell which has a band gap of around $1.1eV$ the maximum efficiency is 29%.

Solar cells' efficiency is also affected by temperature. At higher temperature the band gap is reduced, this causes V_{oc} as well as the fill factor to decrease , but J_{sc} increases. Nevertheless the effect is a net decrease in efficiency. For silicon solar cell the delivered power decreases around 0.5% per ^oC [4]. Appart from these intrinsic losses there are some other factors caused by the non perfect nature of the solar cell that further reduce the efficiency of the cell.

Perhaps the most important effect that effectively affects solar cells efficiency is recombination in the different regions of the cell, the most important recombination mechanisms are reviewed in appendix B.1.1. In general recombination affects negatively both J_{sc} and V_{oc} because less electric charges get to reach the cell's contacts. Recombination happening in the depletion zone causes an increase in the dark saturation current by adding an additional term which causes an increase in V_{oc}. This effect is usually characterized by modifying the ideal diode equation taking the form :

$$J_d = J'_0(e^{qV/mk_bT-1}). \tag{9}$$

where m is an ideality factor varying from 1 to 2. Recombination in the front and back surface of the cells is also an issue when bulk recombination is low as it affects J_{sc} and FF.

Another source of efficiency losses in solar cells is light absorption, as some of the light that hits the front surface of the cell is reflected back. For instance bare silicon is a very reflecting material and unless some texturing is made on the silicon wafer a great portion of the light will not be absorbed. In addition to this, since both the front and back sides of the cell need to be contacted to extract the charge carriers, the regions in the front part of the cell below the metal contacts will be shadowed and no light will ever reach it. The absorption coefficient of the cell depends on the wavelength of the incoming photons, having as general rule that the more energetic ones are easily absorbed than the less energetic ones. So if the cell is not thick enough some high wavelength photons may not be absorbed even though they have enough energy to excite the electrons over the band gap.

Another problem that arises from the front contacts of the solar cells, is the recombination in the metal semiconductor interface. In appendix B.3 it is explained that because of the difference in work functions of metals and semiconductors an energetic barrier that avoids conduction is formed in this interface. This has as consequence to create some series resistance R_s in the cell, which in turn diminish the FF of the cell and lower its performance. If the series resistance value is not excessively high it's effect on the fill factor might be easily calculated. This is done by assuming that the maximum power produced by solar cell is the power produced in the absence of series resistances minus the power lost by the series resistance, thus giving the following

expression for the FF:

$$FF = FF_0 \left(1 - R_s \frac{J_{sc}}{V_{oc}}\right) = FF_0 \left(1 - \frac{R_{series}}{R_{ch}}\right) \tag{10}$$

where FF_0 is the fill factor when there is no series resistance and where we defined the characteristic resistance $R_{ch} = V_{oc}/J_{sc}$. Reduction of this series resistance is an important topic in the present thesis work, because as we will shortly see one of the purposes of having an selective emitter solar cell is to reduce recombination in the metal semiconductor interface.

Finally the last factor that I want to mention that affects the performance of solar cells, is leakage currents between the contacts and junction of the cell, as well on its sides . This problem arises because in this zones the currents find alternate paths to flow which results in a power loss. The shunt resistance is the quantity that characterizes the opposition to the flow through these alternate current paths, thus having a higher shunt resistance will provide better cell performance. The effect that the series and shunt resistances have on the output density current of the cell is summarized in the following expresion:

$$J = J_{sc} - J_0(e^{(qV+JAR_{series})/k_bT-1}) - \frac{V + JAR_{series}}{R_{shunt}} \tag{11}$$

2.3   Typical solar cell design

As we have seen, for a solar cell to have an adequate performance it has to have some basic design features that comply with the requirements necessary to overcome the mayor practical efficiency losses. A typical solar cell is primarily formed by a thick P doped region called the base and a thin N doped region called the emitter. Usually the thickness of the base is around $200\mu m$, whereas the one of the emitter is around $0.3\mu m$. Usually the emitter is heavily doped because this improves charge transport through the contacts, as it is explained in appendix B.3. But this has the drawback that surface and bulk recombination is so high that almost all charges generated in this zone are lost, for this reason it is build as thin as possible. Usually the thickness of the base should be optimized so that it is bigger than the absorption length of light for energies greater than the bandgap, so as to absorb as much light as possible, it should be thinner than the minority carriers diffusion length so to avoid a dead layer. Over the emitter lays a antireflection coating that enhances light trapping, this can be enhanced by texturing the surfaces with an etching chemical. Over the emitter surface also lays the front metallic contacts, whose distance and width should be optimized so as to minimize shadowing of the underlying region and at the same time maximize charge transportation through the metal semiconductor interface. Regarding the back surface contacts the whole area is metalized, again in order to avoid recombination losses by increasing the contact area and creating a back field that avoid charges to recombine in the back surface.

2.4 Selective emitter solar cell

As mentioned in the preceding section, in conventional solar cells the emitter dopant concentration should be carefully selected, to account for a trade off between high minority carriers lifetimes and good charge transport through the front surface metal contacts. In section (B.1) it will be seen that for various of the different recombination mechanisms the recombination rate is proportional to the doping atoms concentration and this in general affects all of the solar cells performance characteristics. Recombination affects V_{oc} because it decreases the amount of minority photogenerated charge carriers that reach the junction, thus it increases the dark saturation current, which from equation (7) is inversely proportional to V_{oc}. J_{sc} is affected by recombination because it reduces the amount of charge carriers that reach the contacts, thus less current is transported out of the cell. Therefore for an emitter to have an acceptable performance the dopants concentration should be below 10^{20} cm^{-3}[15].

On the other hand, as we will see in section B.3 , in order to have a good charge transport across the metal-semiconductor interface in the contacts, the emitter's doping concentration should be high. Several author coincide in that the optimal sheet resistance for the semiconductor underneath the contact region is between 40-45 $\Omega/\square$, for which doping concentrations of at least 10^{19}-10^{20} cm^{-3} must be reached [16], [15]. Not complying with this requirement has as consequence a high recombination rate in the metal semiconductor interface, which considerably increases the series resistance and may reduce the fill factor below 70% for screen printed contacts. Optimization of the non selective emitter solar cell points that the sheet resistance in the emitter should be around $60\Omega/\square$ [14], but this is at the cost of having low blue light response, because charges generated near the front surface will quickly recombinate.

Having seen the problems that are encountered when optimizing the doping concentration of the emitter in a solar cell, it appears that the natural solution is to have a selective emitter. In this approach the area underneath the front metal contacts has a higher doping concentration than the rest of the emitter, thus providing good contact transportation as well as low bulk and surface emitter recombination. However there are some requirements that should be fullfilled by a solar cell for the selective emitter to improve its performance, some of these are:

- The front surface recombination velocity should be low, otherwise the extra lifetime gained by the charge carriers by lowly doping the emitter will be lost in surface recombination. Therefore a selective emitter solar cell requires a good front surface passivation. It is estimated that for front surface recombination velocities under 10000 cm/s, the selective emitter can improve the efficiency in around 0,60%,[17] .

- The resistivity of the base should be low. This is important because the total leakage current of the cell has a contribution from both the base and the emitter, but when the base resistivity is very high the leakage current is almost dominated by the base contribution. Therefore, in this case, any reduction in

the emitter leakage current will not affect the total leakage current, as it is almost equal to the base leakage current [16]

- The reflectivity of high energy photons should be low, otherwise very few charges will be generated in the emitter, thus making any improvement in the lifetimes purposeless.

In general a selective emitter can improve the efficiency of a solar cell up to 0.7 % [17]. However the reason why few comercial solar cells have a selective emitter is that it's fabrication requires incorporating some extra steps that in some cases may be costly and lenghty. The following are some of the most popular fabrication techniques:

Ion implantation. In this technique the selective emitter is made by performing an ion implantation over the wafers, which are covered by a mask that only exposes the desired areas that are going to be highly doped. After ion implantation, an annealing step is carried out in oxidizing environment, in order to activate the dopant atoms as well as to reduce the damage caused by the ion bombardment [19]. Altough this is a simple and straightforward process it has the disadvantages that ion implantation if not done properly may cause damage to the crystal structure and that Ion implantation is a expensive technique, thus not proper for mass production.

Oxide mask Process In this technique introduced by Centrotherm, the substrate wafer is covered by a SiO_2 layer over the regions of the emitter that are desired to be lowly doped. The thin SiO_2 layer will decrease the diffusion rate of the dopant phosphorus atoms during the diffusion doping process [20]. Then the highly doped region pattern is made by means of laser ablation over the desired area. After the diffusion the masking layer is removed by a wet etching process thus having form the selective emitter. The mayor drawback that this process presents is the laser induced damage produced by the high energy photons required to form the oxide mask pattern [18].

Doped Si inks In this technology developed by Innovalight Inc, silicon nanoparticles which are highly doped are deposited onto the wafer by means of screen printing in the areas where the contacts are going to be placed. Then the sample undergoes a phosphorus diffusion that accounts for the formation of the lowly doped emitter. This technology is clean, efficient and only adds an extra step to the manufacturing process [21]. Nevertheless it has the disadvantage that the silicon inc is a pattented costly material, thus it would considerably raise the cost of the solar cells.

Etch back techniques It is widely known that superficial doping concentration in silicon wafers is reduced when it is exposed to acid baths such as HF or HNO_3 during long times. Thus Etch back is a technique for the formation of selective emitters in which the wafer is highly doped and then exposed to acid baths in order to reduce the emitter sheet resistance to the needed value. The desired

high doping areas are properly shielded by means of a screen printing technique. Although this technique is cheap its reproducibility is low, having as major problem the setting of the acid bath.

Laser Doping In the laser doping technique, a phosphosilicate glass layer is deposited on top of the wafer surface to serve as a dopant source. Then the wafer is selectively irradiated by laser energy, this melts the material and incorporates the dopant atoms in the areas where metallization will take place. This is the technique that will be employed in the development of the present thesis because it presents various advantages; it requires no extra diffusion steps or use of additional chemicals, it is cheap and has a very high reproducibility. Since the only additional equipment necessary to perform this technique is a short wavelength laser, it is a process that can be easily incorporated in the baseline production of any manufacturer. The two major challenges that the elaboration of the selective emitter by means of this technique presents are reducing the laser damage and achieving a proper alignment. In the subsequent sections more details about the laser doping technique will be given

Thus having reviewed the basic characteristics of solar cells as well as the basic features of the selective emitter, we will describe in the next section the different manufacturing processes as well as the main characterization techniques used in the elaboration of the present thesis.

3 Solar cell manufacturing processes and characterization.

Solar cells' manufacturing and characterization is a very active and interesting field of research because its background knowledge relies on deep theoretical chemist and physics while is practical application methods make use of many state of the art semiconductor technology techniques. Therefore the purpose of the present chapter is to present an overview of the techniques, materials and equipment that were used in the elaboration and characterization of the laser doped samples and the selective emitter solar cells.

3.1 Solar cell manufacturing.

In figure 2 it is shown a diagram of the basic manufacturing steps used in the elaboration of the selective emitter solar cell made in the present thesis. This process is similar to the standard baseline industrial production process, the main difference being the inclusion of the laser doping step. In order to understand better how the efficiency of the solar cells is affected by the manufacturing process, in this section it will be explained how these process are carried out and what is their specific purpose.
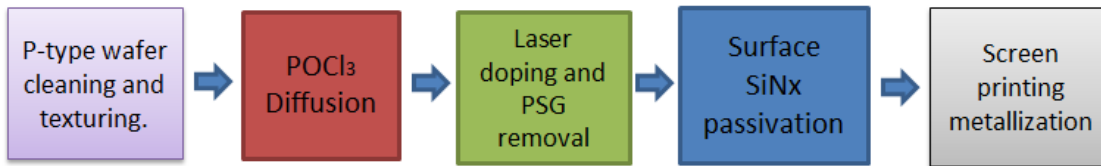
Figure 2: Process flow for the elaboration of SE solar cell based on the baseline process at IFE laboratory.

3.1.1 Czochralski silicon wafers

In the present thesis most of the wafers used were Czochralski silicon wafers, because they are one the best high quality, low price options in the market. The Czochralski process is one of the most popular techniques for growing single crystal high purity silicon wafers. It starts by filling a crucible with high purity polycrystalline silicon material, which has been refined from SiO_2 quartzite, usually by a process called Siemens . The crucible is made of hyper pure material and should be embedded in a clean room environment. Then the crucible is heated to temperatures slightly above the silicon melting point 1500^oC. In order to maintain the temperature constant and oppose the effect of heat convexion across the crucible, magnetic fields are applied. Then, the most crucial step is to dip a silicon seed crystal into the melt over which the bigger crystal structure will grow maintaining the crystal seed properties. Careful orientation ,controlled rotation and slow pulling of the seed crystal are required to create the pure crystal structure. The amount of defects formed in the generated

crystal structure will depend on many factors such as the environment oxygen levels, growing temperature and rotation speeds. In general the slower a wafer is grown the less defects its structure will have. Also bigger wafers tend have more impurities. Therefore the challenge is always to optimize the throughput against the crystal quality [23].

3.1.2 Wafer cleaning, saw damage etch and wafer texturing

In order to maintain the surface of the silicon wafers free of external impurities, all wafers should undergo through standard cleaning processes, between each manufacturing step. A common procedure to clean the wafer is to dip it in 5% HF solution, which removes any growing oxide and external impurities. In certain cases it is necessary to perform a piranha cleaning (4:1:H2SO4:H2O2) which helps to remove any organic residue present in the wafer [24].

Saw damage etch is a process whose purpose is to eliminate possible defects and cracks present in the surface of the wafer. The saw damage etch was done by dipping the wafers in 30% KOH solution at 78 ^0C during 2 minutes. This process in general reduces the thickness of the wafer and should be carefully controlled to not cause any surface damage. Usually after saw damage etch the wafers should be cleaned with HCl solution and DI water so to remove al KOH particles.

One of the methods use to enhance light trapping in semiconductor solar cells is to perform a surface texturing. One of the popular procedures to do this is by KOH baths which result in pyramidal structures which are formed because of the alkaline etching properties of the KOH solution. In our case the texturing was done by dipping the samples in 1% KOH bath with IPA (isopropyl alcohol) for about 40 min with subsequent appropriate cleaning, which included dipping in HF and DI water.

3.1.3 POCl$_3$ diffusion

The introduction of dopant atoms in a semiconductor is one of the processes that is more important in the fabrication of semiconductor devices. In the case of solar cells this is an important step, because it produces the PN structure which provides the essential working mechanisms for the conversion of light into electricity. In most of the common baseline solar cells procedures the front emitter is formmed by performing a POCl$_3$ diffusion in the wafer. This is a process which depends on many variables and which should be optimized to obtained the desired dopant depth concentration profiles. Altough a great amount of research has been done in order to understand the basic diffusion mechanisms of dopant particles into semiconductors [25], due to the complicated nature of the processes most of the standard used recipes have been developed empirically.

The first step in the diffusion process after the wafers have been inserted in the chamber is to heat it to the required diffusion temperature, between 800°C and 1150°C. In order to maintain the recipes reproducibility the temperature should be controlled with accuracy of about 1°C. Then a carrier gas is introduced. Usually this

are nitrogen, oxygen or argon. Then the dopant source gas is introduced an deposited in the surface of the wafers. This stage is called deposition. In normal p type solar cells the most popular phosphorus precursor is POCl$_3$. The following are some of the possible reactions that take place in the diffusion chamber:

$$Si + O_2 \rightarrow SiO_2$$

$$4POCl_3 + 4O_2 \rightarrow 2P_2O_5 + 6Cl_2$$
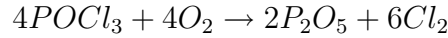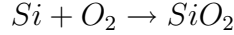
were the formed P_2O_5 and SiO_2 during the deposition will combine to form a phosphorus silicate glass which will subsequently deposit in the wafer's surface. Then the second stage is to produce a drive in of the phosphorus dopants. This is done by increasing the temperature of the furnace, which enhances phosphorus diffusion into the material. In general the concentration profiles are very sensitive to all the different conditions and parameters that can be set for the diffusion furnace. The recipe used for the elaboration of our selective emitter solar cell will be discussed in section 4.3.3.

3.1.4 Surface passivation and antireflection coating.

In the front part of the solar cell two processes that reduce the maximum efficiency of the solar cell take place, i.e surface recombination and reflection losses. These two problems are solved by depositing and antireflection coating and a passivation layer. Fortunately there are materials like SiNx that take care of both at the same time. In general SiNx posses good antireflection qualities and passivation properties, of which both can be controlled by modifying the Si content of the deposited SiNx layer [26]. In addition, due to a high internal positive fixed charge densities, the SiNx coating layer creates an electrostatic field that avoids minority charge carriers to approach the surface, which furthers reduce recombination. For depositing the SiNx layer the most common technique is plasma enhanced chemical vapor deposition. This is a low temperature technique which uses high electromagnetic fields to ionize the gases of the materials that will be deposited in the substrate. Usually the precursor gasses is a combination of NH$_3$ and SiH$_4$, which due to the plasma process creates additional hydrogen atoms which help to reduce the amount of dangled bonds [27].

3.1.5 Front and back surface metallization

In order to extract the photogenerated charge carriers, metal contacts should be deposited in the front and back surfaces of the solar cell, being screen printing one of the cheapest and most used solution in commercial silicon solar cells.
An screen printing system is mainly composed by a screen, a squeegee and the metal paste. The screen contains the pattern that will be printed in the solar cell, which is composed by a few busbars and several metal fingers connecting them. The metal paste is composed of an active powder metal plus some organic binders which keep the mix in a suspension . After the metal paste has been deposited in the screen

the squeegee pushes it through the openings thus forming the desired metal pattern on the wafer surface. In the present thesis Ag paste was used for the front contacts formation while for the back Al was used. Ag is known for having good conductivity and low diffusion coefficient.

Then, in order to make the contact, the metal paste should penetrate through the front surface passivation layer and go deep into the emitter. This is done by performing a contact firing at temperatures between 700^oC and 900^oC in a belt furnace. This results in the diffusion of Ag into the silicon substrate with formation of an alloy that provides a low resistivity metal semiconductor interface [27]. In general the firing process highly determines the depth and quality of the contacts, therefore for different emitter profiles should be optimized.

3.2 Solar cells characterization.

In solar cells development characterization techniques are as important as the manufacturing it self, because they allow to evaluate the performance of the elaborated product and thus trace the future paths to follow. Therefore in the present chapter it will be presented an overview of some of the different characterization techniques used in evaluating the properties of the different samples made.

3.2.1 Sheet resistance and four point probe method.

Probably the most important characterization method employed in the present thesis was sheet resistance measurement, because it allowed us to quickly obtain information on the emitter dopant concentration without causing damage to the analyzed sample. The reason for this is that the conductivity in a semiconductor material depends on the amount of available conducting charge carriers, which in turn depends on the dopant atom concentration in the crystal lattice.

Sheet resistance is formally defined as:

$$R_s = [q \int \mu(C)C_e(z)dz]^{-1} \tag{12}$$

where $C_e(z)$ is the carrier concentration depth profile and $\mu(C)$ is the mobility which depends on the carrier concentration. Sheet resistance is the preferred used quantity, when characterizing the resistance to current flows in thin homogeneous layers of semiconductors. This quantity is related to the usual resistivity measure by:

$$R_s = \rho/t \tag{13}$$

where ρ is the resistivity of the measured sample and t the thickness of the layer being analyzed. Sheet resistance has the same units as the usual resistance but is only applicable over two dimensional homogeneous systems, therefore its units are written like $\Omega/\square$ to specify the quantity measured.

The usual method used to evaluate sheet resistance is the four point probe method. In this method four conducting probes in a linear configuration are placed over the studied sample, then a known current is passed between the two external probes and

the voltage drop is measured between the two internal ones. The sheet resistance is the value of the ratio between the voltage drop and the forced current [23]. These values have to be corrected by a geometrical factor which depends on the ratio of the probe spacing to the thickness of the studied layer. If the spacing of the probes is much bigger than the layer and they are symmetrical between each other the factor is 4.5325. In figure 3 a schematical diagram of the 4 point probe system is displayed.
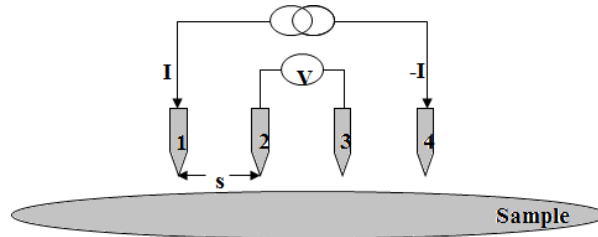
Figure 3: Four point probe method to measure sheet resistance.

The reason why a four point configuration is preferred over a two points one is that it avoids problems arising from contact resistance, which sometimes can be as big as the one in the measured sample it self.
Thus even though it is hard to extract the doping concentration from sheet resistance alone, comparative measurements allowed us to study the amounts of doping atoms concentration after the different doping processes.

3.2.2   Surface roughness

In order to measure the roughness of a wafer surface, some depth measurements were made by means of an optical microscope. The microscope is controlled by a computer software, which by making a variation on the focus depth makes a 3d model of the pictured area. Using this it is possible to know with great accuracy the depth of each point in the studied surface. Then in order to measure the surface roughness the microscope's software is used. This has an incorporated function in which the depth at each point in a line traced by the user is measured. This is illustrated in figure 4. Then the software calculates quantities such as the average depth, the standard deviation, root mean square standard deviation and the maximum peak to valley distance.
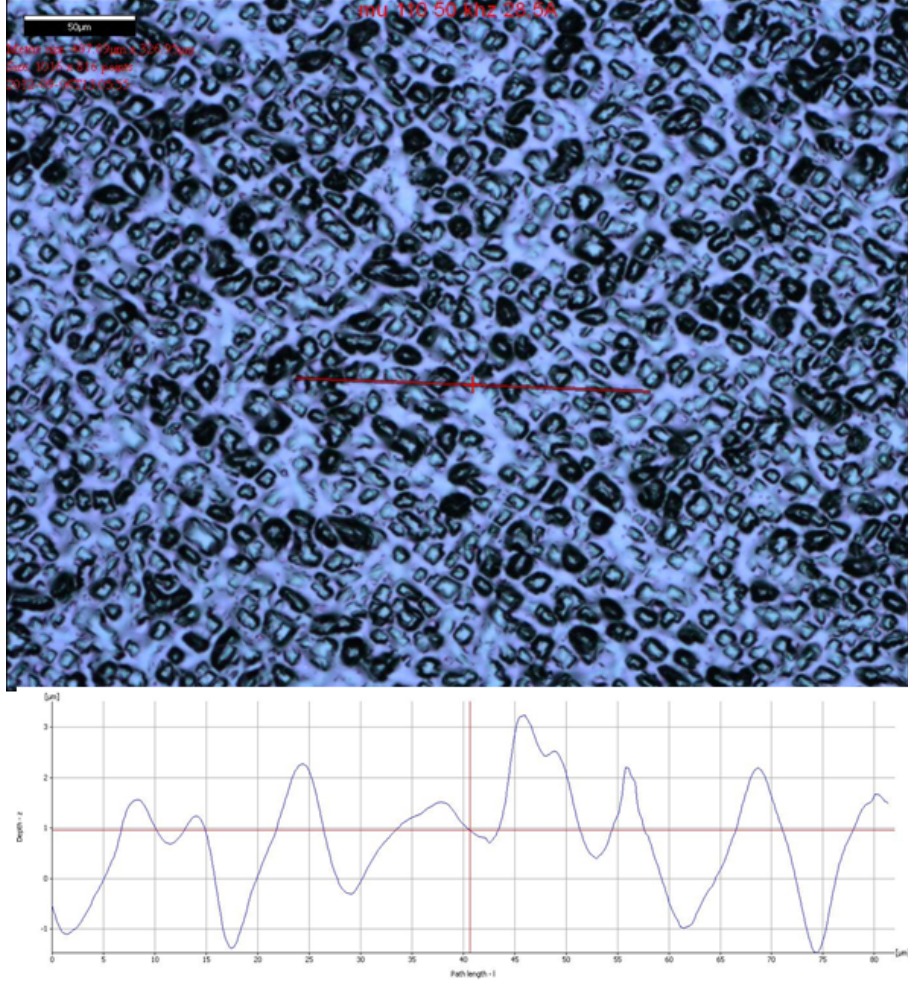
Figure 4: Measuring the surface depths after laser irradiation. In the bottom part of the figure the surface depths at each point over the traced line are displayed

Therefore in order to calculate the surface roughness we used the root mean square deviation of the depths at all the measured points r_q. For each sample various lines were traced in different directions and the the quantity r_q was averaged and this was taken as the surface roughness.

3.2.3 Lifetime measurements

Carrier lifetimes is one of the parameters that is more critical when studying and designing semiconductor devices, because it determines most of the electronic transport properties of the crystal and its measurement gives important information about the quality of the material . A complete explanation on the meaning of this quantity and the factors that affect it is given on appendix B.1.1. When one is studying lifetimes one is not measuring a property of the semiconductor it self but a property of its carriers, whose states are greatly influenced by the measurement technique [30], therefore different measurement techniques may provide different results which

may in principle be correct, thus when characterizing lifetimes it is usually necessary to use more than one calibration method. Therefore the equipment used in the development of this thesis uses photoluminescesnce decay (PLD) and Quasi-steady Photoconductance QSSPC as lifetime measurement methods.

QSSPC method: In this method, the minority carriers lifetimes are obtained by first illuminating the sample with a flash lamp during periods of time long enough that the sample is considered to be in a quasi steady state during the time of the measurement. Usually the requirement for the quasi steady state condition is that the effective carrier lifetime is smaller than the lamp time constant [30]. The measurement consist on detecting the photoconductance signal coming from the sample during the illumination time, which is done by means of an inductive coil placed below the sample. Then from the decayment time of this signal the minority carriers lifetimes τ_{eff} is obtained. But in order for this information to be useful the amount of excess minority carriers produced by the the illuminating photons should be known. This is easily accomplished if the light intensity incident on the sample is measured, because then the generation rate G can be obtained by:

$$G(t) = \frac{f\Phi(t)}{d} = G_0 e^{-t/\tau_{flash}} \tag{14}$$

where f is the absorbed fraction of photons, Φ the incident flux and d the sample thickness. The last equality of the equation is the generation rate, assuming the pulse intensity decays exponentially with time constant τ_{flash}. From this the excess minority carriers density is calculated to be [30]:

$$\Delta n = \frac{\tau_{eff}}{1 - \tau_{eff}/\tau_{flash}} G_0 \left(e^{-t/\tau_{flash}} - e^{-t/\tau_{eff}} \right) \tag{15}$$

Thus from this relation curves relating the effective minority carrier lifetime vs injection level can be obtained.

Photoluminescence Decay method: In PL measurements the excess minority carriers are generated by a short pulse of photons with energies greater than the band gap, then the lifetimes are measured by detecting the light emitted from the recombination process and its dependence on time. In general the PL signal is proportional to the rate of recombination, thus to the excess carrier density. The relation between the radiated photon flux $\Phi_{pl}(t)$ and the excess minority carriers is given by:

$$\Phi_{pl}(t) = K \int_0^d \Delta n(x,t) dx \tag{16}$$

where K is a constant accounting for solid angle emission variations and the reflectivity of the radiation emitted. The effective lifetime τ_{eff} is calculated from the generation rate (equation 14) and Δn by:

$$\tau_{eff} = \frac{\Delta n}{G} \qquad (17)$$

In general PL is used for obtaining spatial mappings of the carriers lifetimes for a given injection level, while QSSPC is used for obtaining τ_{eff} vs Δn curves.

3.2.4 Emitter saturation current

As was mentioned earlier lifetimes measurements is a powerful tool to study the quality of a semiconductor sample, but it has the flaw that it does not distinguish between different recombination mechanisms, nor where in the sample does the recombination takes place. Since in the present thesis we are interested in studying the quality of the crystal in the emitter which were formed by laser doping, it is necessary to have a technique that separates recombination in the emitter from the rest of the sample. The more appropriate technique is saturation current measurements. The emitter saturation current is a measure of the amount of current that is loss because of recombination in the emitter and the front surface region. It is formally defined as:

$$J_{0e} = \frac{q n_i^2}{N_a} S_{em} \qquad (18)$$

where S_{em} is the recombination velocity of charge in the region mentioned. In appendix B.1.7 it will be seen that recombination lifetimes can be separated by terms whose contribution comes from the bulk of the sample and those whose contribution comes from the regions near the surface. From equation 47 of appendix B.1.7 and equation 18 the effective lifetime can be expressed as [28]:

$$\frac{1}{\tau_{eff}} - \frac{1}{\tau_{Au}} = \frac{1}{\tau_{SRH}} + \left(J_{0e(front)} + J_{0e(back)} \right) \frac{(N_D + \Delta n)}{q n_i^2 W} \qquad (19)$$

where τ_{Au} and τ_{SRH} are the terms coming from the Auger and SHR recombination mechanisms. Thus, from this equation it can be seen that the minority carrier effective lifetime is inversely proportional to the saturation current. Thus the technique for measuring saturation currents consist in elaborating symmetrical samples, so that the contributions inside the first parenthesis of the right hand side of equation 19 is just $2J_{0e}$. Then the idea is that at high injection levels the SHR recombination lifetimes is independent of the injection level Δn w, so that in this case $1/\tau_{eff}$ increases linearly with the injection level, and thus by finding the slope of the $1/\tau_{eff}$ vs Δn curve one is able to find J_{0e}.

In the present thesis a Sinton instrument was used to find J_{0e}. This is an equipment that uses a QSSPC coil together with a flash lamp to obtain $1/\tau_{eff}$ vs Δn curves. The advantage that this instrument has over the PL equipment, which also does QSSPC, is that it easily produces the high light intensity necessary for obtaining the required high injection levels . The software controlling the equipment calculates automatically the $1/\tau_{eff}$ vs Δn slope and thus gives the value for J_{0e}, but it it necessary to visually check that the curve are approximately linear, otherwise the flash intensity should be increased.

3.2.5   SIMS profiles

One of the most accurate technique to characterize doping concentration profiles is secondary ion mass spectroscopy. In this method the tested sample is placed in an ultra high vacuum chamber and then impinged by a beam of high energy ions (between 1-5 keV). This causes some sputtering of the sample's atoms[30]. Then some of this ejected atoms are electrically charged, thus they can be subject to electromagnetic fields that drives them towards an spectrometer which measures the mass/charge ratio. This ratio is characteristic of each element, thus it allows to calculate the amount of the element in the sample. By increasing the sputtering rate it is possible to obtain the concentration of the impurities as a function of depth. In silicon this technique allows to measure phosphorus concentrations as low as 1×10^{15} cm^{-3} by using Cs as bombardment ions source [23].

3.2.6   IV measurements

Perhaps the ultimate test performed on solar cells to evaluate its performance is the IV curve measurements. This is done by connecting the front and back terminals of the solar cell to a variable voltage source that in addition measures current. The measurement consist in applying a voltage between the cells terminals while exposing the cell to illumination from a source lamp with known intensity and then measuring the output current density produced by the cell. Initially the voltage is 0 and then is increased until the V_{oc} value where the cell does not produce current anymore. The output current is constantly measured in this process, thus a J vs V curve is obtained. From this curve the values of J_{sc},V_{oc}, FF and efficiency are obtained. To obtain the efficiency the values of the incident flux power should be known.

Since the values of the output current are also dependent on many different external factors, in order to characterize solar cells in a comparable way certain standard conditions have been established. These are:

1. Light intensity of 100mW/cm^2. This is called one sun illumination.

2. Cell temperature of 25 ^{o}C.

3. Four point probe to remove the effect of the probe-cell contacts resistance.

Besides the already mentioned quantities other cell parameters like series resistance and shunt resistances can be obtained by making appropriate fittings to the IV curve [29].

3.2.7   Internal quantum efficiency

In a solar cell the quantum efficiency is the ratio between the amount of carriers collected in the cell's terminals to the number of photons of a given wavelength. Since the reason why a photon was not converted to electricity might be either that it was not absorbed or that it recombined before reaching the cell's terminal two kinds of

quantum efficiencies are defined: internal and external. In external quantum efficiency the ratio of all photons hitting the cell against the amount of collected charges is measured. In internal quantum efficiency the ratio of absorbed photons is measured against the amount of collected charges. This measurement then requires measuring the reflectance of the cell for the wavelength range studied.

In a quantum efficiency measurement an applied voltage is applied to the cell terminals and then the output current is measured while the cell is illuminated by monochromatic light from a lamp source. The light wavelength is varied from high energy values to the semiconductor bandgap energy where the cell does not produce any current. Then the reflectance for the same wavelength range is measured an by extracting the amount of reflected photons the internal quantum efficiency is measured.

4 Laser doping theory and experiments

Laser doping (LD) is a technique in which a thin layer of dopant source is deposited over a semiconductor surface to subsequently be irradiated by a laser energy source in order to incorporate the dopant atoms into the substrate. This technique was introduced in the early 60's by Fairfield and Schwutke [38], and since then it has been widely used in the semiconductor industry for the elaboration of different devices such as CMOS or bipolar structures.

The advantages that laser doping offers over other traditional doping techniques such as ion implantation and oven annealing are: quick and cheap processing times, selective area doping and novel doping profiles that allow to elaborate ultra shallow highly doped junctions [37]. The mayor drawback that the laser doping technique presents is the introduction of defects into the crystal material caused by laser irradiation damage [41]. This topic has been widely researched and it has been found that the damage inflicted on the semiconductor greatly dependent on the laser parameters settings.

Regarding the fabrication of a selective emitters solar cell LD presents the advantage of localized doping, which allows to elaborate the required highly doped areas while at the same time creating the metallization patterns.

The great challenge presented when performing this technique is to acquire the desire doping level while maintaining the materials laser damage as low as possible, thus in order to do so it is necessary to understand well the laser doping mechanism and the nature of the created silicon defects. Therefore in the present chapter some theoretical considerations as well as a brief review of some works already made on this topic will be presented.

4.1 Laser doping review.

When a silicon surface is irradiated with laser photons, those with energy above the bandgap will excite the electrons to the conduction band, with the rate of light absorption being described by the material absorption coefficient λ (equations 26 and 27). If the energy absorption rate is faster than the heat dissipation rate by conduction, the material heats up due to electron collisions with the latice ions, until it reaches the silicon melting point (1414^oC) [39]. At this point, the present dopants will diffuse into the silicon material, with characteristic diffusion depths dependend on the diffusion coefficient of the particular dopant source .

When the material starts to lose more energy by conduction than it gains by photon absorption the temperature begins to decrease and then when the melt has lost enough energy to account for the latent heat, the molten silicon will recrystallize. Recrystallization of a molten volume that is deposited over a Si crystal structure will occur epitaxially at ultra high speeds, which is believed to be one of the most important factors affecting the crystal's quality [41].

Laser doping has been extensively studied by means of computer simulations which use the classical heat diffusion equation to analyze different probable doping profiles.

In one dimension the heat diffusion equation with an additional light absorption term gives [40]:

$$\frac{\partial T(x,t)}{\partial t} = \frac{\partial}{\partial x}\left[D(T)\frac{\partial T(x,t)}{\partial x}\right] + S(x,t), \qquad (20)$$

where D is the thermal diffusivity and $S(x,t)$ is the rate of laser light absorption (equation 31). Laser pulses only provide a finite amount of energy given by its Gaussian profile, thus $S(x,t)$ is given by:

$$S(x,t) = \sqrt{\frac{4\ln 2}{\pi}}\frac{(1-R)F_p\alpha}{\tau_p}\exp(-\alpha x - 4\ln 2(t-t_{peak})^2/\tau_p^2) \qquad (21)$$

where F_p is the maximum pulse fluence ,t_{peak} is the time at which it occurs and τ_p is the half width pulse length.
What the heat equation without the radiation term tells us, is that the temperature at certain moment t at a certain point x will go up or down depending on if its warmer neighbor is warmer than its coldest is colder, so that the speed of the heat diffusion is in general controlled by the thermal diffusivity D of the material, and the temperature vs depth position curve curvature. This is expressed in the second derivative of the right hand side of equation (20) . This will later be important in the interpretation of the obtained results. Usually, in order to include the possibility of phase transitions, equation (20) is transformed to an enthalpy version instead of a temperature one [39].

The other important equation used in computer simulations is the dopant atoms diffusion equation, which describes the rate at which the dopants diffuses into the crystal . This equation is,

$$\frac{\partial C(x,t)}{\partial t} = D_D(T,x,t)\frac{\partial^2 C(x,t)}{\partial^2 x} + Q(x,t) \qquad (22)$$

where C is the dopant atom concentration, D_D is the dopant diffusion constant in the material and Q is the source term at the surface. For phosphorus diffusing into liquid silicon it is found out that $D_D = 3.4 * 10^{-4} cm^2/s$ [42], which is five orders of magnitude higher than in solid silicon. For this reason it is assumed that diffusion only takes place when the substrate is in liquid state.

As mentioned before computer simulations have allowed researches to obtain a detailed description of the laser doping process which along with some experimental results have led them to some very interesting conclusions, some of these are:

1. Incorporation of the dopant atoms into the crystal take place during epitaxial regrowth by means of latice silicon atoms substitution [47]. This implies that after laser doping the dopant is electrically active and no further annealing is needed.

2. The amount of structural defects formed in the recrystallized area is proportional to the recrystallization velocity, which means that longer melting times will give higher quality material. [41]. This is so because by having longer

molten times, epitaxially regrown atoms will have more time to accommodate them selves into the crystal latice. Usually the melting and recrystallization velocity is described by the front melt velocity, which is the rate at which the interface between the liquid and solid state in the material penetrate in or out of the material. This is another point that will be crucial when analyzing our obtained data.

3. Increasing laser pulse energy increases the materials molten time and depth, but the time it takes to reach the maximum melting depth is almost constant [42]. Therefore the recrystallization velocity and thus the quality of the material is mostly controlled by the pulse laser energy. Figure (5) illustrates the front melt position as function of time (taken from [45]). Later on we will find out that this is true only when laser pulse duration are equal as is the case in figure (5)
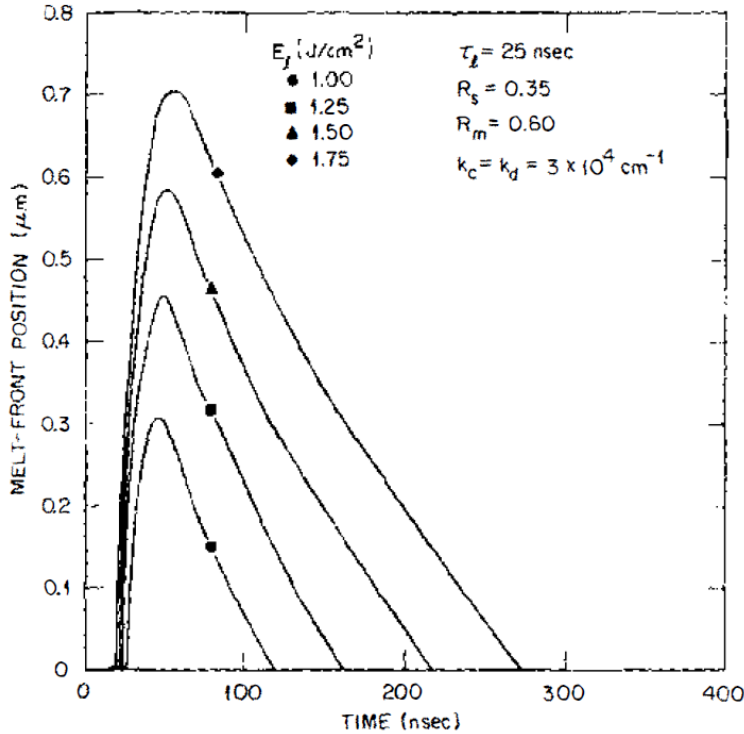
Figure 5: Melt front position as a function of time. taken from [45].

4. Recrystallization velocities in silicon are very fast, in the order of $\mu m/s$[41].This implies that the material will go through a whole cycle of melting and recrystallization during one laser pulse. For instance in the present thesis we used laser doping frequencies of about $45 - 75kHz$, which means that the time between two pulses is of the order of $1x10^{-5}s$, while the time that it takes for a 200 nm zone to recrystallize is of the order of $1x10^{-7}s$. This means that the maximum melting depth is in each pulse almost the same.

5. The amount of doping atoms incorporated into the silicon depends both on

24

the diffusion velocity of the dopants and the front melt penetration velocity . Figure (6) displays the maximum melt and junction depths for various incident laser energies . At low energies the diffusion process is limited by the position of the front melt while at high laser energies the front melt penetrates much faster than the doping atoms thus the process is limited by the atoms diffusion velocities.
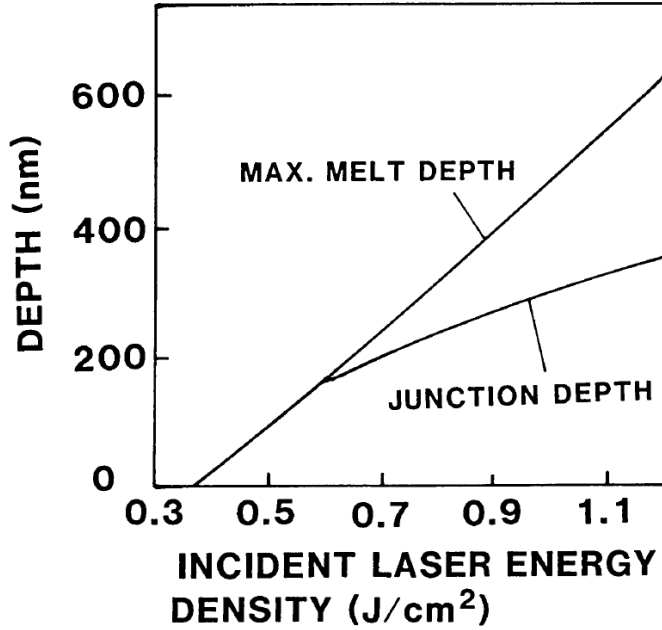
Figure 6: Simulated maximum melt depth and junction depth as function of laser energy density. Taken from [45]

6. The depth of the molten region is strongly dependent on the absorption depth at the laser's wavelength. In general the melting depth is proportional to the absorption depth. High wavelength laser will produce deeper profiles, while low wavelength lasers produce shallower ones,[41], [44]. For this reason when performing very high and shallow doping profiles lasers with more energetic photons are preferred. In general the absorption coefficient in silicon is temperature dependent, an empirical approximation that has been found for this is:

$$\alpha(T) = 5.02e^{T(K)/430} \tag{23}$$

This means that as the material gets hotter it absorbs more light, this can lead to runaway solutions when making computer simulations.

Besides computer simulations many other techniques have been used to understand the nature and effect of laser doping on silicon materials. Regarding defect formation due to laser damage some of the conclusions that have been found are:

25

7. Up to 90 % of the extra defects formed in the crystal due to Laser doping are found in the nearby region of maximum light absorption. This was found by Mooney et al by using deep level transient spectroscopy [50].

8. The most prominent type of defect found after LD on silicon substrates are electrically active point defects. This is mainly due to the substitutional nature of the incorporated dopant atoms [49]. In general higher dimensions defects have not been observed when using (100) silicon substrate, whereas in (111) silicon stacking faults were observed, this was studied by means of transmission electron microscope images by Young et al [47]. This comfirms that melted silicon recrystallizes epitaxially. Young et al suggested that heating up the wafer while recrystallization takes place would reduce the number of point defects formed in the solidification process, because the incorporated dopant atoms will have more time to find their place in the lattice.

9. Large concentrations of oxygen atoms have been found near the surface of the laser doped areas. These impurity atoms could act as traps thus reducing the electrical performance of the material.

The above considerations will help us to interpret the results obtained and thus choose the best laser parameters to make our selective emitter solar cell.

4.2   Qswitch Laser

A laser is a semiconductor device which generates coherent light rays by means of stimulated emission of radiation. Literature reviewing the basic principles of laser are easily found, for instance one of the early classical articles reviewing this subject is the one presented by one of the laser pioneers, Gould, R. Gordon [52].
For the elaboration of the present thesis a Q switched diode pumped laser was used. Q-switching is a laser mode which allows pulsed operation by storing optically pumped energy in the laser crystal while preventing feedback into the gain medium. When the maximum stored energy is reached the feedback is allowed into the gain medium thus generating the stimulated emission process. This permits the generation of short pulses with high peak fluence. Usually this pulses have a Gaussian form which are mostly characterized by the following parameters: the fluence (J/cm^2), light wavelength (nm), pulse duration width (ns) and in focus spot $1/e^2$ diameter(μm). The parameters of the laser over which we have control are the diode current, the pulse repetition and the scanning velocity. The current and repetition frequency of the laser will determine the output power and thus the pulse fluence, which is the average energy per unit area. This quantity is obtained by dividing the laser output power by the frequency and the pulse area.

The Rofin Sinar laser used for this thesis does not have an incorporated power meter, and since in particular the one we were using suffers from stability problems the power had to be measured before and after each doping process by an external laser power meter.

In general higher diode current gives higher output power, while higher pulse repetition, results in lower laser power. This is illustrated in figure (7), where we measured the laser power output in function of the repetition frequency.
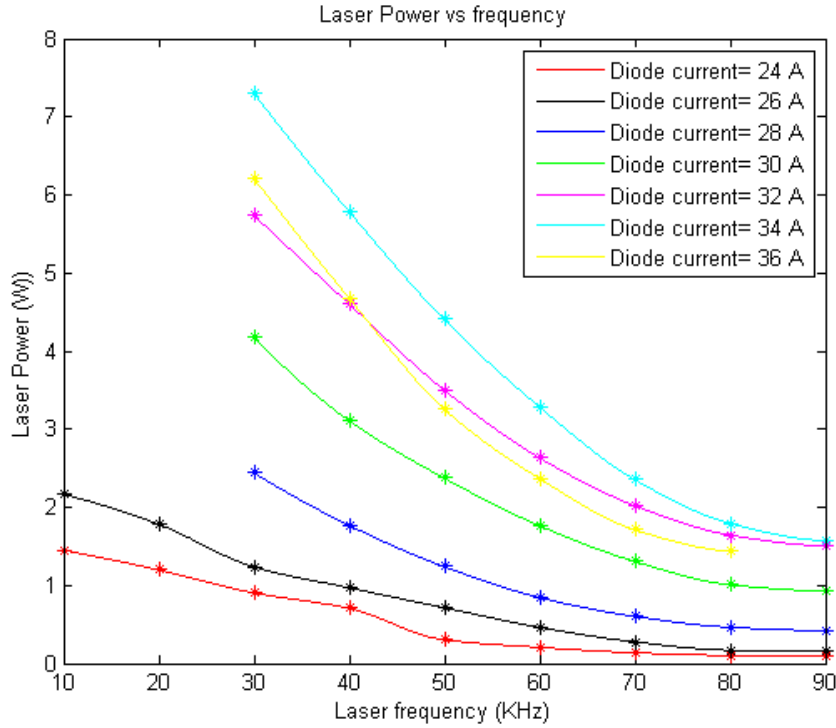
Figure 7: Measured laser power vs laser repetition frequency for different laser diode currents.

The wavelength of the laser depends on the diode's crystal characteristics, thus for a given laser it is determined. In our case the laser light wavelength is 532 nm which is very suitable for laser doping purposes because it produces a rather shallow doping.

In general the laser pulse duration is a very variable parameter that depends both on the laser diode current and in the laser repetition frequency. For higher laser diode current, the pulse duration tends to decrease, while the peak fluence of the pulses increase. For higher laser repetition frequencies the pulse duration increases while the peak fluence decreases. This will be a very important point later in our thesis because we will see that the doping profiles are highly influenced by the laser pulse shapes. In figure 8 we display the measured pulse duration for various laser diode currents as well as laser energies. The measurement was made by means of an oscilloscope and it was at laser frequencies of 65 and 75 kHz because this are of the most used in this thesis.

In figure 8b it can be observed that in general the pulse width is higher for the high repetition frequency pulses. This implies that the low frequency pulses will have higher peak fluences. Note that it is not always a rule that for pulses with same energy density, the ones at higher laser frequency have longer pulse duration, because

27

for two pulses to have same energy density but different laser frequency the power should be adjusted with the one at higher frequency having higher laser power, but in general the pulse duration decreases with increasing laser power.
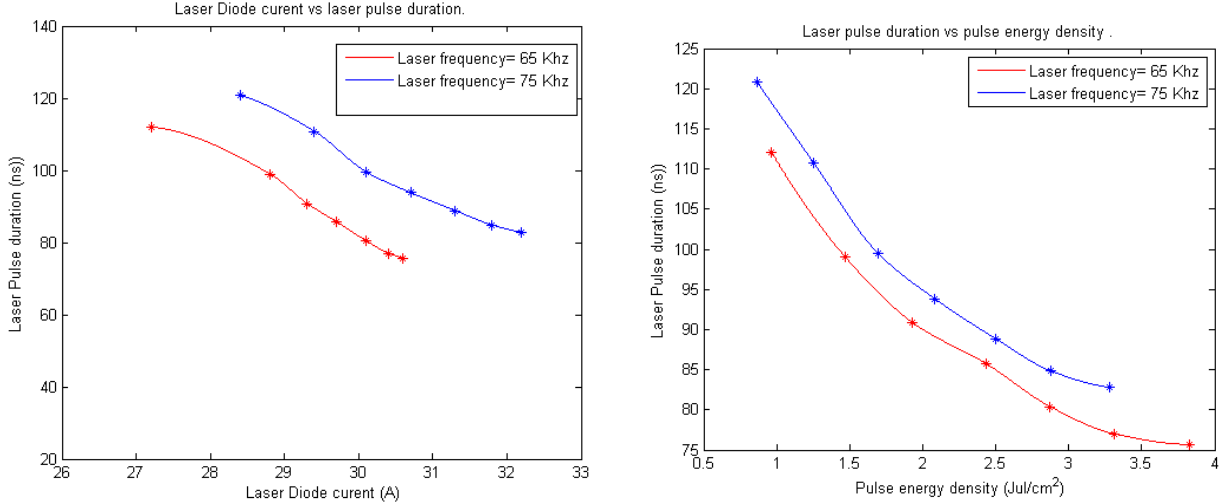
(a) Pulse duration vs laser diode current for laser repetition frequencies of 65 kHz and 75kHz.

(b) Pulse duration vs Pulse energy density for laser repetition frequencies of 65 kHz and 75kHz.

Figure 8: Laser pulse characteristics for two of the most used laser repetition frequencies in the present thesis.

The laser in focus spot diameter(μm) is a quantity that varies with the laser power. The manufacturer of the laser claims that it is 20 μm we measured it for various laser powers and it gave and approximately constant values.

4.3   Experimental results

In the following section a report and analysis on the experiments done on laser doping will be given. The Laser doping experiments done in the present thesis were performed by using a diode pumped laser of wavelength , 532 nm with reference Nd:YVO4 RSM 20E from Rofin-Sinar.

The wafers over which the doping was performed had different preparations and initial doping depending on the experiment as explained later. In general, except for the wafers used for the SIMS measurements, all experiments were performed on monocrystalline boron doped unpolished wafers of dimension 125+/- 0.5 mm , resistivity 0.5-3 ohm·cm and thickness 200 micrometers. In general it was a common procedure to clean the wafer with 5% HF solution before depositing the dopant glass layer whatever the deposition method was, so to remove any growing oxide.

The general Laser doping procedure was to first deposit in the surface of the substrate a phosphorus glass layer (two different methods were used for this), and then irradiate it with the laser energy to perform the diffusion of the dopant into the wafer.

28

The purpose of the experiments was to characterize the laser parameters which would give the best doping results causing fewer damage to the crystal structure of the wafer.

One of the factors that limits the range of values that can be chosen for making the laser doping is the stability of the Laser. Unfortunately the power output of the Rofin-Sinar laser available at the IFE laboratory is not stable for a great range of values for which the manufacturer claims the laser is operational. Therefore one of the necessary tasks was to choose parameters that would give laser power outputs reasonably stable for periods long enough to make the laser irradiation of the needed areas. For doing so the power output of the laser was measured before and after each laser doping process . The power meter used was manufactured by Coherent INC. Several experiments were performed in which current and frequency were varied but the power was not measured, but since from day to day the output power of the laser may notably vary they would not give accurate information, therefore they will not be reported.

4.3.1 Laser power stability and preliminary sheet resistance measurements.

Since the parameters that can be adjusted in the laser have a wide range of possible values the first experiments that were made during the present thesis were aimed to obtain a first approach and overview of the range of sheet resistances that could be obtained, as well as the range of parameters that would give decently stable power outputs. The wafers used in this experiment were saw damage etched in KOH by usual procedures but not textured.

In this experiment the doping process was made by first using a spray on system which used phosphorus pentoxide (P_2O_5) dissolved in alcohol in a 1:4 proportion as a doping source. The wafers where sprayed two times and then transported to a heating oven at 150 ^{o} C for 15 min. Next the wafers where transported to the laser chamber the laser doping process was performed. Afterthe laser doping the wafers were dipped in 5% HF bath during two minutes to remove the phosphorus glass. Finally the sheet resistance was measured by using a four point probe system.

The study of the parameters was carried out as follows: For a fixed value of the laser current the frequency was varied from values from 30kHz to 80 kHz in steps of ten. This was done for current values of 30, 32, 34, 35 and 36 Amps . The overlapping was set to 75%. In order to keep this value fixed for the different frequencies the scanning speed should be adjusted. This experiment was not very well designed because by varying the laser frequency while leaving the current fixed one is varying the rate at which the laser pulses hits the wafer and also at the same time the power of the laser, therefore two laser doping parameters are being varied. Also since the laser power is not stable and same values for current and frequency may give different power values at different times the power is not studied systematically with this method.

It is to note that not all the samples processed in this experiment presented good

29

readable sheet resistace values. This would happen in two different circumstances. One would be that the laser power and energy density is so high that silicon ablation would take place. This could easily be observed by eye inspection because the irradiated zone looked brilliant. The result of this would be that when trying to measure the sheet resistance R_{sh} the values given by the four point probe were not stable, giving enormously varying values for two different measurements. The second circumstance that would lead to non readable R_{sh} values, was that the laser power output was to unstable during the laser doping process. This could be in many cases easily observed by eye because a strong color gradient could be noticed in the irradiated area. This could also be observed if the power before and after the measurements would greatly differ, though that they don't differ would not always mean that the power during the process was stable, because during the measuring process the laser could stabilize it self again. In many cases both situations could be presented.

The results and parameters used in this experiment are shown in table 9 in appendix A.

Even though this experiment had some flaws it allowed us to draw some conclusions regarding the frequency and power of the laser, which helped us to design the future doping experiment's. First of all it was observed that the laser was very unstable for laser frequencies higher than 90 kHz, therefore this was established as the higher laser frequency limit to be used. Second it was observed that for laser configuration with energy densities higher than 10 J/cm^2 ablation would take place, however physical change in appearance would take place for much lower energy densities. Down to 4 J/cm^2 the wafer surface would become brilliant, indicating that laser damage was inflicted. In table 9 it can be seen that the lower sheet resistance that could be achieved was $14.1\Omega/\square$. Further increasing the laser energy density would increase dramatically the sheet resistance, thus showing that a severe damage in the crystal structure had taken place.

Regarding the laser frequency it was decided that a good range for looking for the frequency was between 45 kHz and 80 kHz, because for values below this range it could be easily seen that the wafer was ablated and for values above the laser output power was to unstable.

4.3.2 Second Doping experiment: Sheet resistance on laser doped wafers using POCl$_3$ diffusion as dopant source method.

In the second doping experiment the doping source was not deposited by means of an Spray on dopant system as in the first one, but instead a POCl$_3$ furnace diffusion system was used. The general method was to make a POCl$_3$ diffusion on the wafers, which would already incorporate some amount of dopant in the wafer and at the same time deposit a superficial phosphorus glass layer which could subsequently used as a dopant source. The heavily doped regions were formed by irradiating the wafers with the still present phosphorus glass layer with the Laser.

The experiments where done for two different recipes of the POCl$_3$ diffusion. One which gave the wafers an initial sheet resistances of around 60 $\Omega/\square$ and another 200

$\Omega/\square$ respectively. We will refer to them as the $R_{sh}200\Omega/\square$ and $R_{sh}60\Omega/\square$ samples respectively . For each one of these wafers we varied the frequency and power. The frequencies studied were 45, 50 and 55 kHz. For each one of these frequencies the laser power was varied from 1.5 W to 4.5 W in steps of around 0,5 W by varying the laser current. The values of the power cannot be set exactly to a desire value because the same current does not always give the same power. Therefore the power had to be varied manually by constantly measuring and doing a trial and error method. For each set of values the doping was performed on areas of squares with dimension 2.5cm X 2.5cm.

After performing the doping the sheet resistance was measured , the results are displayed in figure 9 and the laser parameters can be found in table 11 of appendix A.
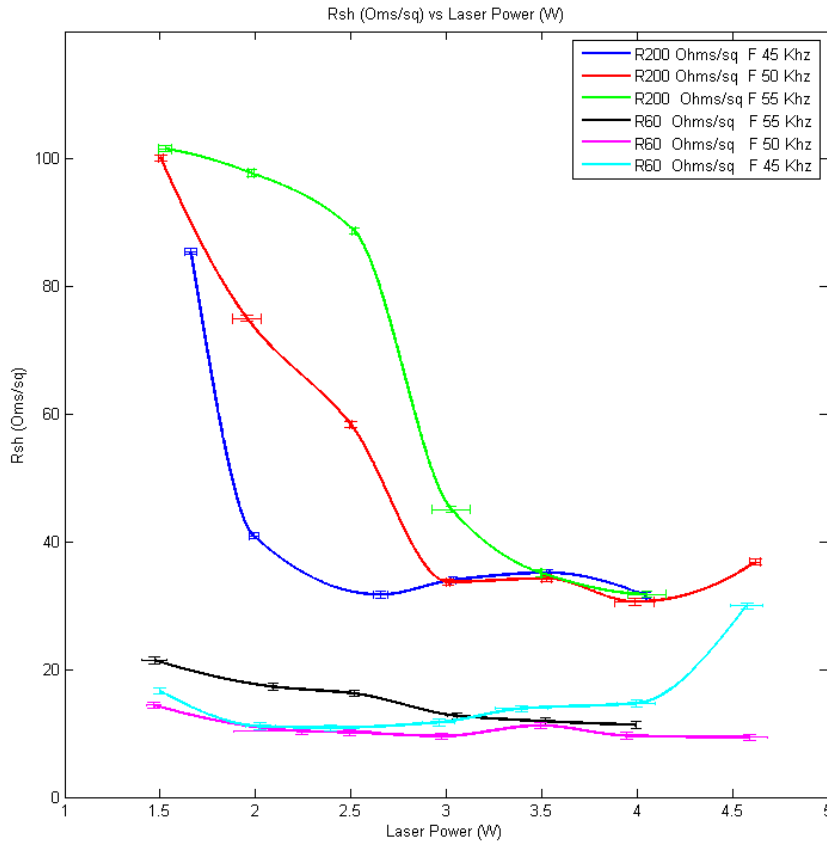
Figure 9: Sheet resistance vs Laser doping power for the various samples. The subscript R200 and R60 refers to the sheet resistance of the wafer after the POCL3 diffusion. The joining lines are only guides to the eye, the measured points are only where the error bars are.

In figure (9) it can be observed that the laser doping process indeed decreases considerably the sheet resistance of the irradiated wafer. In the $R_{sh}200\Omega/\square$ samples

it can be observed that first the sheet resistance decreases rapidly but at around 2.5W it does not decrease appreciably any more, at some points it does even increase. There are two possible explanations of why this could have happened.

The First one is the availability of dopant source. It could be that above 2.5W all the available doping phosphorus atoms diffused in the wafer thus no further lower sheet resistance could be attained.

The second explanation is that above certain energy density the front melt diffuses into the crystal much faster than the dopants do. This means that the doping process is limited by the atoms diffusion velocities. This was illustrated in Figure (6).

In table (11) it can be seen in the rows corresponding to the $R_{sh}200\Omega/\square$ samples that the samples made at 55 kHz and 50kHz laser frequency attain a first minimum sheet resistance at around $31\Omega/\square$ at a laser energy density of 7.34 J/cm^2 and 7.48 J/cm^2 respectively. The 45 kHz sample reaches this sheet resistance value at around 7.9 J/cm^2. Thus for a given overlapping percentage there is a laser energy density threshold, in which further increase in the laser energy density does not decrease considerably the sheet resistance but instead will inflict damage to the wafer. Probably the reason why this energy density limit differs between the different laser frequency samples is that the laser pulse duration varies with frequency as seen in subsection (4.2).
Thus since for higher frequency the laser pulse duration is longer, the laser doped samples done at higher laser frequency reach the maximum energy limit at lower energy. More on this will be explained later. In the simulations done by Toshiyuki and Setsuo [43] (figure 6) the energy density threshold is at around 0.6 J/cm^2 which is much lower than our case, but this is because this simulation is for a single pulse, whereas in our case we had a pulse overlapping of 75%.

Thus what happens, is that at certain point in the wafer when the first pulse hits the wafer some amount of dopant atoms diffuses into a certain depth limited by the diffusion velocity of the phosphorus atoms, then the next nearby pulse diffuses this atoms further more and so on with the following pulses. But since the pulse overlapping is not 100%, eventually the pulse is too far away to cause any melting and no more diffusion occurs. Obviously if the pulse overlapping was 100% the dopant atoms could reach the maximum melting depth of the pulse, but since it is not, the dopant atoms do not reach the maximum melting depth. This can be deduced by looking at figure (5), there we can see that the maximum melting depths are about 0.5 μm whereas as will later see in the SIMS experiments the doping depth don't exceed 250 nm. For this reason increasing the energy density beyond the mentioned threshold does not increase the doping level.
Therefore if one wants to increase the doping level in this case, what should be done is to increase the pulse overlapping percentage and maybe the dopant source. The fact that increasing the energy density increases also the melting to the sides of the irradiated regions was not mentioned because again as can be seen in figure (5), the changes in energy produce increase in the melting depth in amounts of the order of

$0.1\mu m$ while the laser diameter is around $20\mu m$, thus all doping is assumed to happen only under the irradiated areas.

In figure (9) it can be seen that the 60 $R_{sh}\Omega/\square$ samples attained a lower sheet resistance after laser doping than the $R_{sh}200\Omega/\square$. This probably means that the minimum sheet resistance in this experiment was limited by the atoms diffusion velocity rather than the amount of dopant source available, otherwise the $60\Omega/\square$ and $200\Omega/\square$ samples would have reached similar minimum sheet resistances.

4.3.3 Emitter sheet resistance simulation and Elaboration

The central idea of the selective emitter solar cell is to have a lowly doped front surface with highly doped regions underneath the metal contacts. This decreases the emitter recombination and enhances transport through the metal contacts. Nevertheless since the solar cell is composed of a PN structure it is clear that some level of doping should be maintained in the emitter in order to maintain a reasonable open circuit voltage. Therefore in order to determine an optimal doping concentration of the emitter a quick PC1D simulation was performed.

The idea of the simulation was to determine the variation of the efficiency of the cell as function of the emitter sheet resistance, while leaving the front surface contact resistance constant. For doing so we varied the junction depth and by this we controlled the sheet resistance.. We used as ground cell parameters the ones used for the baseline manufacturing of the IFE institute. The parameters are shown in table 13 of appendix A.

In figure 10 the resulting cell efficiencies is plotted as function of the emitter's sheet resistance. It can be observed that after $100\Omega/\square$ the efficiency gained by increasing the sheet resistance does not increase considerably. This means that the increase in the efficiency due to the increase in blue response has some kind of asymptotic value. Therefore it was considered that an optimal sheet resistance for the emitter of our selective emitter solar cell would be between $115\Omega/\square$ and $120\Omega/\square$.
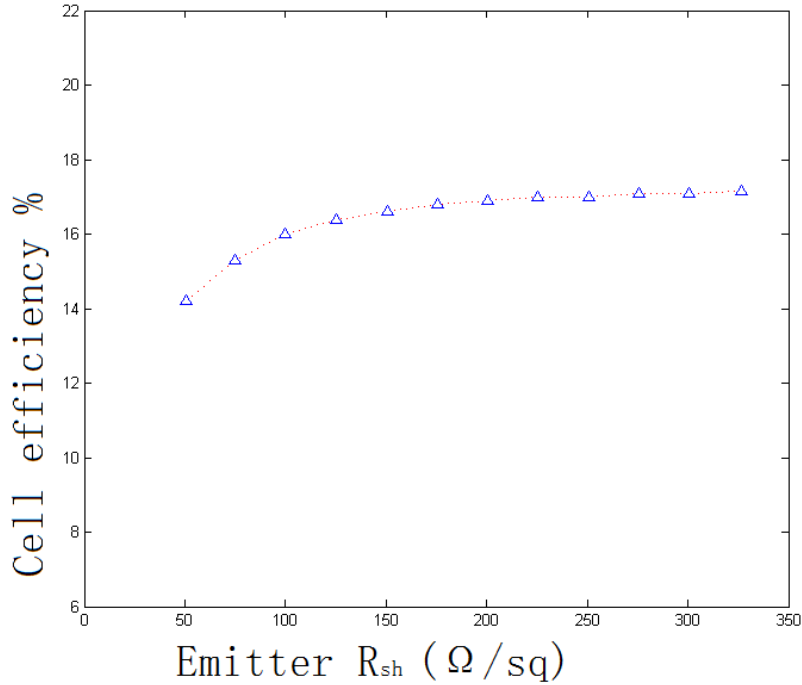
Figure 10: Simulated total cell efficiency vs emitter sheet resistance.

Having decided the optimal sheet resistance for the emitter it was necessary to develop a recipe for the POCl3 diffusion process that would give us this value, thus various recipes were tried in the $POCl_3$ furnace. Before every $POCl_3$ diffusion was made, usual 2 minuted 5% HF cleaning and spin drying procedures were carried out. The main parameters that were varied are the deposition time, drive in time, drive in temperature and nitrogen flow. After the POCl3 diffusion the sheet resistance of the wafers was measured using the four point probe method over 13 different points along the wafer. In table 1 the average sheet resistance toked over t 13 points of the wafer and its standard deviation are shown for each one of the diffusion experiments. It is observed that recipe number 7, which is low temperature, has a sheet resistance value in the desired range with a low standard deviation, which means a good homogeneity. It was decided that this recipe was going to be used in the elaboration of the selective emitter. Therefore the following laser doping experiments were performed using wafers that were $POCl_3$ diffused using this recipe.

Table 1: POCl$_3$ diffusion experiment parameters.Recipe number 7 was decided to be the appropriate one to elaborate the selective emitter.

Recipe	Deposition (min)	Drive in (min)	Nitrogen flow (SLM)	Drive in Temperature ^{o}C	empty slots between wafers	R_{sh} average $(\Omega/\square)$	R_{sh} STD $(\Omega/\square)$
1	15	42	10	837	1	81	8,1
2	12	35	10	837	1	138,9	20,48
3	13	34	10	837	2	74,7	5,24
4	10	37	10	837	2	122,9	9,05
5	13	34	13	837	2	152	8,37
6	12	28	10	815	2	98	1,57
7	12	28	10	806	2	116,6	0,47

4.3.4 Sheet resistance on textured wafers.

Having developed a recipe for the POCl$_3$ diffusion, we used it to elaborate the following doping experiment in which we measured the sheet resistance for samples made at different laser doping parameters .It was made on textured wafers because when elaborating the selective emitter solar cells it will be done on this kind of wafers. This time the pulse overlapping percentage was set to 80%, whereas the laser frequency was set to 65, 75 and 85 kHz. For each one of these frequencies the laser power output was also varied from about $2W$ to $0.5W$. In table 14 of appendix A the exact parameter values are presented. The laser doping was performed on textured samples that were POCl$_3$ diffused with the previously developed formula. In figures 11a and 11b the resulting sheet resistance values are plotted in function of the laser output power and laser energy density respectively.
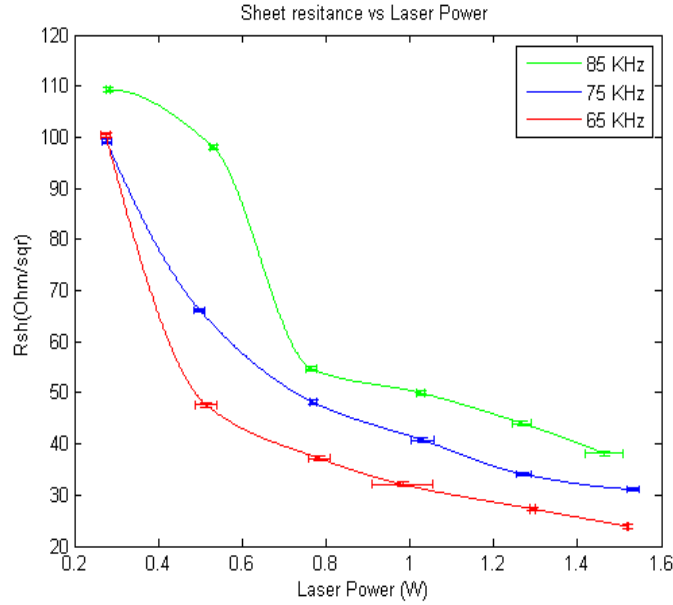
(a) Sheet resistance Vs Laser output power for various laser frequencies. Measured points only where error bars are present
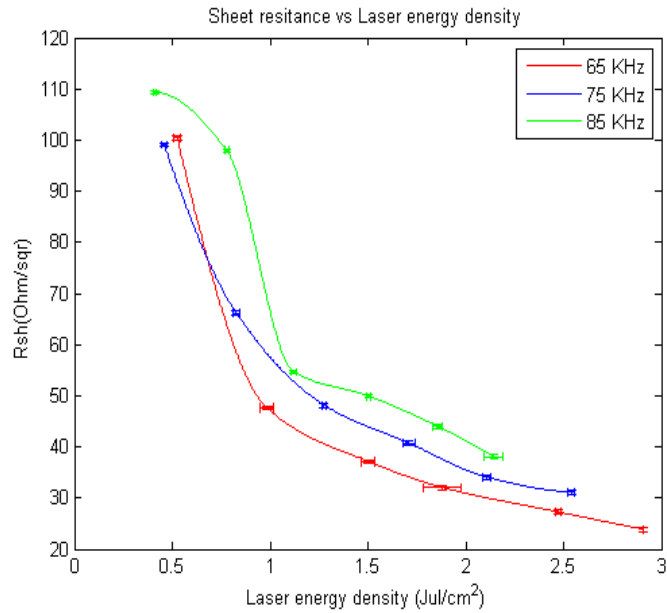
(b) Sheet resistance Vs Laser energy density for various laser frequencies. Measured points only where error bars are present

It is observed in figure 11a that with the new $POCl_3$ recipe sheet resistances below 35 $\Omega/\square$ are easily attainable. Visually the samples with sheet resistances above 40 $\Omega/\square$ look quite acceptable, not burned at all. As it was expected increasing the laser power decreased the sheet resistance. In figure 11a it can also be seen that samples made at similar laser power but lower laser repetition frequency present lower sheet resistance. This is because at same power output but lower repetition frequency each laser pulse has higher energy.

What was not completely expected is what is observed in figure 11b, that is that samples that were made at similar laser energy densities but higher laser frequency presented higher sheet resistances. This has to do with the fact that two pulses that have the same energy density but were made at different repetition frequencies have different pulse shapes.

As we saw in section 4.2 when the laser is set at a lower repetition frequency the output light pulse has a longer duration but a smaller peak fluence. This has as consequence that for lower repetition frequencies the substrate melting time is longer but the melting depth is shallower. Later on after the results for the SIMS measurements are presented we will give a deeper explanation on this.

In addition to this experiment on textured wafers also some similar experiments were carried out on flat surface ones. The results were quite similar only that the laser power outputs had to be sligthly higher, because of the increased reflectivity.

4.4 Laser induced damage quantification by means of surface roughness.

The idea of the following experiment was to obtain a more quantitative idea of the damage done by the laser on the irradiated crystal area, this was done by measuring the surface roughness after the laser doping.

Two experiments were made which involved surface roughness measurements. One in which we investigated the effect of varying the laser repetition frequency on the surface roughness and other in which we investigated the effect of varying the laser power. Both experiments were done on untextured wafers which had been $POCl_3$ diffused using the chosen recipe 7 developed in the last section. In both experiments the samples were dipped in HF bath after the laser doping in order to remove the $POCl_3$ glass layer.

In our first experiment we wanted to study the damage caused by the laser irradiation over the wafer for various laser repetition frequencies . In order to do so we prepared samples with R_{sh} values on the range of 43-45 ($\Omega/\square$). The parameter varied to obtain the desired samples was the laser diode current which in turn controls the laser power output. Elaborating this samples required at some extent some trial and error tests, but since we had already accumulated some knowledge in the laser doping technique it was not difficult to obtain the desired R_{sh} values. The reason why we choose this range of R_{sh} values was that this was the determined desired value for the substrate region below the front metal contacts in our selective emitter solar cell (see section 5).

The doping parameters can be observed in table 15 of appendix A. In figure 11 the resulting average roughness was plotted for each of the different laser doping frequency samples. In this graph it can be clearly observed that the surface roughness decreases with the laser repetition frequency.
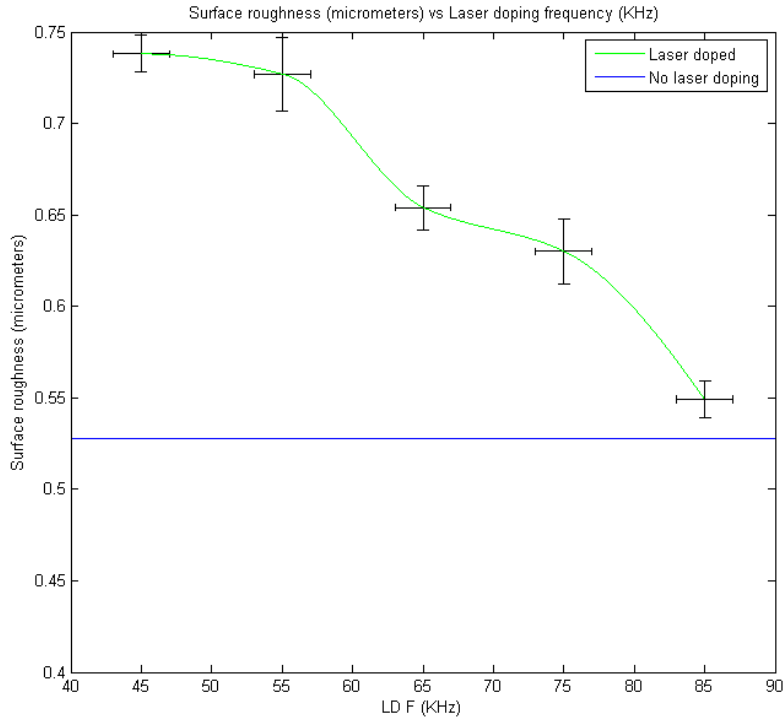
Figure 11: Wafer roughens measured by the root mean squared depth variation method, for 45 $\Omega/\square$ samples prepared at 45, 55, 65 ,75 and 85 kHz laser repetition frequency. Measured points only where the error bars are.

In table 15 it can be seen that not all the samples were prepared using the same energy density, but the ones done at higher laser frequency required higher energy density. The reason why higher energy density and laser repetition frequency implies less surface roughness is that this conditions produce a higher melting time and smaller recrystallization velocities, thus giving the atoms more time to epitaxially recrystallize. Later on after the results for the SIMS experiment are present an hypothesis of why this happens will be presented.

In the second experiment the laser output power was varied while keeping the laser repetition frequency fixed at 65 kHz and the overlapping percentage at 80%. The laser power output was varied in steps of about $0.25W$. The laser parameters as well as the experiment results are resumed in table 17.

In figure 12 the average surface roughness is plot in function of the laser output power. In this figure it can be observed that the surface roughness increases with the laser power and since the laser frequency is fixed it also increases with the laser energy density. This may seem contradictory with the last experiment were we concluded that higher energy density gave better surface uniformity. But the reason why this happens is that in the last experiment the energy was varied by varying both laser repetition frequency and laser output power whereas in this experiment we were only varying the laser output power.

38
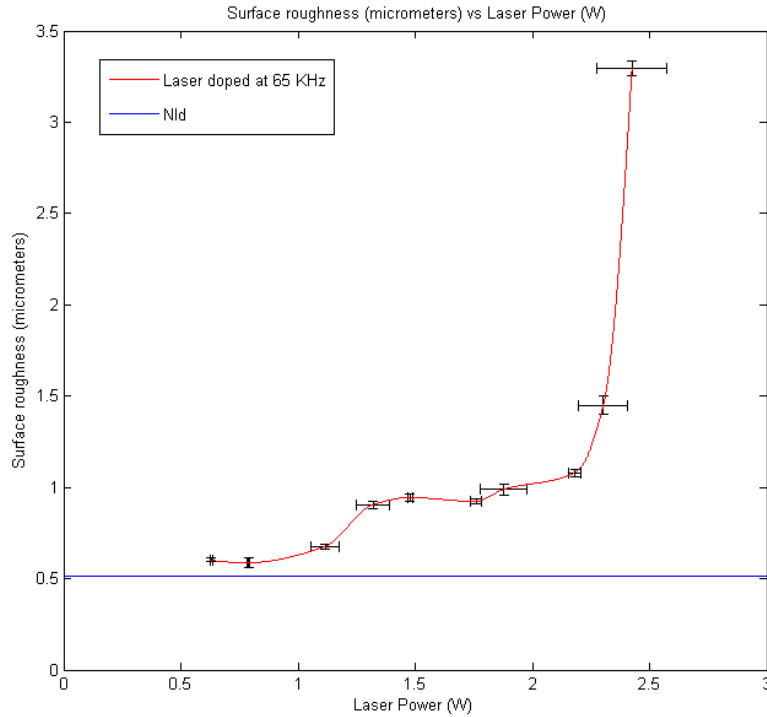
Figure 12: Wafer roughness measured by the root mean squared depth variation method vs Laser power output. Measured points only where the error bars are.

As it was mentioned on section 4.2, the effect that varying the laser output power with fixed repetition frequency has on the pulse shape, is that higher power gives higher peak fluences and decreasing laser pulse duration. The net effect that increasing the energy on the second experiment had on the irradiated area was to increase the melted volume while in the first experiment the effect was to increase the melting time. Thus in the second experiment with increased energy recrystallization velocities should have been higher therefore giving more rough areas. In figure 12 it can also be observed that for laser powers higher than $2W$ the roughness increases dramatically which means that probably ablation is taking place.

4.4.1 Secondary ion mass spectrometry analysis

In the next experiment laser doped samples were prepared for SIMS analysis. This time we used 4 inch polished wafers, which were initially boron doped with resistivity in the range $0.5 - 3\Omega \cdot cm$. The wafers were first POCl$_3$ diffused using initially boron doped the $115\Omega/\square$ recipe developed in section 4.3.3 . In this experiment we wanted to compare the doping concentration profiles for samples made at different laser repetition frequencies and different powers. In table 2 the parameters used in the laser doping process are displayed.

Table 2: Laser doping parameters used in SIMS experiment.

					Overlapping =80%
Sample	I(A)	P(W) average	Laser Frequency (kHz)	Energy density (J/cm^2)	R$_{sh}$($\Omega/\square$)
t0	0	0	0	0	105
t1	29,8	1,19	65	2.27	37,0
t2	29,2	0,93	65	1.77	44,4
t3	28,6	0,70	65	1.34	60,5
t4	26,6	1,65	75	2.73	35,3
t5	30,2	1,39	75	2.30	38,8
t6	29,8	1,19	75	1.98	51,4
t7	30	0,90	75	1.49	59,6
t8	31,6	1,40	85	2.04	68,8
t9	32,2	1,22	85	1.78	44,4
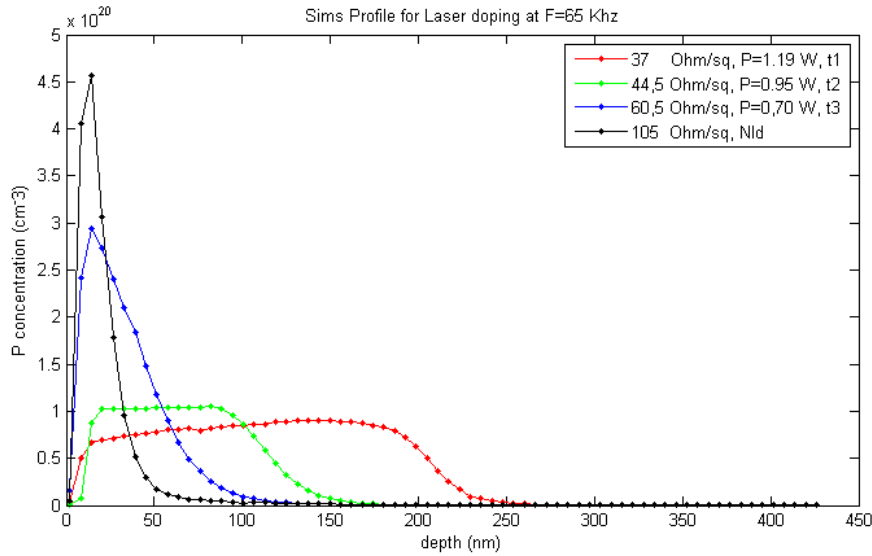
Figure 13: SIMS profiles for laser doped samples prepared at laser frequency of 65 kHz. The black curve represents the non laser doped sample.
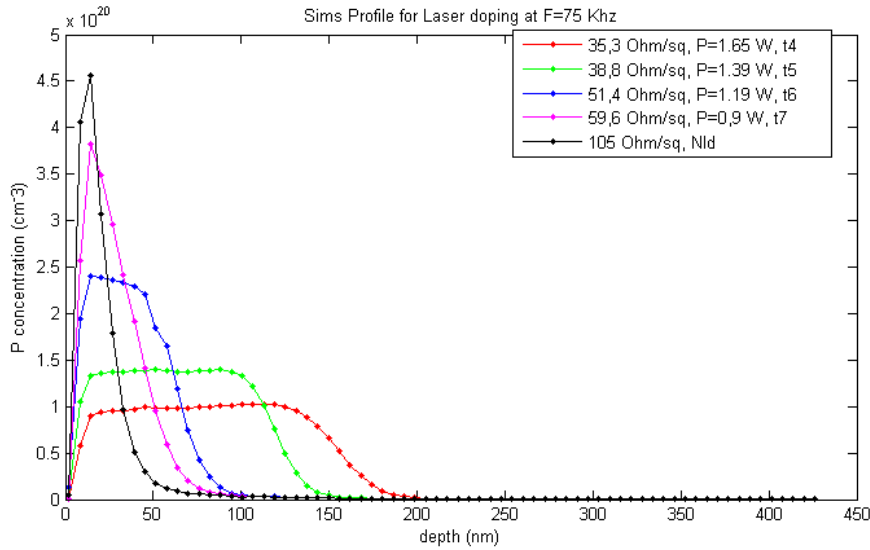
Figure 14: SIMS profiles for laser doped samples prepared at laser frequency of 75 kHz.The black curve represents the non laser doped sample.
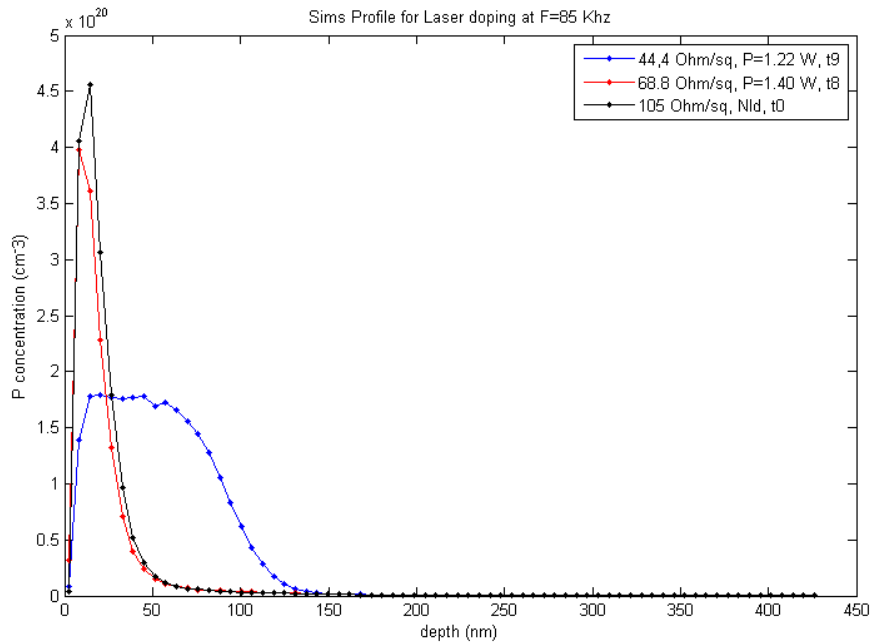
Figure 15: SIMS profiles for laser doped samples prepared at laser frequency of 85 kHz. The black curve represents the non laser doped sample.

In figure 13, 14 and 15 the profiles for samples made at same frequency but different powers are displayed in each graph. It can be observed that initially the sample that was POCl3 diffused but not irradiated with laser energy had a very high but also very shallow phosphorus atom concentration. Then as was expected

increasing the laser Power increases the amount of dopant atoms that diffuses into the silicon substrate. This is so because increasing laser power increases laser energy density which means that more volume of the substrate will be melted.
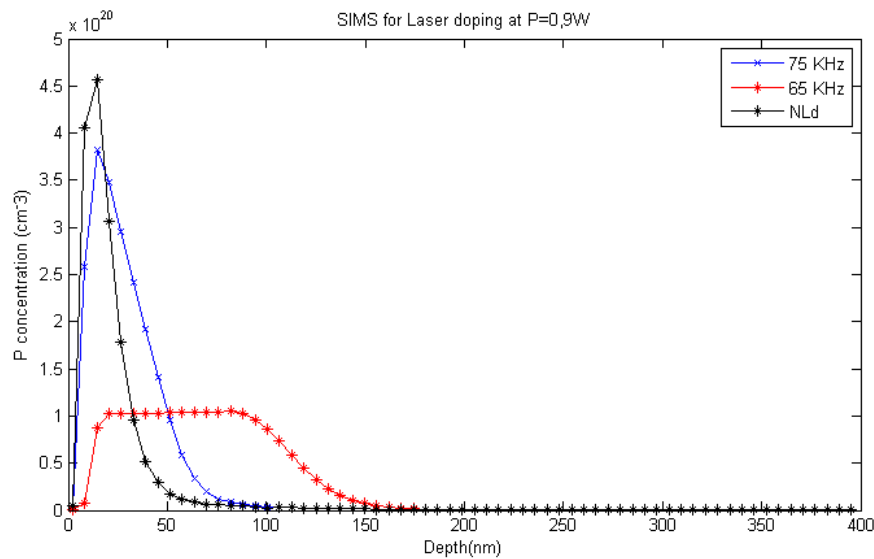
Figure 16: SIMS profiles for laser doped samples prepared at laser power around $0.9W$. See table 2 , samples t2 and t9 for exact data
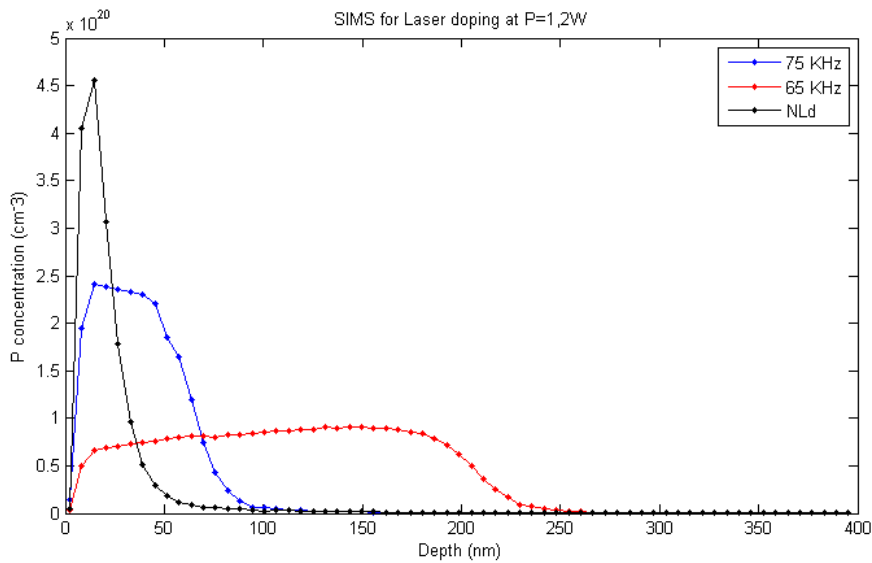
Figure 17: SIMS profiles for laser doped samples prepared at laser power around $1.2W$. See table 2 , samples t1 and t6,for exact data

In order to study the effect of the laser repetition frequency on the doping profiles we plot in figures 16 and 17 the SIMS profiles of different samples prepared at differ-

ent laser frequencies but with similar laser output power. In figure 16 for $P_l = 0.9W$ and in figure 17 for P_l=1.2 W. It can be seen in both of this figures that the samples prepared at lower laser frequency have deeper diffusion profiles. This was also expected because by having the same laser power output and decreasing the frequency by 10 kHz one is considerably increasing the irradiation laser energy density.
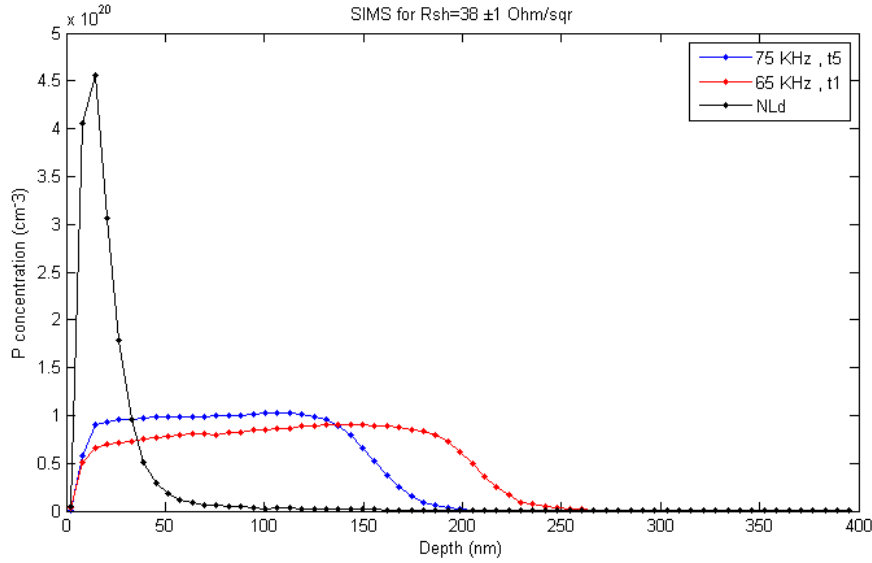
Figure 18: SIMS profiles for laser doped samples prepared at different laser frequencies but which gave similar R_{sh} of about $38\Omega/\square$. See table 2 for exact data
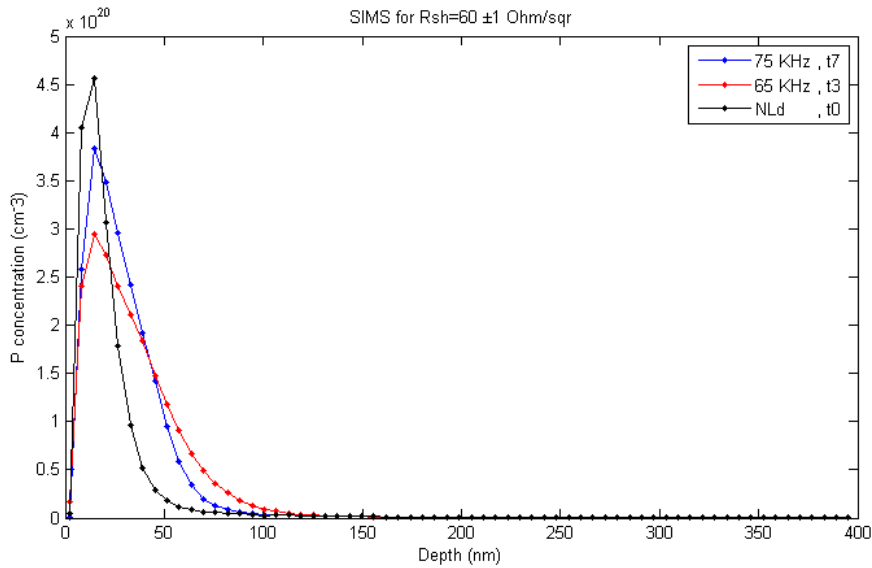
Figure 19: SIMS profiles for laser doped samples prepared at different laser frequencies but which gave similar R_{sh} of about $60\Omega/\square$

Also we wanted to compare samples which had similar sheet resistance but which were made at different laser frequency repetitions. Therefore in figures 18 and 19 we plot the SIMS profiles for samples prepared at different frequencies of 65 kHz and 75kHz but which presented similar sheet resistance values. It can be observed that in the samples made at 65 kHz the dopant atoms diffused deeper than in the sample made at 75 kHz. If you look at table 2 you can notice that sample t5 has slighter bigger energy than sample t1 , but the dopants in t5 diffused less depth. Similar situation happens with samples t7 and t3. Therefore it is clear that samples made at higher laser frequency present more shallow dopant concentration profiles. Again this has to do with the fact that the high frequency laser pulses have longer duration but smaller peak fluence.

4.5 Lifetime Measurements.

In the following experiment we wanted to study the degradation of the crystal's quality due to laser irradiation by means of lifetimes measurements. As we have already seen, lifetimes measurement is a technique that provides accurate information about the quality of a semiconductor material, because the minority carriers lifetime is inversely proportional to the amount of defects present in the material. Therefore the purpose of the following experiment is to compare the reduction of the minority carriers lifetimes in laser irradiated samples.

For this experiment various nontextured wafers were POCl$_3$ diffused using the usual $115\Omega/\square$ recipe. Some of these wafers were laser doped using different laser parameters. The laser doping was performed on $3cm \times 3cm$ squares on both sides of the wafer to form a symmetrical structure. Two wafers were not laser doped but were left as references . After the laser doping all wafers were passivated in the PECVD machine with amorphous silicon, at a deposition temperature of 230 ^oC during 5 minutes. After the passivation, the lifetimes were measured for different injection rates by means of the PL imaging machine.

In table 3 the parameters for each one of the samples used in the Passivation experiment are shown. In the first Column the name of each sample is displayed. s1, s2 and s4 are the three different wafers which were laser doped, s1 and s2 were doped using a laser frequency of 65 kHz and s4 laser frequency of 75 kHz. They in turned had 4 different squares which were irradiated by different laser powers going from about 1.25 W to 0.5 W. The laser power was measured before and after the laser doping , column 2 displays the average power. The samples called POCl3-1,2 are the ones that were POCL3 diffused but were not laser doped. The samples called Clear-1,2 were clear samples that were not diffused only passivated.

Column 4 displays the average laser energy density.Column 5 displays the sheet resistance of each sample measured by the four point probe method. In column 6 the lifetime at an injection level of $\Delta n = 2 \cdot 10^{15} cm^{-3}$ are displayed. In column 7 we compared the decrease in lifetime of the laser doped samples with the average lifetime of the two POCl$_3$ samples. Column 8 shows the measured inverse saturation current values of which will talk again later.

Table 3: Laser parameters for lifetimes measurement experiment.

Sample	P(W) average	Laser Frequency (kHz)	Laser Energy density (J/cm^2)	R($\Omega/\square$)	τ (s) at $\Delta n = 2 \cdot 10^{15} cm^{-3}$	lifetime % decrease (compared to POCL3 wafers)	J_{0e} (mA/cm^2)
s1-t1	1.26	65	2,42	31.4	9.34E-05	46.8	4.03E-13
s1-t2	1.09	65	2,09	35.4	8.58E-05	51.1	3.43E-13
s1-t3	0.76	65	1,46	48.06	1.01E-04	42.4	3.11E-13
s1-t4	0.57	65	1,08	60.64	1.30E-04	25.9	2.80E-13
s2-t1	1.23	65	2,35	31,45	1.12E-04	36.2	4.04E-13
s2-t2	1.01	65	1,93	38.2	8.55E-05	51.3	3.83E-13
s2-t3	0.71	65	1,36	49.73	1.22E-04	30.5	3.10E-13
s2-t4	0.53	65	1,02	70.26	1.54E-04	12.3	2.87E-13
s4-t1	1.61	75	2,67	34.85	1.00E-04	43.0	3.08E-13
s4-t2	1.17	75	1,94	47.13	1.15E-04	34.5	2.70E-13
s4-t3	1.00	75	1,66	59.1	1.45E-04	17.4	2.22E-13
s4-t4	0.77	75	1,28	101.2	1.67E-04	4.8	2,03E-13
POCl3-1	0	0	0,00	114	1.75E-04	0.3	1.79E-13
POCl3-2	0	0	0,00	115	1.76E-04	-0.3	1.95E-13
Clear-1	0		0,00	260	2.34E-04	-33.3	
Clear-2	0		0,00	260	2.01E-04	-14.5	
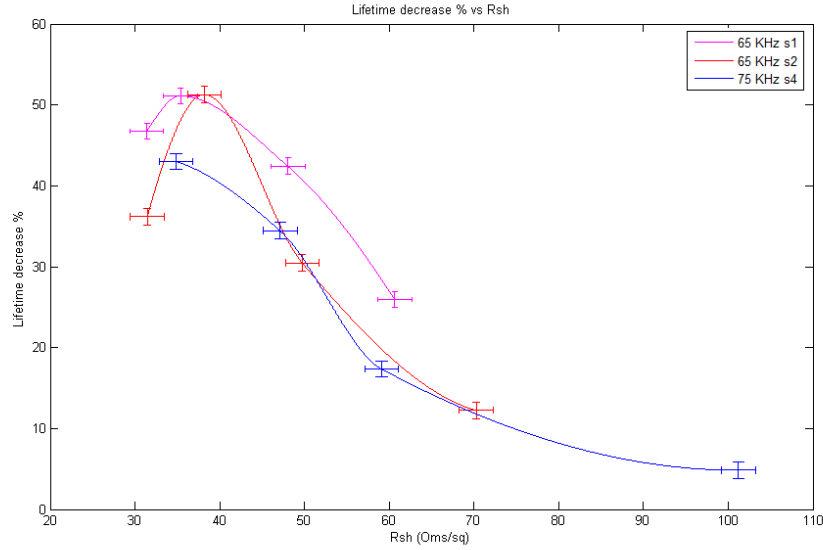
Figure 20: Lifetimes % decrease compared to non LD samples vs sheet resistance. s1,s2 and s4 samples plotted see 3 for parameters.

In figure 20 the lifetimes percentage reduction for each sample is plotted vs its sheet resistance value. It can be observed that in general the lifetimes decreased less for the samples prepared at laser frequencies of 75 kHz than for the ones at 65 kHz. It can also be seen that increasing the laser power decreases the minority carrier lifetimes, except for the samples at around $30\Omega/\square$ where we can see that there is an unexpected increase in lifetime compared to the ones at around $40\Omega/\square$, but in briefly we will see that this anomality was because an specific irregularity on the wafer.

Figure 21: Lifetimes vs injection level for samples prepared at laser frequency of 65kHz and different laser powers. See table 3 for laser parameters

Figure 22: Lifetimes vs injection level for samples prepared at laser frequency of 65kHz and different laser powers. See table 3 for laser parameters
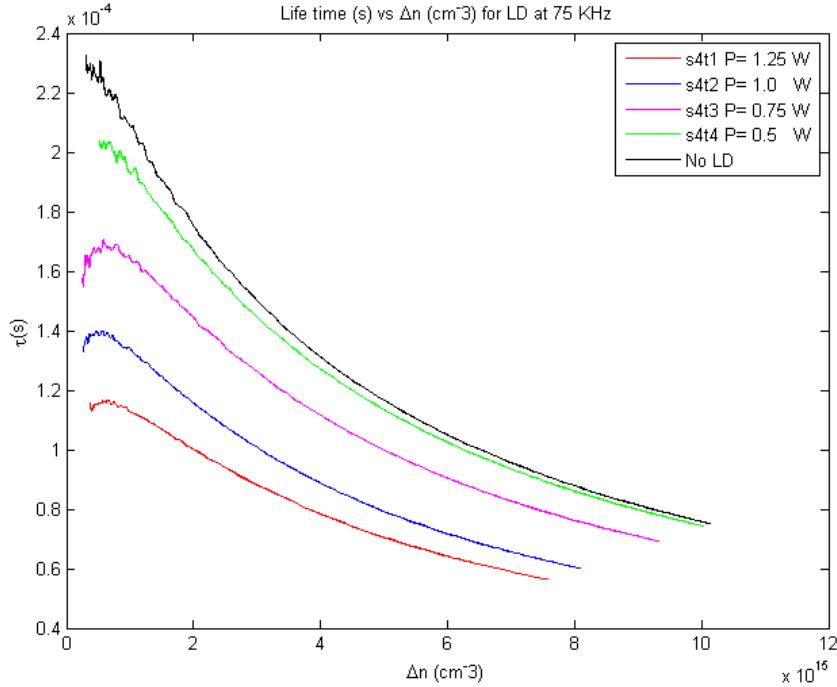
Figure 23: Lifetimes vs injection level for samples prepared at laser frequency of 75kHz and different laser powers. See table 3 for laser parameters

In figures 21 and 22 and 23 the $\tau(s)$ vs Δn curves are plotted for each wafer. Figures 21 and 22 correspond to the samples doped at 65 kHz laser frequency. There it can be observed that the samples made at laser power around 1.25 W present better lifetimes than the ones made at 1.0 W. This could have happen for two reasons:
The first is that indeed the damage caused by the laser at 1.25 W was smaller than the one caused at 1.0 W.
The second is that the wafers on which the experiment was performed had a nonuniformity in the passivation quality thus giving better lifetimes for a certain region. In order to investigate this in figures 24a and 24b we plot a lifetime mapping of the wafer for both the samples that were POCL$_3$ diffused . In figure 24a it can be seen that in the left upper corner there is a unusual high lifetime spot, which is not present in 24b. This explains why we had such high lifetime values in the s1t1 and s2t1 samples of table 3. This nonuniformity in lifetimes probably was caused by some unknown factor during the passivation process. Since in the second POCl$_3$ sample this nonuniformity is not observed we can conclude that this was not present in all samples and that is why in the samples made at $75kHz$ not unexpected behavior was present. Comparing the two samples it can also be seen that besides the anomaly, spot the rest of the wafer of figure 24a is quite uniform, so the results are still valid.

48
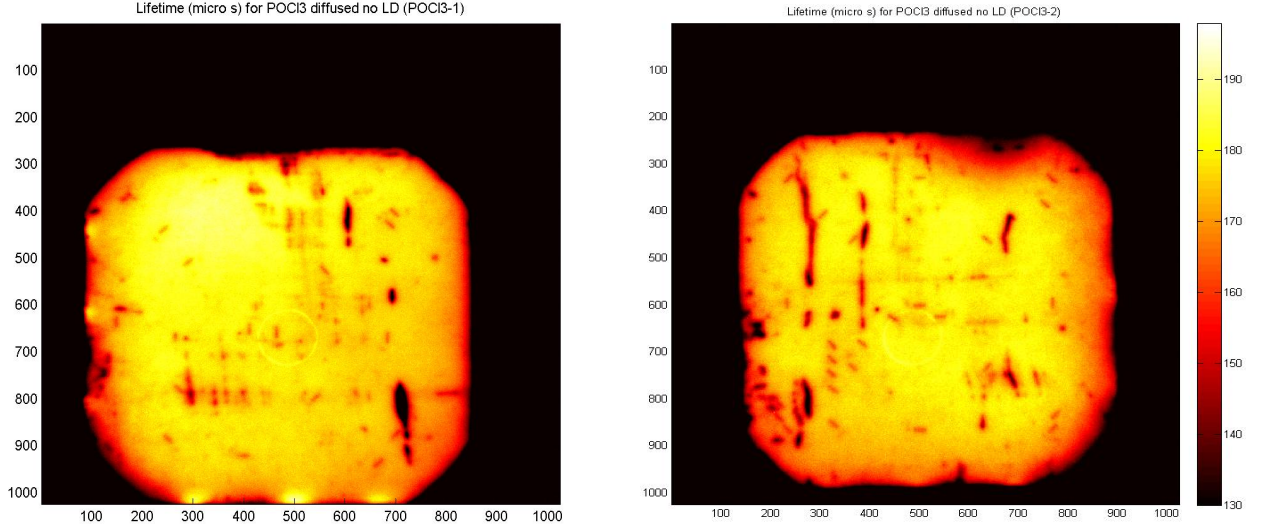
(a) POCL3-1.Sample.

(b) POCL3-2.Sample .

Figure 24: Lifetime mapping for POCl$_3$ diffused wafers without Laser doping at injection level of around $1.9 \times 10^{15} cm^{-3}$

Table 4: Laser parameters for second lifetime measurement experiment.

Sample	P(W) average	Laser Frequency (kHz)	Laser Energy density (J/cm^2)	R($\Omega/\square$)	τ (s) at $\Delta n = 2 \cdot 10^{15} cm^{-3}$	lifetime % decrease (compared to POCL3 wafers)	J_{0e} (mA/cm^2)
s5t1	1.22	65	2.34	32.35	7.07E-05	59.9	4.11E-13
s5t2	1.04	65	1.98	38.3	8.41E-05	52.4	3.56E-13
s5t3	0.75	65	1.43	49.1	9.77E-05	44.7	3.02E-13
s5t4	0.53	65	1.01	61.4	1.21E-04	31.5	1.93E-13
s5nl1	0.00	0	0.00	114	1.71E-04	2.9	1.76E-13
s5nl2	0.00	0	0.00	115	1.82E-04	-3.1	1.56E-13

Nevertheless we decided to repeat the laser doping experiment for the sample made at $65kHz$.The procedure was the same as before, the doping parameters are shown in table 4. The samples referred as s5nl1 and s5nl2 are the reference samples that were POCl3 diffused and passivated but with no laser doping process . The resulting lifetimes vs injection level curves are show in 25. In this figure it can be observed that the lifetime decreases with increasing laser power and the phenomenon observed before is not present.
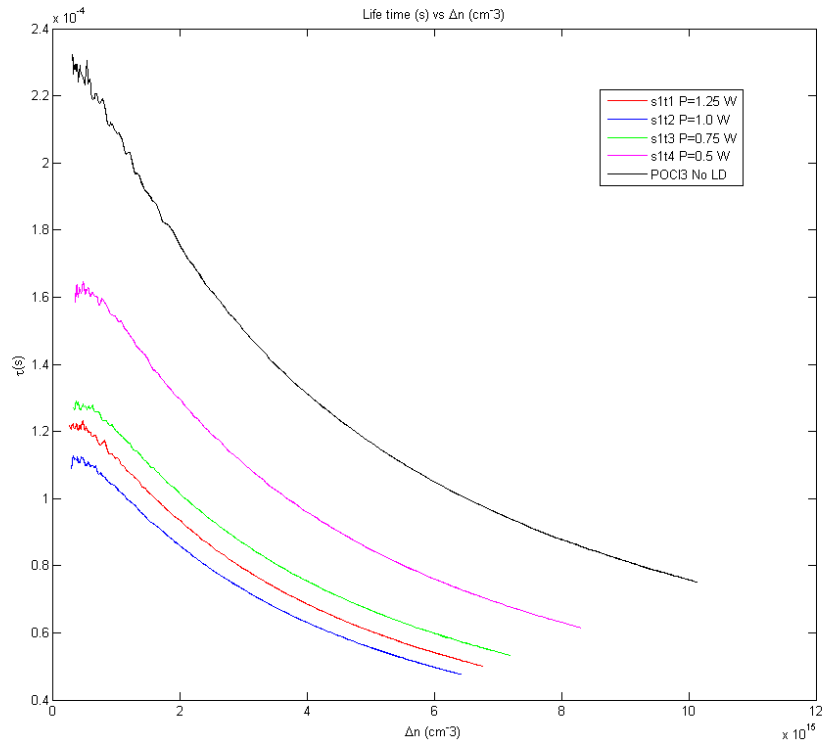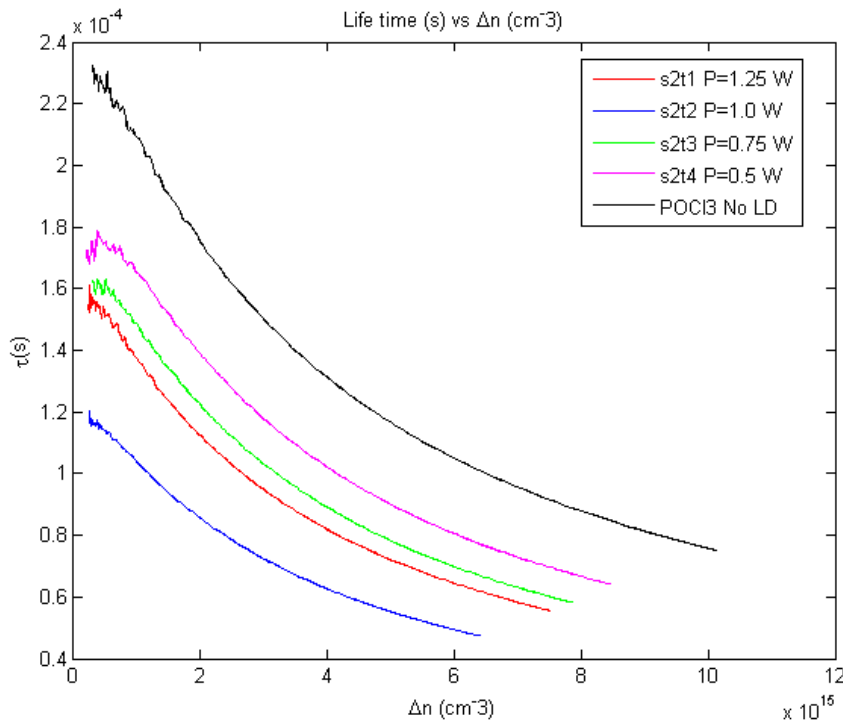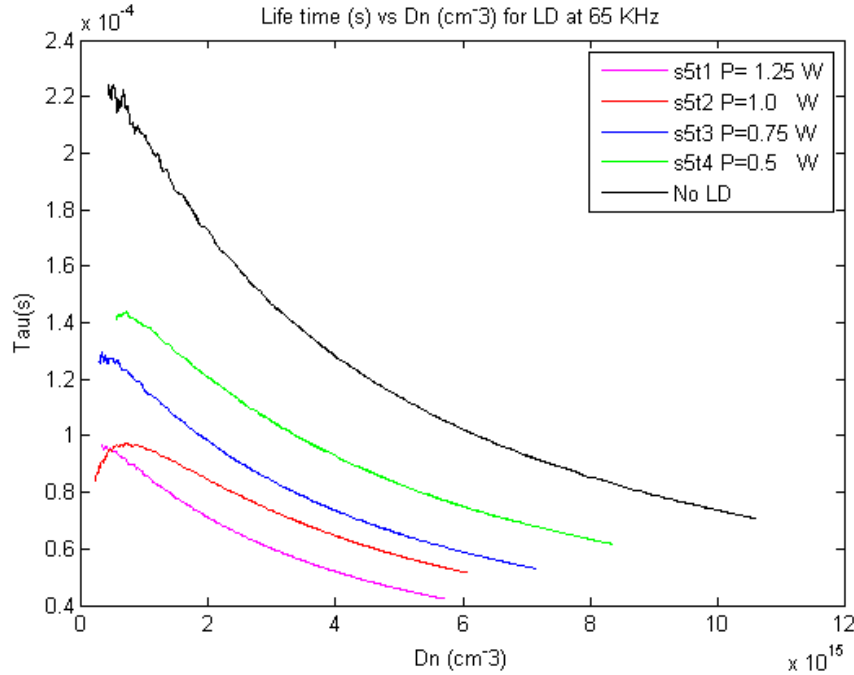
Figure 25: Lifetimes vs injection level for samples prepared at laser frequency of 65kHz and different laser powers. See table 3 for laser parameters.

In figure 26 we plot again the lifetime % decrease compared to non LD samples. It can again be observed that the samples made at 65 kHz laser frequency were more damaged by the laser doping process than the ones made at 75 kHz. In order to visualize the effect that laser frequency has on the minority carriers lifetimes, we plot in figures and the lifetime vs injection level curves for samples that have similar sheet resistance but which were laser doped at different laser frequencies.

Figure 27a correspond to samples with $R_{sh} = 35 \pm 0.5\Omega/\square$ whereas Figure 27b correspond to samples with $R_{sh} = 60 \pm 1\Omega/\square$. It is clear in both figures that the samples made at 65 kHz present lower lifetimes for all injection levels, even though they were made at lower laser pulse energy density (see table 3). Therefore the results obtained in section 4.4 are confirmed: Laser doped samples made at higher laser frequencies present less crystal degradation than the ones made at lower laser frequency. In the elaboration of our selective emitter solar cell we are interested in having a R_{sh} value of around $R_{sh} = 43\Omega/\square$ for the highly lased doped regions.

In figure 26 it can be seen that for the samples made at 65 kHz we would get a lifetime degradation compared to the non laser doped samples of around 55% at R_{sh} values near the desire one whereas for the sample made at 75 kHz we get a 45% lifetime degradation. Taking into account that the non laser doped sample has $R_{sh} = 115\Omega/\square$ and that the recombination lifetime is inversely proportional to the concentration of dopant atoms we conclude that the lifetime degradation obtained is quite acceptable for the choosen laser parameters, thus they should be suitable for the elaboration of

the selective emitter solar cell.
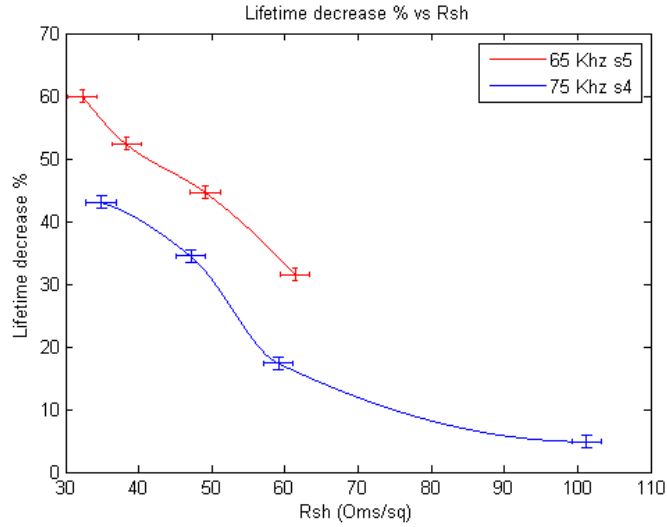
Figure 26: Lifetimes % decrease compared to non LD samples vs sheet resistance for samples at laser frequencies 65 kHz and 75 kHz. See table 4 for laser parameters.
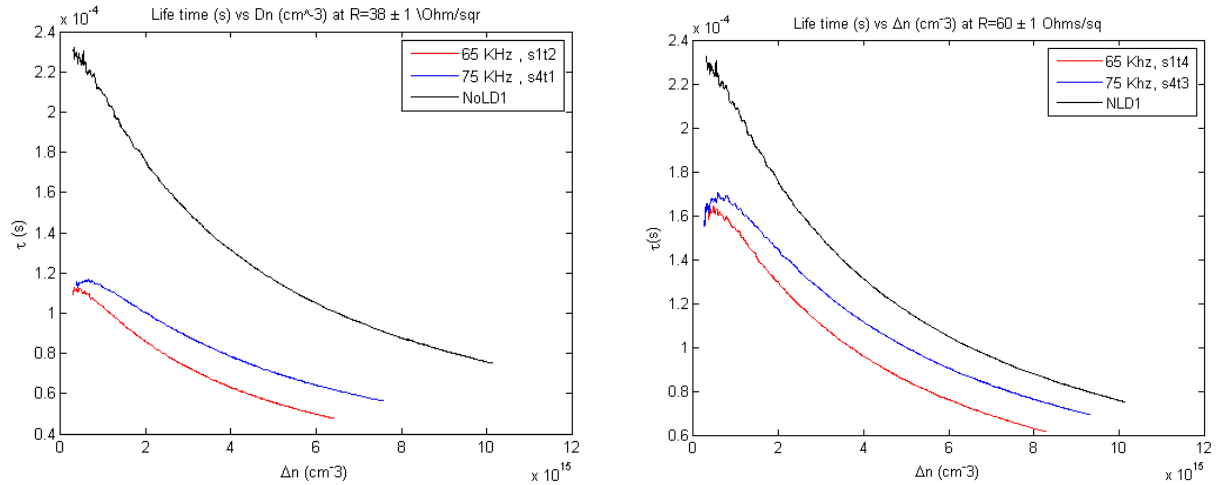
(a) Samples with $R_{sh} = 35 \pm 0.5\Omega/\square$.

(b) Samples with $R_{sh} = 60 \pm 1\Omega/\square$.

Figure 27: τ (s) vs Δn for samples with similar R$_{sh}$ but irradiated at different laser frequencies of 65KHZ and 75KHZ .

4.6   Saturated emitter current.

Another quantity that can be measured using the elaborated double sided laser doped symmetrical structure is the saturation current. As we saw in section 3.2.4 the saturation current J_{0e} is a very appropriate quantity to study the crystal quality in highly doped samples, because it measures the amount of recombination that is taking place in the regions close to the wafer surfaces .In the last columns of tables 3 and 4 the

51

measured J_{0e} values for each of the samples is displayed.

The first thing to note in tables 3 and 4 is that eventhough samples s1t1 and s2t1 present unusual high lifetimes, their J_{0e} value is similar to the s5t1 one. This confirms that the damage done on the surface by laser irradiation is similar and that the high lifetimes values observed for the s1t1 and s2t1 samples were caused by some anomaly in the wafer or in the passivation process.
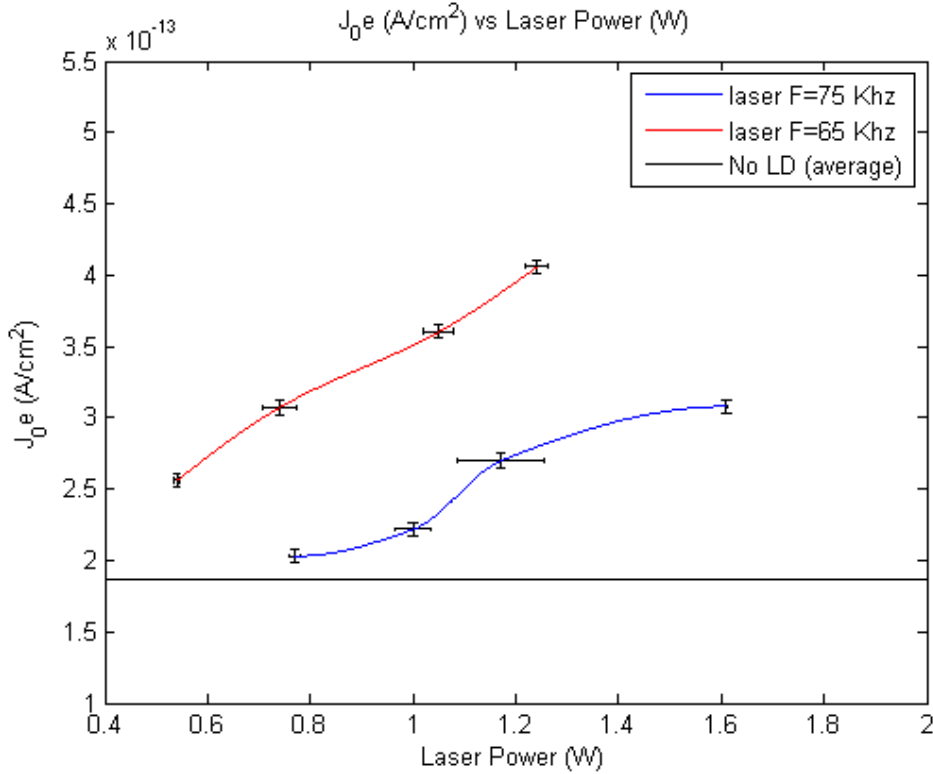
Figure 28: Saturated current vs Laser Power. The values for the 65 kHz curve are the average of samples s1,s2 and s5.

In figure 28 we plot the saturated current in function of the doping laser power. For the 65 kHz samples we plot the average of the measured values of samples s1, s2 and s5. As it was expected the saturation current increases with the laser power, indicating that indeed the defect density increases considerably after the laser doping process. Some authors like M. Muller report decreasing J_{0e} values for increasing laser power after certain threshold[55]. However, in the present experiment such behavior was not observed . They do not report the exact laser parameters that they used so it is not easy to compare. It could be that if we try higher laser powers such decreasing behavior would be observed. Comparing again the performance of the 65 kHz samples with the 75 kHz ones, it is again clear that more laser damage was produced in the low laser frequency samples.

4.6.1 Laser doping conclusions and results analysis.

In section 4.3.2 it was observed that the sheet resistance of laser doped samples decreases with increasing laser power. However it was observed that for a fixed pulse overlapping percentage, there is a a R_{sh} minimum that cannot be trespassed by increasing laser power. When this threshold is reached, in order to decrease the sheet resistance and have deeper and more highly doped profiles an increase in the pulse overlapping percentage should be made. It was concluded that this is because the dopants diffusion is limited by the dopant atoms diffusion velocity and not the front melt penetration velocity.

In section 4.3.3 it was observed that samples irradiated by similar laser energy densities, but with lower laser frequency repetition, present lower sheet resistance. For this reason when in section 4.4 we prepared samples with similar sheet resistances, the ones made at higher laser frequency had to be made at higher laser pulse energy densities. Also in section 4.4 it was observed that for samples which had similar sheet resistances, the ones made at lower laser frequency presented higher surface roughness. It was observed that for a fixed laser frequency the roughness increases with laser power.

In section 4.4.1 the SIMS analysis showed that higher laser output power increased the dopants diffusion depths, as it was expected. Also it was found that for samples made at similar laser pulse energy densities, but different laser frequency, the ones at lower frequency present deeper dopant concentration profiles.

In section 4.5 where lifetimes and saturation current was studied, it was found out that increasing laser power decreases the minority carriers lifetime and increases the saturation current. This indicates that recombination in the emitter region is increased by the laser doping process, thus some damage in the crystal structure was made. For the desired 43 $\Omega/\square$ high doped region we would have a lifetime decrease of about 45-55 % with respect to the 115$\Omega/\square$ region. Regarding laser frequency it was found out that for samples that have similar sheet resistances the ones elaborated at higher laser frequency present better minority carriers lifetimes. Similarly saturated current values gave the same result that is that higher laser frequency decreases crystal degradation.

So in conclusion two laser parameters were studied. Laser output power and laser repetition frequency. The results obtained for the laser output power studies were expected and are easily explain. But the results regarding the laser frequency are not very obvious. The following is my interpretation and hypothesis of the results obtained.

First of all as already seen for two pulses carrying similar total energy the pulse duration is longer for the one for which the laser is set to a higher repetition frequency , but at the same time it has a smaller peak fluence. Lets called the high frequency pulse HFP and the low frequency one LFP.

At the beginning of the irradiation process the sample is acquiring energy by light absorption and since the absorption rate is higher than the diffusion rate, the sample

is heating up. Thus the maximum temperature is reached some time after the pulse peak fluence is reached. Afterwards it losses more energy by conduction than what it gains by irradiation and it starts to cool down. The LFP sample will locally reach a higher temperature because it received a similar amount of energy in less time, so this energy had no time to diffuse. In order to get a clearer view of what is happening let's take a look at Figure 29, which is a computer simulated temperature vs sample depth plot made by Young and Wood [46].
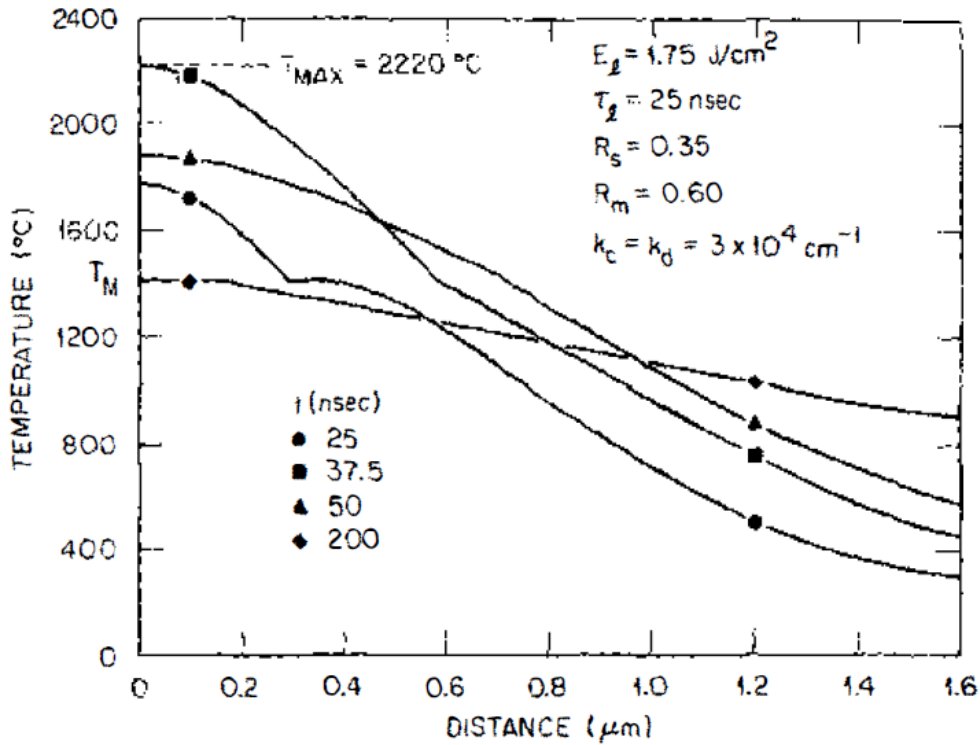
Figure 29: Computer simulated temperature vs crystal depth. Taken from [46]. The different curves correspond to different times after the laser pulse hitted the wafer. Pulse length is taken to be 25ns.

The different curves correspond to different times. We observe that the maximum temperature is reached at about 37.5 ns after the laser pulse started . The melting temperature is about 1450 ^oC and it can be seen that at this point there is a brake in the curves, which is due to the phase transition. If you compare the curves at 37.5 ns, 50 ns and 200 ns you can see that the concavity of the curves in the melted region decreases with time, which by equation 20 means that the rate of heat transferring decreases with time.

It can also be seen in the $25ns$ curve and in smaller extent in the 37.5 ns one, that just after the phase break the shape of the curve is also concave which means that this region is getting warmer, therefore it will get melted, whereas in the 50 ns there is no concavity after the phase break, it is even a little convex which means that the temperature is starting to go down.

54

When the maximum front melt position is reached the concavity just after the break point will be zero, a bit later it will become convex thus cooling down. Now the LFP will reach higher temperature in less amount of time, therefore the curvature of its melted region curve just after the maximum temperature is reached, is higher than the curvature for the melted region curve of the HFP. This means that the front melt penetrates into the material faster in the LFP sample than in the HFP one. My hypothesis is that since it penetrates faster it also penetrates deeper. The reason why I think this is that in figure29, in the curves in which the material has already reached its maximum temperature and the front melt is still penetrating (like in the one at 37.5 ns) the curvature in the melted zone is higher than the curvature in the crystallized zone, which means that the energy is transmitted faster witthin the melted zone than in the crystallized one. For illustrating this I made the drawing shown in figure 30, showing what would be the difference in the temperature vs depth profiles for the HFP and LFP samples just after the maximum temperature has been reached (note that this does not have to be simultaneous in both samples).

In the LFP sample the curvature in the molten region is higher than in the HFP sample. In the HFP sample in general the temperature in the solid region after the front melt position is higher than in the LFP sample.
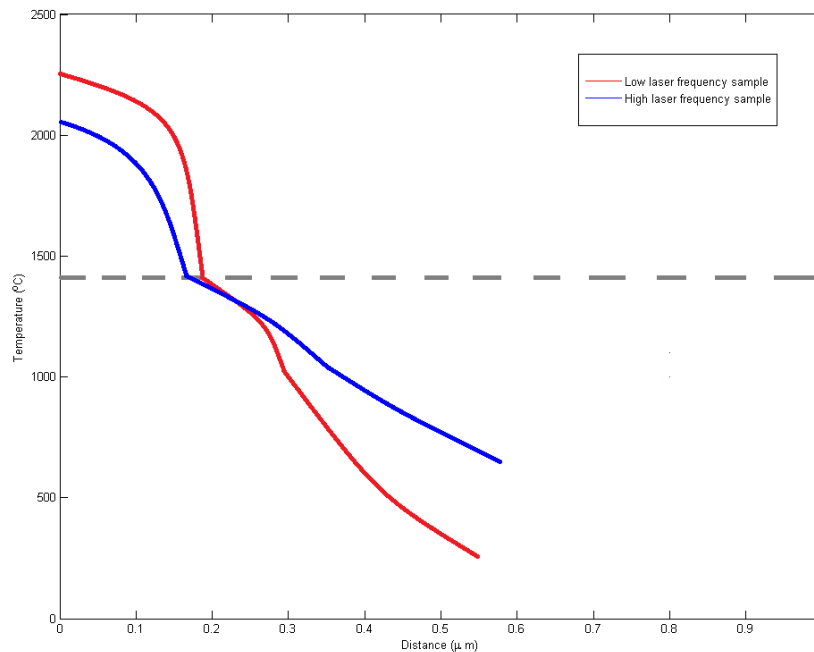
Figure 30: Illustrative drawing for showing the difference in temperature vs depth profiles. Just after the sample has reached its maximum temperature but the front melt is still penetrating. Two curves are displayed, one for samples made at high laser frequency and one at low one.

Thus since compared to the HFP sample, in the LFP sample the energy is going faster from the hot parts of the melted zone to its colder parts where the front melt is, in the LFP sample more energy is being used in heating up the front melt zone , whereas in the HFP sample more energy is being used heating up the regions beyond the front melt zone. This implies that the front melt will reach a deeper distance in the LFP sample than in the HFP sample, whereas the HFP sample will stay molten for a longer period of time and its recrystallization velocity will be smaller.

That the recrystallization velocity is smaller in the HFP sample follows from the fact that since the front melt was penetrating at a smaller rate, the rate at which the energy was being transmitted from the molten to the solid zone was smaller, so the energy in the solid zone had more time to distribute thus giving less abrupt profile than in the LFP case. I illustrate this with the drawing showed in figure , where how a temperature vs depth profiles would look like for a time just after the front melt has reached its maximum depth is displayed.
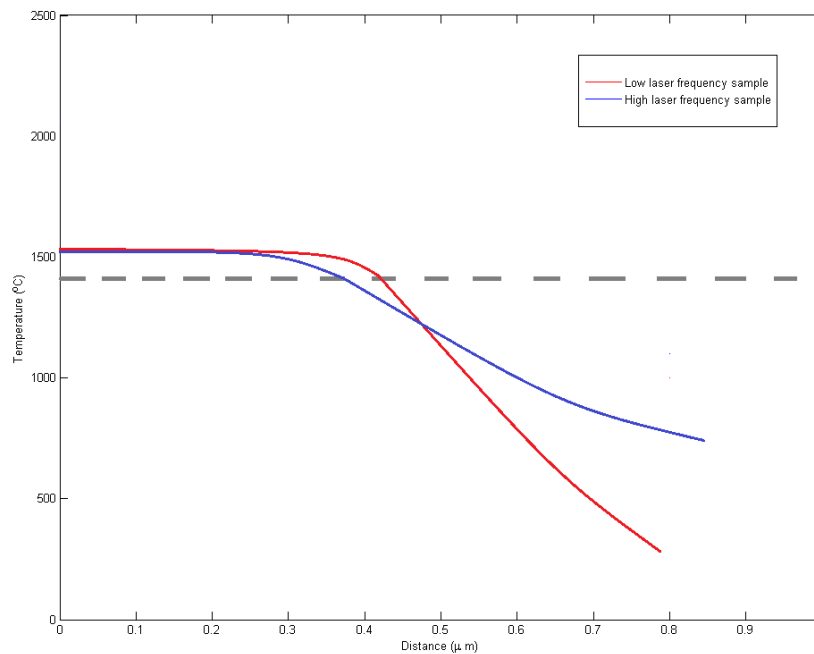
Figure 31: Illustrative drawing for showing the difference in temperature vs depth profiles just after the front melt has reached its maximum depth. Two curves are displayed, one for samples made at high laser frequency and one at low one.

So since the temperature vs depth profile in the solid region is less abrupt in the HFP case the energy flows at lower rate. When the front melt is penetrating the velocity at which this is done is mostly dependent on the rate at which the energy flows inside the molten zone from its hotter regions to the front melt, but when the front melt is retreating its velocity is more dependent on how the energy in the solid

zone near the front melt flows, so since in the HFP case in this region the energy flows at a slower rate the recrystallization velocity is smaller.

All this does not mean that doping atoms get to reach the front melt depth, because as we already saw the front melt might penetrate up to $0.5\mu m$ while our samples where less than $0, 1\mu m$. So the reason why in the LFP samples the doping atoms penetrate deeper than in the HFP ones is that since in the LFP sample the front melt reached a deeper depth when the sample is recrystallizing the front melt has to go through a longer distance to meet up with the deepest diffused atoms than in the HFP case. In figure I illustrate this with a drawing.
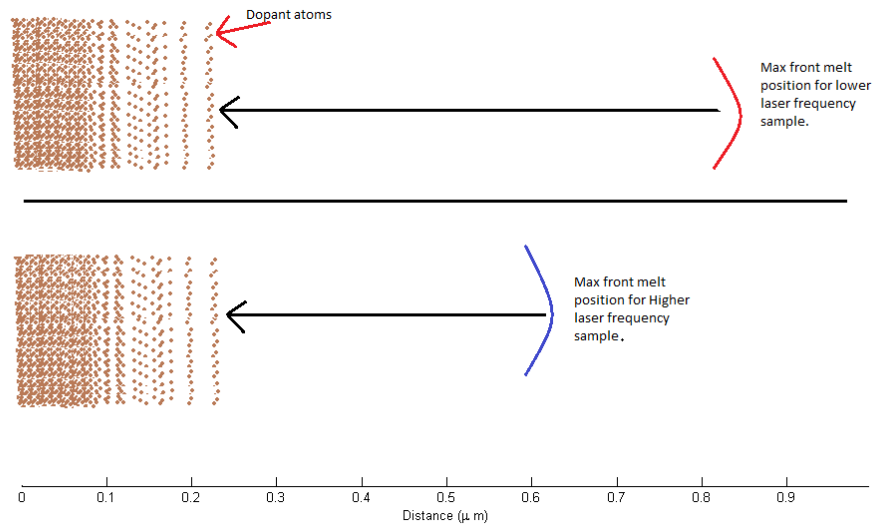
Figure 32: Illustrative drawing for showing why when the sample is recrystallizing it might in some cases take longer for the deepest diffused front melt to reach the dopant atoms.

Thus for some cases it might happen that since the recrystallization velocity for the LFP case is higher than for the HFP case it takes shorter time for the front melt to encounter the dopant atoms. If the doping was done by a single pulse probably this would happen . But since we have a 80% pulse overlapping, with each incoming pulse the atoms are diffusing deeper and deeper, so at some point the dopant atoms are closed enough to the front melt that the extra distance that the front melt has in the LFP case compared to the HFP case, does make some diference regarding the amount of time that the front melt will take to meet up the diffusing dopant atoms.

Thus from the former analysis one concludes that for laser pulses with similar energy density but different shapes, the one with shorter pulse duration but higher peak fluence will produce a higher melting depth but shorter molten times, the doping profiles will be deeper and the recrystallization velocity will be higher thus giving a poorer crystal quality.

This explains why the samples that were made at 65 kHz laser frequency had in general lower sheet resistances, deeper doping profiles and worst lifetimes than the ones made at 75kHz even though they were irradiated with pulses with similar laser energy densities.

Based on the results obtained in this section I recommend the following procedure to optimize the laser parameters when making a laser doping: In general for achieving a desired sheet resistance with low crystal damage it is recommendable to first establish the maximum laser repetition frequency available for the laser. Then depending on the throughput desired one should establish the pulse overlapping percentage, higher overlapping will give better crystal quality because less energy in each pulse will be needed, but this will produce lower throughput. With these two parameters vary the laser power output until the required sheet resistance is achieved. If the crystal quality is not high enough and the pulse frequency cannot be increased then a further increase in the overlapping percentage should be made.

5 Selective emitter solar cell results.

Having chosed suitable laser parameters to perform the laser doping process, we proceed to elaborate the selective emitter solar cells. These were 5cm×5cm area cells, which were cutted from 15,6cm×15,6 cm wafers Cz silicon wafers which went through a KOH texturing process. The manufacturing steps were carried out following the baseline procedure of the IFE laboratory as described in section 3. For the elaboration of the selective emitter we used the developed formula number 7 of table 1 for the $POCl_3$ diffusion. By this method we elaborated double side P doped wafers with sheet resistances around 115 $\Omega/\square$. As said before the desired sheet resistance for the highly doped areas is around 43 $\Omega/\square$. The laser doping was made at repetition frequencies of 65, 75 and 85 kHz. The laser parameters were chosen using the results of the experiment exposed in section 4.3.4 which were also made on textured wafers. Nevertheless in order to make sure that the desired sheet resistance would be obtained some testing experiments were made on wafers from the same batch. In table 5 we resume the laser parameters that gave the best approach to the desired sheet resistances.

Table 5: Laser parameters for 43 $\Omega/\square$ doping on textured $POCl_3$ diffused wafer.

frequency (kHz)	Diode current (A)	Power (W)	Scan velocity (mm/s)	R_{sh} ($\Omega/\square$)
65	27.9	0.66	260	43.1
75	29.8	0.85	300	43.7
85	32	1.53	340	42.8

After the laser doping the samples were passivated with SiNx by PECVD. Then the metallization of the cells was carried out by means of an screen printing process. As already mentioned the cells had a size of 5×5 cm^2. The laser doped pattern consisted of 21 fingers equally spaced of 180 μm wide. These were connected to a central perpendicular busbar of 1600 μm wide . The rear part of the cell had an homogeneous contact with no busbar. For the rear part metallization, aluminum was used and was deposited by means of screen printing and dried out at 250 ^oC. For the front part metallization, silver contacts were used. In order to have a good alignment with the laser doped pattern some fiducial marks had to be made in the corners of wafer.

After the deposition and drying of the front contacts, a firing in the LA-309 furnace was made. In the firing process the depth that the contacts reach depend on the temperature of the four chambers of the furnace and the time the wafer spends on each one, which is determined by the belt velocity. Samples with three different firing conditions were elaborated. The following are the recipes used, they are defined by the temperature of each chamber and the belt velocity.

1. 780^oC,835^oC,890^oC,945^oC at 520 cm/min

2. 780^oC,830^oC,880^oC,930^oC at 520 cm/min

3. 780^oC,825^oC,870^oC,915^oC at 520 cm/min

For each firing condition various samples were elaborated. In table 16 the laser frequency and firing recipe conditions for each cell are displayed, along with their respective IV performance characteristic values. In order to visualize better the results obtained an average of the quantities obtained by the IV characteristics measurement was made for the samples with equal manufacturing conditions, with the results being showed in table 6.

Table 6: Averaged IV measurement results for each manufacturing condition.

LF (kHz)	Firing recipe	Efficiency	Voc(mV)	Jsc (mA/cm^2)	FF %	R$_s$ (Ω)	R$_{shunt}$ (Ω)
65	1	17.41	616.30	36.94	76.49	1.21E-02	6.62E+01
65	2	17.19	615.29	36.87	75.79	1.39E-02	4.57E+01
65	3	17.11	610.89	36.80	76.10	1.40E-02	3.94E+01
75	1	17.26	615.39	36.81	76.21	1.30E-02	4.92E+01
75	2	17.12	611.41	36.94	75.82	1.47E-02	4.24E+01
75	3	17.22	615.21	36.78	76.11	1.41E-02	5.27E+01
85	1	17.36	614.94	36.83	76.66	1.20E-02	7.36E+01
85	2	17.31	614.28	36.88	76.39	1.33E-02	8.41E+01
85	3	17.09	612.89	36.78	75.84	1.63E-02	6.54E+01

The first thing to note in table 6 is that for each laser frequency the best efficiencies were obtained by the samples that were fired with recipe number 1, which is the recipe that presented higher firing temperatures. Among this samples the best results were obtained by the samples that were laser doped at 65 kHz, which is the lowest laser frequency. For firing condition 1 and 2 the samples at 85 kHz Laser frequency had a higher efficiency than the ones at 75 kHz, but looking at the shunt resistances we observed that 75 kHz samples have lower shunt resistances, therefore the lower efficiencies might be due to manufacturing mistakes, specially the ones using recipe 2.

It is seen that the V_{oc} is higher for the samples that were fired at higher temperature. The first possible reason for this is that because of the higher firing temperature more H atoms from the SiNx coating diffused into the silicon which resulted in a better passivation . Thus the samples fired at higher temperature have deeper profiles which results in bigger junction depths and this produces higher V_{oc}. The second reason could be that higher firing temperature produces deeper front contacts, which as we saw in section B.3 reduces the contact recombination because it increases the interface area. For the samples fired at the highest firing temperature we see that the ones that produce higher V_{oc} are the ones that were laser doped at lower frequency. This is similar to what we mentioned before. As we saw in section 4.4.1 the samples made at lower frequency produce deeper doping profiles and this results in greater

V_{oc}.

Regarding J_{sc} the situation is less clear and should be analyzed looking at the other quantities. For the samples done at 65 kHz J_{sc} increases with firing temperature. This might have to do with the increase in contact area. If we look at the series resistance for the same samples we observe that this quantity decreases with increasing firing temperature.This means that having deeper contacts reduces the series resistance, because by increasing the contact area one reduces the contact recombination. But in the cases for samples made at 75 kHz and 85 kHz the situation is different. In both of this cases the maximum J_{oc} is reached in using recipe 2.

One possible explanation for this can be given by looking at the SIMS measurement results. For instance the one at 85 kHz which is labeled as sample t9 and has $R_{sh} = 44\Omega/\square$ (figure 15). There it is observed that the doping profile that this sample has, is neither Gaussian or ERFC but something in between. This profile has a peak concentration of around 1.75 cm^{-3} and is almost constant until a depth of around 80 nm. After this it starts to abruptly decrease. Therefore the possible reason why the J_{sc} in the samples made at 85 kHz LF is better for recipe 2 than for recipe 1 is the following: Since in recipe 1 the contact is deeper, its bottom part could be in the zone were the doping concentration started to decrease, and lower Si doping as we saw implies higher interface recombination, therefore less current crossing the contacts. M.Hilaly reports contacts penetration depths of 55 nm for the PV168 Ag paste fired at 900 C/80 ipm [54], it is seen the SIMS profile of the t9 sample that the maximum doping concentration is constant until about 50nm. This does not mean that the deeper contact are shunted, because they still in a N doped zone. This is supported by the fact that the shunt resistance is higher for recipe 2 than for recipe 1. This did not happen in the case were the highly doped zone was irradiated by 65 kHz laser frequency because in this case, as we have seen, the doping profile is deeper (figure 13). This leads us to think that the contacts penetration is about 50-90 nm in our samples.

It is observed that the best fill factors of the samples are obtained by the cells made at 85 kHz. This is for two reasons. The first posible explanation for this is that for the 85 kHz sample the maximum doping concentration is 1.75×10^{20} cm^{-3} while for the 65 kHz sample it is 1.05×10^{20} cm^{-3}. In general to up to 90 nm the doping concentration of the 85 kHz sample is higher than for the 65 kHz. This means that in general in the bottom region of the contact the semiconductor doping concentration is higher for the 85 kHz than for the 65 kHz. The second reason is that the laser doped zones of the 85 kHz samples presented higher lifetimes and smaller saturation current. It is seen that indeed the maximum efficiencies obtained by a sample made at 65kHz and a 85 kHz don't differ greatly. The best 65 kHz cell has an efficiency of 17.45% and the best 85 kHz has 17.41%. The difference is mainly because the deeper doping profiles provide higher V_{oc}, but also since the doping concentration near the surface is lower for the 65 kHz samples, the passivation is better so it presents a smaller surface recombination.

In order to further study the performance of the cells in figure 33 we plotted the IV characteristics of the best cells of each laser frequency and those for a cell that has was elaborated by a similar process, but with homogeneous emitter of 115 $\Omega/\square$ sheet

resistance.
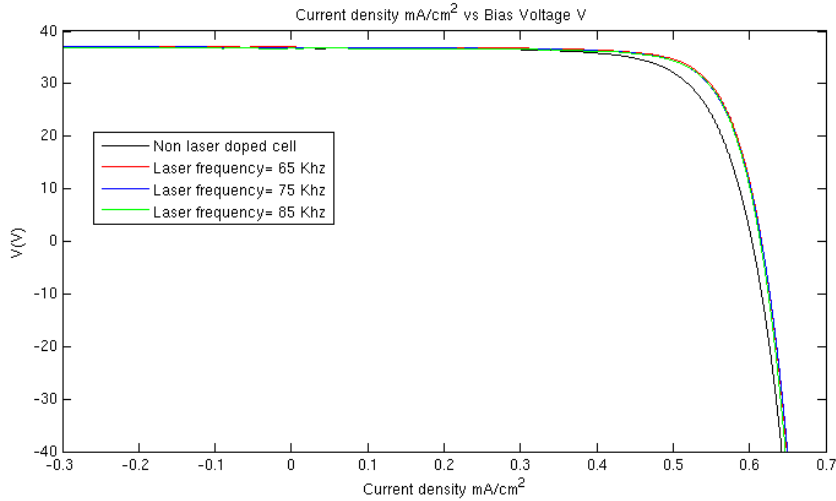
Figure 33: IV characteristics of best elaborated selective emitter solar cells and solar cell without SE.

It is observed in this figure that the main effect that the selective emitter has is to increase the fill factor,this is due to the decrease in the metal semiconductor resistance due to the high doping level.

In order to characterize better the selective emitter solar cells, internal quantum efficiency (IQE) measurements were made. The improvement in the blue response was analyzed by comparing the IQE of the selective emitter cells with that of some cells with homogeneous of emitter 73 $\Omega/\square$ sheet resistance . This value is closed to the optimal for non selective emitters. The cells that we used for this purposes are those of the baseline of the IFE laboratory. These cells were made by similar process than the ones with selective emitter, except that they had a homogeneous emitter (HE) and that they had been through an edge isolation process. The rest of the fabrication steps were the same. The wafer quality was very similar because they were fabricated from same batches. In figure 34 the resulting quantum efficiency vs wavelength curves are plotted for some selective emitter samples. For each of the studied frequencies we plotted the samples that presented best efficiency. Also the IQE of the reference homogeneous emitter sample is plotted
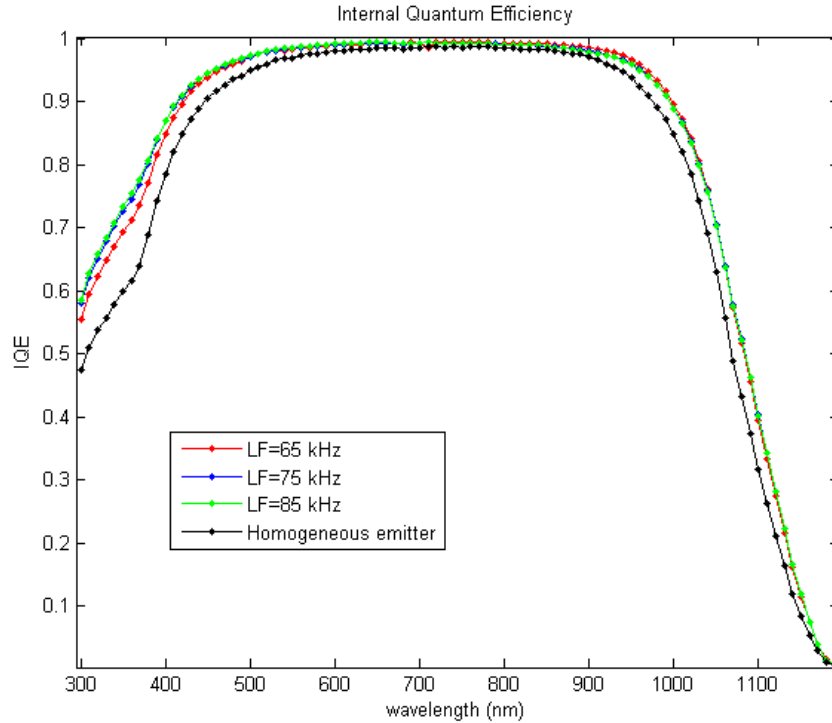
Figure 34: Internal Quantum Efficiency for selective emitter cells and reference sample.

In figure 34 it can clearly be observed that the blue response of the selective emitter cells improved with respect to the homogeneous emitter one. It is also seen that the samples that were made at higher laser frequency presented higher IQE. One thing that was not expected is that in the low energy photons region there is also an improvement in the IQE with respect to the sample with homogeneous emitter. This is probably because in the selective emitter sample the emitter is more shallow so there is a stronger back surface field compared to the baseline sample.

Besides the IQE the spectral response measurement also gives information on how much recombination occurs in the emitter and how much in the base, which is quite appropriate to evaluate the selective emitter cell. In table 7 we display the recombination velocities in the different regions of the cells for the samples plotted in figure 34.

Table 7: Recombination velocities in different parts of the cell, for selective emitters (SE) and homogeneous emitter.

Sample	SE. LF=65 kHz	SE. LF=75 kHz	SE. LF=85 kHz	Homogeneous emitter $R_s = 73(\Omega/\square)$
Emitter recombination [mA/cm^2]	0.8892	0.7655	0.7322	1.182
Volume recombination [mA/cm^2]	0.0309	0.0528	0.0585	0.1293
Rear recombination [mA/cm^2]	0.4044	0.5256	0.5629	0.5708
Decrease % in emitter recombination	24.8	35.2	38.0	0

In this table it is confirmed again that the samples made at higher laser frequency present less recombination in the emitter, which again proves that higher laser frequency imflict less laser damage.

It is also seen that compared to the HE cell the SE cell has less emitter recombination. This was expected because except for the regions underneath the contacts the SE cells have a higher sheet resistance than the HE cells.

Eventhough the decrease in the emitters recombination velocities in the SE cells go from 24% to 38%, it is seen in figure 34 that the increase in the blue response is only increased in around 10%. This made us suspect that probably some current was being loss in the contacts, meaning that the metallization pattern did not exactly match the laser doped one. To find this out some microscope pictures were taken . The results were that indeed there was a misalingment between the contacts and the laser doped region. This can be seen in figure 35.

(a) Left side   (b) Right side
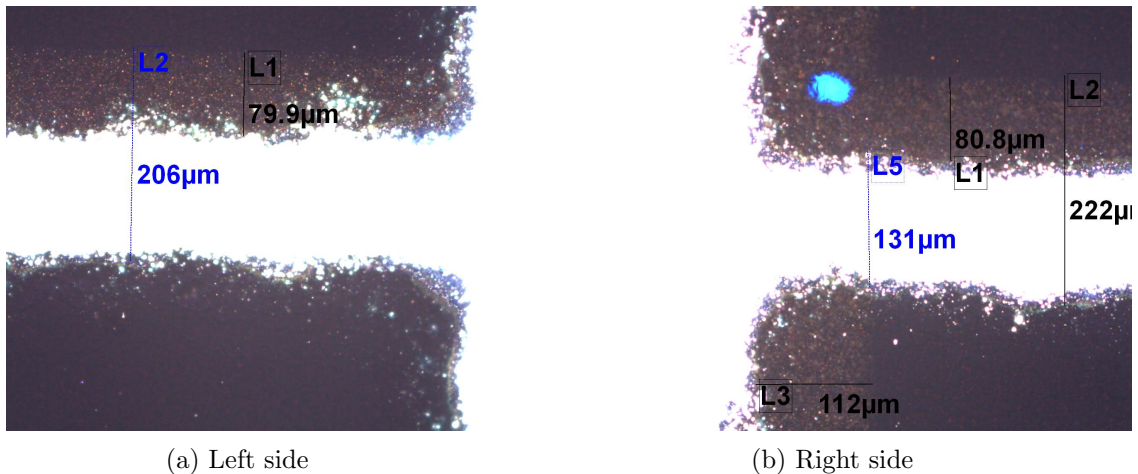
Figure 35: .Microscope picture of the contacts in the area were the fingers (horizontal) meet the busbar (vertical). The laser doped area can be noticed by a different color.

In this figure it can be noticed that there is a portion of the contacts that is outside the laser doped area. Indeed it can be seen that above the fingers there is a region of about 80 μm of uncovered laser doped area. Since the fingers are about 130 μm width

whereas the laser doped region was 180 μm width. This means that about 24% of the contact is outside the laser doped area, this leads to high recombination rates in this part of the metal semiconductor interface, even more than in the baseline sample, because the low doped area of the emitter has higher sheet resistance. In the busbar region the situation is not as bad because of the busbar dimensions. The metal is about 1500 μm width while the laser doped region is 1600 μm width. In the picture it can be seen that around 112 μm of laser doped region is not covered by metal contacts. This means that less than 1% of the busbar has a high metal semicondutor recombination interface. We took pictures of the contact region for various of the cells made, it was found out that all of them had a misalignment with some small variations between them. The main consequence that the misalignment produce is to decrease the FF of the cells, for this reason the fill factors of our cell were not as good as expected.

In order to make a final comparison of the elaborated selective emitter solar cells, in table 8 it is displayed the electrical characteristics of three cells with different types of emitter. The first is the selective emitter one (SEc16) . The one displayed is sample c16 of table 16, which presented one of the best performances. The second one is a homogeneous emitter cell with $R_s = 73(\Omega/\square)$ (HE R73), which was taken from the IFE baseline reference cells. It is to mention that because this cells had not SE, and they had higher sheet resistance under the metal contacts, the space between the fingers was bigger. The third cell is the homogeneous emitter cell with $R_s = 115(\Omega/\square)$ (HE R115) whose features are similar to the SE one.

Table 8: Comparison of cells with three different types of emitter. One with selective emitter (SE c16), one with homogeneous emitter with $R_s = 73(\Omega/\square)$ and other with homogeneous emitter with $R_s = 115(\Omega/\square)$

Sample	Efficiency	Voc (mV)	Jsc (mA/cm^2)	FF %	R_{series} (Ω/cm^2)	R_{shunt} (Ω/cm^2)
SE c16	17.3	614.2	36.7	76.7	2.88E-1	1.74E+3
HE R73	17.3	617.7	36.2	77.18	5.57E-1	2.93E+4
HE R115	16.1	604.5	37.0	71.66	7.00E-2	2.10E+3

In this table it is seen that the efficiency of the SE cell is not really higher than the HE R73 cell. The reasons for this are: First the missalignment mentioned before in the SE cells. Second that the HE R73 cells had gone through an additional edge isolation process which has as purpose to avoid leakage currents. This can be noticed in the fact that the shunt resistance of the HE R73 cell is almost an order of magnitude higher than the SE cell. Both of this factors have the effect of enhancing the fill factor of cell HE R73 over that of the SE one. Nevertheless the fill factors of the SE cells are not much lower than the ones HE R73 ones. Indeed looking at various cells from the IFE baseline their fill factors range from 75%-78% which is kind of the same fill factors obtained for the SE cells.

Comparing the SE cell with the HE R115 cell it can be seen that the fill factor

of the first is much higher than the second, meaning that in spite of the misalignment the effect of the high doping underneath the contacts is quite valuable. Also if comparing the series resistances of the three cells, it is seen that the SE cell has the lowest value, meaning again that the quality of the contacts was not bad.

The HE R73 cell presents the highest V_{oc} value. The SE cell has the second highest and the HE R115 has the lowest. This has to do with the amount of doping concentration in the emitters. Regarding J_{sc}, the effect of the lightly doped emitter can be easily appreciated, because the more lightly doped HE R115 cell has the highest value, then the SE emitter is second and then HE R73 cell has the lowest.
In general eventhough there was some problems in the elaboration of the selective emitter solar cell, it was seen that it's effect is appreciable and that with some small improvements it can really present a much better performance than the homogeneous emitter cells. Based on the above results we present the following list of improvements and optimizations that can be made to obtain a SE cell with higher efficiency:

Better metallization alignment : This can possibly be solved by increasing the visibility of the alignment marks made on the wafer, in this way the screen printing machine would recognize them better and more accuracy would be obtained. As already said a good contact-high doped pattern alignment would considerably increase the fill factor. This would further allow to better optimize the fingers width and distance.

Perform and edge isolation : This would reduce the edge leakage currents arising from the manufacturing problems.

Optimize SiNx surface passivation coating for the 115 ($\Omega/\square$) emitter : This was not mentioned before, but the surface passivation recipe used is optimized for a emitter with sheet resistance around $73(\Omega/\square)$. This increases the surface recombination in the SE cells, which as mentioned in section 2.4 can substantially diminish the positive effects of the selective emitter.

More optimization on the laser parameters: Even though the laser parameters used presented satisfactory results, there still room for more optimization here. It was seen that higher laser frequency presented better J_{sc} but lower V_{oc} , because this creates less crystal damage but shallower doping profiles. Thus I think that one method to improve both of this parameters would be to increase the pulse overlapping for a high frequency mode (probably the most suitable for our laser would be 75 kHz because of estability issues).
Trying to obtain a high doping area of around 43 ($\Omega/\square$) with higher pulse overlapping and high frequency has two positive consequences: first that since the number of melting cycles for each spot is higher the dopant atoms would reach deeper into the crystal, which would increase V_{oc}. Second that for obtaining the same sheet resistance with higher pulse overlapping, the energy of each pulse should be decreased, this would decrease the amount of laser induced defects and would further improve J_{sc}. The reasons for this is that to produce a

lower energy pulse at the same frequency one needs to decrease the laser output power, which would decrease the peak fluence of the pulses and at the same time increase the pulse duration. Both of these effects were seen in section 4.6.1 to improve the recrystallized area quality.

More optimization of the firing parameters . In order to do this some SEM pictures could be taken to measure exactly the contact depth for various firing conditions. It was mentioned that possibly the contact depth peneration are between 50 and 90nm.

For limited time reasons we were not able to implement the above mentioned improvements in the selective emitter solar cells, but we hope to do it in a very close future. This concludes our analysis of the selective emitter solar cells made by laser doping.

6   Conclusions

In the present thesis a study of the laser doping technique on crystalline silicon was carried out. This was done with the purpose of implementing a selective emitter solar cell. The main laser parameters that were studied were the laser power, laser repetition frequency and in some extent pulse overlapping. With these we arrived at conclusions regarding the effect that the laser pulse duration and peak fluence has on the doping profiles as well as in the quality of the recrystallized areas. This had not been previously studied experimentally, for most of the studies focus only on the effect of the total energy density but not the particular shape of the pulses. A small theoretical explanation hypothesis based on computer simulations of other authors was given. The conclusions were:

- Laser doping experiments made at same laser energy densities but produced at different pulse repetition frequencies and power will not produce the same doping profiles. The sheet resistances produced by laser doping experiments at lower repetition frequencies are in general higher. There is no single laser parameter that can exactly predict the outcome sheet resistance of the laser doped sample, even for very similar dopant precursors. Therefore for any particular laser doping application the laser parameters should be optimized.

- For two laser pulses carrying similar energies but with different shapes, the one with higher peak fluence but smaller pulse duration will produce deeper doping profiles but because of higher recrystallization velocity the amount of laser induced crystal defects will be bigger. Therefore, since higher laser repetition frequencies produce pulses with longer durations but smaller peak fluences this results in better quality laser doped areas.

- Higher laser power output produce deeper doping profiles. Nevertheless for a fixed pulse overlapping there is a threshold on which increasing the laser

power output will not increase the dopants concentration but instead will create more laser damage. To further increase the dopant concentration the pulse overlapping should be increased.

- In general for a given required sheet resistance it is desirable to work with the highest pulse repetition frequency available. And depending of the throughput requirements with high pulse overlapping percentage.

In general the laser doping technique is a very versatile technique that if appropriately optimized can provide very useful results. Some further works regarding this topic could be a computer simulation study of the effect that the laser pulse shape has on the recrystallized area quality.

Regarding the selective emitter elaboration the following are the conclusions:

- A suitable $POCl_3$ diffusion recipe was developed for the formation of the $115\Omega/\square$ emitter with phosphorus glass layer appropriate for the laser doping

- Suitable laser parameters for the laser doping of the contacts area were found. It was confirmed that samples elaborated with high laser frequency can ultimately present better performance because this reduces laser induced crystal defects thus increasing the J_{sc}

- It was confirmed that the selective emitter solar cells present a better blue response than the homogeneous one. We did not achieve higher efficiencies for the selective emitter cells than for the baseline ones, but this was mostly because of the missalignment in the metallization. Nevertheless various possible improvement steps for the selective emitter cell were presented, some of these are hoped to be soon implemented.

- It was found out that in general the elaboration for elaboration the selective emitter by the laser doping technique it is preferable to do it at high laser pulse repetition frequencies, because this reduces the damage inflict on the crystal structure.

- It was shown that in spite of the alignment problems, highly doping the area underneath the contacts increases the fill factors of the cells. This was done by comparing the selective emitter cell with a homogeneous high resistance emitter one.

Finally in was shown that that despite the elaboration of a selective emitter solar cell by a laser doping technique present some optimization challenges, is a process that is compatible with most of the standard solar cell baselines, and if correctly implemented it can lead to a considerable improvement on the net efficiency of the silicon solar cells.

Appendices

A   Laser doping parameter Tables.

Table 9: Laser doping results for experiment 1 of section 4.1.

I=30A	Overlaping=75%		
F (kHz)	Power(W)	Power STD (W)	SR (Ω/□)
30	3,6	0,13	burned
40	2,7	0,02	654 Burned
50	2,0	0,03	19
60	1,4	0,02	50
70	1,0	0,01	175
80	0,9	0,01	512
90	0,8	0,04	Unstable
I=32A	Overlaping=75%		
F (kHz)	Power(W)	Power STD (W)	SR (Ω/□)
30	6,1	0,39	707 (burned)
40	4,9	0,37	183,6
50	3,8	0,34	17,0
60	3,2	0,62	131,4
70	2,3	0,40	186,3
80	1,9	0,38	332,2
90	1,7	0,36	unstable
I=35A	Overlaping=75%		
F (kHz)	Power(W)	Power STD (W)	SR (Ω/□)
40	5,6	0,1	burned
50	4,5	0,05	21
60	3,2	0,02	160
70	2,3	0,03	200
80	1,7	0,01	481
90	1,4	0,12	unstable
I=34A	Overlaping=75%		
F (kHz)	Power(W)	Power STD (W)	SR (Ω/□)
40	5,3	0,15	burned
50	4,1	0,01	14,1
60	3,0	0,04	127,8
70	2,3	0,03	156,8
80	1,8	0,01	321,3
90	1,7	0,02	unstable
90	1,7	0,36	unstable

Table 10: Laser doping parameter for experiment in section 4.3.2

The following samples had initial R_{sh} of 65 $\Omega/\square$				
Frequency=45 kHz , vscan=225				
I (amps)	P(W)av	P STD(W)	E (J/cm^2)	R($\Omega/\square$)
28.30	1.50	0.00	4.14	18.78
28.90	2.03	0.06	5.60	25.37
29.70	2.40	0.09	6.62	29.99
30.70	2.96	0.06	8.18	37.08
31.30	3.39	0.10	9.38	42.51
32.50	4.00	0.07	11.05	50.07
33.70	4.58	0.06	12.64	57.30
Frequency=50 kHz , vscan=250				
I (amps)	P(W)av	P STD(W)	E (J/cm^2)	R($\Omega/\square$)
28.30	1.47	0.03	9.33	42.27
29.50	2.25	0.26	14.30	64.79
30.40	2.50	0.05	15.88	71.99
31.30	2.98	0.05	18.96	85.91
32.20	3.49	0.02	22.24	100.80
33.00	3.95	0.06	25.13	113.92
34.50	4.59	0.07	29.22	132.42
Frequency=55 kHz , vscan=275				
I (amps)	P(W)av	P STD(W)	E (J/cm^2)	R($\Omega/\square$)
29.50	1.47	0.05	8.50	38.55
30.80	2.09	0.01	12.12	54.93
31.50	2.52	0.01	14.56	66.00
32.40	3.05	0.03	17.67	80.10
33.40	3.52	0.02	20.36	92.27
36.00	3.99	0.00	23.12	104.77

Table 11: Laser doping parameter for experiment in section 4.3.2

The following samples had initial R_{sh} of 200 $\Omega/\square$				
Frequency=45 kHz , vscan=225				
I (amps)	P(W)av	P STD(W)	E (J/cm^2)	R($\Omega/\square$)
28.50	1.66	0.02	4.59	20.78
29.00	1.99	0.02	5.50	24.92
30.00	2.66	0.03	7.34	33.27
30.50	3.04	0.01	8.39	38.01
31.30	3.54	0.01	9.77	44.28
32.00	4.05	0.00	11.18	50.68
Frequency=50 kHz , vscan=225				
I (amps)	P(W)av	P STD(W)	E (J/cm^2)	R($\Omega/\square$)
28.50	1.50	0.01	3.74	16.94
29.50	1.96	0.05	4.87	22.05
30.40	2.50	0.00	6.22	28.18
31.20	3.01	0.01	7.48	33.92
31.90	3.53	0.02	8.77	39.73
32.80	3.99	0.07	9.92	44.94
34.30	4.62	0.02	11.49	52.06
Frequency=55 kHz , vscan=250				
I (amps)	P(W)av	P STD(W)	E (J/cm^2)	R($\Omega/\square$)$\pm$ 0.1
29.60	1.53	0.02	3.45	15.64
30.30	1.98	0.01	4.47	20.28
31.20	2.52	0.01	5.69	25.78
32.00	3.03	0.07	6.84	31.02
32.80	3.50	0.00	7.90	35.83
34.00	4.05	0.07	9.16	41.50

Table 12: Laser parameters for doping experiment of section 4.3.4.

P (average)	P STD (W)	Frequency (kHz)	Energy density (J/cm^2)	$R(\Omega/\square)\pm 0.1$
1.52	0.00	65	2.90	23.8
1.29	0.01	65	2.47	27.3
0.98	0.07	65	1.87	32.1
0.79	0.03	65	1.50	37.1
0.51	0.03	65	0.98	47.6
0.27	0.01	65	0.52	100.5
1.53	0.01	75	2.54	31.2
1.27	0.02	75	2.10	34.1
1.03	0.03	75	1.70	40.7
0.77	0.01	75	1.28	48.1
0.50	0.01	75	0.82	66.1
0.28	0.01	75	0.46	99.1
1.46	0.05	85	2.14	38.2
1.27	0.02	85	1.85	44.0
1.03	0.01	85	1.50	49.9
0.77	0.01	85	1.12	54.6
0.53	0.01	85	0.77	97.9
0.28	0.00	85	0.41	109.3

Table 13: PC1D simulation parameters

Material	Silicon
device area	$1cm^2$
Thickness	180 μm
Dielectric constant	11,9
Band gap	1,124 eV
Intrinsic conc	1e10 cm^{-3}
P type background doping	3,633e 15 cm^{-3}
Front surface doping	1 e 19 cm^{-3}
recombination lifetime	100 μs
Light intensity	0,1 W/cm^{-2}

Table 14: Laser parameters for sheet resistance experiment in textured wafers, section 4.3.4

P (average)	Frequency (KHz)	Energy density(Jul/cm)	R(Ohm/sq)
1,5195	65	2,9067	23,874
1,2925	65	2,4724	27,29
0,9825	65	1,8794	32,0737
0,785	65	1,5016	37,136
0,514	65	0,9832	47,626
0,2745	65	0,5251	100,51
1,532	75	2,5398	31,17
1,2705	75	2,1063	34,09
1,0305	75	1,7084	40,74
0,7695	75	1,2757	48,146
0,499	75	0,8273	66,17
0,277	75	0,4592	99,13
1,464	85	2,1416	38,11
1,2675	85	1,8541	44,03
1,0265	85	1,5016	49,95
0,7655	85	1,1198	54,64
0,5315	85	0,7775	97,96
0,2805	85	0,4103	109,31

Table 15: Laser parameters for roughness experiment 1, section 4.4

Power (W)	Frequency (kHz)	surface Roughness (μm)	Energy density (J/cm$\hat{2}$)
1,85	85	0,549	2,706
1,31	75	0,63	2,172
0,88	65	0,654	1,683
0,501	55	0,727	1,133
0,41	45	0,728	1,133

Table 16: Selective emitter cells manufacturing conditions and performance characteristics.

Sample	LF (kHz)	Firing recipe	Efficiency	Voc(V)	Jsc (mA/cm^2)	FF %	R_s (Ω)	R_{shunt} (Ω)
c1	65	1	17.4	616.1	37.0	76.5	1.21E+04	6.69E+01
c2	65	2	17.2	615.5	37.0	75.6	1.24E-02	2.81E+01
c3	65	3	17.1	610.9	36.8	76.1	1.40E-02	3.94E+01
c4								
c5								
c6	75	1	17.3	615.8	36.9	76.2	1.30E-02	5.85E+01
c7	75	2	17.1	611.4	36.9	75.8	1.47E-02	4.24E+01
c8	75	3	17.2	615.6	36.8	76.1	1.39E-02	4.25E+01
c9	75							
c10	75							
c11	85	1	17.4	615.6	36.9	76.6	1.24E-02	7.77E+01
c12	85	2	17.4	615.4	37.0	76.3	1.34E-02	6.67E+01
c13	85	3	17.1	611.9	36.7	75.9	1.64E-02	5.20E+01
c14	85							
c15	85							
c16	85	1	17.3	614.2	36.7	76.7	1.15E-02	6.96E+01
c17	85	2	16.5	618.5	33.9	78.8	5.04E-02	2.29E+08
c18	85	3	17.1	613.8	36.8	75.8	1.62E-02	7.87E+01
c19	85	2	17.2	613.0	36.8	76.5	1.26E-02	1.20E+08
c20	85	2	17.3	614.4	36.8	76.4	1.40E-02	6.60E+01
c21	75	1	17.2	615.0	36.7	76.2	1.30E-02	3.99E+01
c22	75	2	17.0	614.1	36.9	74.9	1.34E-02	1.91E+01
c23	75	3	17.2	614.8	36.8	76.1	1.42E-02	6.28E+01
c24	75	2	17.0	615.1	36.2	76.0	1.46E-02	4.34E+01
c25	75							
c26	65	1	17.4	616.6	36.9	76.4	1.20E-02	6.55E+01
c27	65	2	17.2	615.1	36.7	76.0	1.53E-02	6.33E+01
c28	65	3						
c29	65	2	16.9	617.1	35.6	76.8	1.22E-02	6.91E+01
c30	65	2	16.9	614.5	36.1	76.1	1.29E-02	3.20E+01

Table 17: Laser parameters for roughness experiment 2, section 4.4

P$_{average}$ (W)	P$_{STD}$ (W)	Energy density (J/cm$\hat{2}$)	R(Ohm/sq)	Roughness (μm)
0.63	0.006	1.20	52.1	0.60
0.80	0.005	1.53	45.8	0.57
1.07	0.059	2.05	35.8	0.68
1.27	0.070	2.43	31.8	0.90
1.48	0.009	2.84	30.5	0.95
1.74	0.025	3.33	28.7	0.92
1.95	0.100	3.73	27.8	0.99
2.20	0.027	4.21	27.2	1.08
2.38	0.105	4.55	24.1	1.45
2.53	0.151	4.84	22.7	3.29

B Lifetimes and metal-semiconductor interface

In section 2.4 it was seen that the purpose of the selective emitter is to optimize the emitter doping level without having to account for the trade of between descent lifetimes in the bulk of the emitter and good charge transportation through the front surface contacts. In order to understand why this problems arise in the first place it is necessary to understand the nature of the recombination and transport mechanisms both in the bulk of the material as well as in the metal semiconductor interfaces. Therefore the purpose of the present section will be to understand with some level of detail the nature of the recombination processes.

B.1 Carrier Generation-Recombination Lifetimes

In solar cells the first step in the conversion of solar into electrical energy is the generation of conducting charge carriers out of light photons. Generation are processes in which some electric charges present in a material absorb enough energy to pass from a statical bind state to a mobile conducting state. Usually in semiconductors, the generation is carried out by the creation of an electron hole pair (ehp) , by promoting an electron from the valence band to the conduction band, leaving a hole behind in the valence band. Since conducting charge carriers are in a excited state with respect to the nonconducting ones, all generation processes require an input of energy to the system.

On the other hand in recombination processes conducting charge carriers release some energy by decaying to less energetic non conducting states as a consequence of the system trying to attain equilibrium. These processes are contrary to the generation ones, for in general every recombination mechanism has a generation counterpart. The main generation-recombination mechanisms are: Optical and radiative, thermal,

Auger and Shockley-Read-Hall recombination-generation.

Radiative and Auger recombination are intrinsic processes which happen when an excited charge carrier decays into a less energetic level by realeasing some energy in form of heat, light or both, depending on the specific mechanism. Shockley-Read-Hall is a recombination-generation mechanism in which electron-hole pairs are trapped or realeased by a impurities or defects of the crystal which have discrete energy levels present in the band gap. This process requires that the charges absorb or release some energy, which is transferred to the lattice molecules in form of phonons. This is an extrinsic recombination mechanism which is highly dependent on the quality of the crystal.

In general, even under equilibrium conditions conducting electron hole pairs (ehp) are always being created and destroyed in any semiconductor with nonzero temperature, at generation and recombination rates G and U characteristic for each specific mechanism. The average time that the excess minority carriers takes to recombine and decay to a non conducting state is called the recombination lifetime τ_r . Contrary to this, the generation lifetime is the average time intervals at which ehp's are being created by processes usually opposite to the recombination ones. The carrier lifetimes are related to the recombination and generation rates by

$$
\begin{aligned}
G &\equiv \triangle n/\tau_G \\
U &\equiv \triangle n/\tau_R
\end{aligned}
$$

$$(24)$$

$$(25)$$

where $\triangle n$ are the excess carrier densities [30] .

These generation recombination processes occur both in the bulk and at the surface of the semiconductor, but since the surface is an abrupt interruption of the crystal structure the nature of the generation-recombination mechanisms are in principle different from the ones in the bulk, therefore they should be studied separately and characterized by its own surface recombination-generation lifetimes.

Carrier lifetimes is one of the parameters that is more critical when studying and designing semiconductor devices, because they determine most of the electronic transport properties of the crystal and its measurement gives important information about the quality of the material . But in order to understand the information obtained by the different measurement techniques it is important to understand how this is being done. When measuring the carrier lifetimes one is not measuring a property of the semiconductor it self but a property of its carriers, whose states are greatly influenced by the measurement technique [30]. Therefore different measurement techniques may provide different results which may in principle be correct.

Therefore in the following section the nature of each of the main generation recombination mechanisms will be explained with more detail.

B.1.1   Optical Generation

Optical generation is a processes in which conducting charge carriers are generated in a semiconductor by absorbing incoming light photons. Usually when photons

are absorbed by a semiconductor, the electrons in the valence band get excited and jump to the conduction band and are able to transport electric charge. Therefore the probability that a photon gets absorbed by the material depends on both the photon's energy and the material's band gap. In general the main requirement for an absorption event to take place is that the energy of the photon be greater than the bandgap of the semiconductor. In direct band gap semiconductors the absorption can be directly made by converting the energy of the photon into the electrons kinetic energy. In indirect bandgap semiconductors the creation or destruction of a phonon is sometimes required in order to conserve energy and momentum. Macroscopically the most used quantity used to describe how much light is absorbed as it passes a material is the absorption coefficient $\alpha(E)$. This quantity is an energy dependent proportionality factor which comes from a form of the Beer-Lambert law. This states that at a depth x in a material under the effect of an incident beam of light of intensity $I(x)$, the amount of light absorbed by the material is proportional to the intensity of the beam at that point [33]. Therefore:

$$\frac{dI}{dx} = -\alpha I. \tag{26}$$

This is a easy first order differential equation whose solution is easy to find if we know the α coefficient, it takes the form:

$$I(x) = I(0)e^{-\int_0^x \alpha(E,x')dx'}. \tag{27}$$

So from this it is seen that for incident photons of suitable energy E, which we can assume that when absorbed generate free carriers, the generation rate at a material depth x due to an incoming flux of photons $F(E)$ at an energy E is:

$$g(E,x) = (1 - R(E))\alpha(E)F(E)e^{-\int_0^x \alpha(E,x')dx'}. \tag{28}$$

where $R(E)$ is the reflectivity of the surface. For obtaining the total generation rate due to the incoming photons of all wavelengths we should integrate equation (27) over all photon energies.

So $\alpha(E)$ is a coefficient which is in general dependent on the material, and which in order to characterize it the best way to proceed is to measure it. But as mentioned before, the most important process that occurs in the material during light absorption is the transition of electrons from the valence band to the conduction band, which means that the absorption is mostly dependent on the electron transition probabilities. This transition rate can be calculated using the so called **Fermi golden rule**, which is a quantum mechanical analysis of the coupling between the electrons in the atom and the electromagnetic field composed of the incoming light photons. This rule gives the transition rate between and initial and final state of a system composed of an electron and a photon. Usually the initial state is constituted by the electron in a base state and the photon whereas the final state is composed by the excited electron and no photon. These two states are coupled by an interaction Hamiltonian with which we obtain the interaction matrix elements $|T_{if}|$ [34]. In order to apply this rule to the case of absorption of photons by electrons in a semiconductor we multiply the

transition rate given by the Fermi golden rule by the density of conduction band states g_c, the density of valence band states g_v and the difference in the probabilities that valence and conduction band states are occupied given by the Fermi Dirac statistics. Then we integrate over all the possible crystal's wavevectors k_v and k_c and we obtain that the net rate of absorption of photons energy E is given by

$$r_{abs}(E) = \frac{2\pi}{\hbar} \int \int |T_{cv}|^2 \delta(E_c - E_v - E) f_i (1 - f_f)(f_v(\mathbf{k}_v) - f_c(\mathbf{k}_c)) g_v(\mathbf{k}_v) g_c(\mathbf{k}_c) d\mathbf{k}_v d\mathbf{k}_c \tag{29}$$

Therefore the rate at which the material is absorbing energy from the light photons $\frac{\partial U_e}{\partial t} = -E * r(E)$. Since equation (26) tells us how the electromagnetic field losses intensity as it passes the material, $r_{abs}(E)$ can be related to α by making some electromagnetic considerations [33]. It is found that:

$$\alpha = \frac{n_s}{c} \frac{E}{U_e} r_{abs}(E) \tag{30}$$

where c is the speed of light an n_s is the materials index of refraction. It can be seen from equation (29) that calculating α from this method is not straightforward procedure because it requires a exact knowledge of the bands structure and densities of states for the material being analyzed. Nevertheless some general approximations can be made for instance by using the parabolic band approximation it can be shown that for direct gap semiconductors near the band minimum:

$$\alpha = \alpha_0 (E - E_g) 1/2 \tag{31}$$

where α_0 is a constant dependent of the material and E_g is the materials band gap [5]. For indirect band gap semiconductors the situation is more complicated, because the absorption depends on the creation or destruction of a phonon. Sometimes the parabolic band approximation can be again used and if the incoming photon is very energetic, such that $E - E_g >> E_p$ where E_p is the a energy of a created phonon, then

$$\alpha \propto (E - E_g)^2 \tag{32}$$

So in general this means that high energy photons are absorbed before than low energy ones, therefore they tend to be trapped towards the front part of the cell. So as we already saw this is one of the important issues for the current thesis because by decreasing recombination in the emitter of the cell one improves the blue light response of the cell which is the one responsible for the generation of charge carriers in this region of the cell.

B.1.2 Radiative Recombination

Radiative recombination is an unavoidable process in which an excited electron in the conduction band decays to an empty state in the valence band by emitting a photon which carries away the excess electron energy. In direct band gap semiconductors

the decayment of the electron can directly be made by the destruction of an ehp, whereas in indirect bandgap semiconductors the creation of a phonon is sometimes required. For this reason radiative recombination is not a very important limiting factor in indirect materials, as is the case for Si, while for direct ones it is the main recombination mechanism, thus one of the most important efficiency limiting factors. Since radiative recombination is a process contrary to photon absorption, the spontaneous photon emission rate r_{sp} can be calculated by equilibrium considerations with the absorption mechanism. From this it is found that the r_{sp} in one direction is [33] :

$$r_{sp} = \frac{2\pi n_s^2}{h^3 c^2} \frac{\alpha(E)E^2}{e^{(E-\triangle\mu)/k_b T} - 1} \tag{33}$$

where $\triangle\mu$ is the chemical potential arising from the splitting of the quasi Fermi levels under a external disturbance such as light exposure or voltage bias. In order to find the total radiative recombination rate is necessary to integrate equation (33) over all photons energies.

$$U_{rad_t} = \int r_{sp} d_E \tag{34}$$

Radiative recombination is a process that is necessary in order to maintain thermal equilibrium, therefore it is always occurring even in equilibrium conditions and in order to obtain the net radiative recombination rate the value at thermal equilibrium must be subtracted. When disturbances happen the population of holes an electrons increase and their densities follow the relation $np = e^{\triangle\mu/k_b T}n_i^2$, and from this relation and equations (33),(34) it is found that the net recombination rate follows a relation of the form:

$$U_{rad} = B_{rad}(np - n_i^2). \tag{35}$$

So it is seen that the radiative recombination rate is a quantity that is mostly dependend on population of carrier densities out of equilibrium. Furthermore it is found that if the semiconductor is doped U_{rad} takes the forms:

$$U_{rad} = \frac{n - n_0}{\tau_{n,rad}}, \qquad \text{for p doped materials,}$$

$$U_{rad} = \frac{p - p_0}{\tau_{p,rad}}, \qquad \text{for n doped materials,}$$

where are n_0 and p_0 are the electron and holes equilibrium densities, $\tau_{p,rad}$ and $\tau_{n,rad}$ are the minority carriers lifetimes given by

$$\tau_{p,rad} = \frac{1}{B_{rad}N_a}, \qquad \text{with } N_a \text{ the acceptors doping density} \tag{36}$$

and

$$\tau_{d,rad} = \frac{1}{B_{rad}N_d}, \qquad \text{with } N_d \text{ the donors doping density.} \tag{37}$$

In general radiative recombination is an important recombination mechanism because it is the ultimate efficiency determining factor in solar cell, but as mentioned before for practical real semiconductor solar cells as the Si ones there are other recombination mechanisms that affect more the operation of the cells.

B.1.3 Thermal generation

When a semiconductor is at a temperature above the absolute zero the lattice ions have some thermal vibratory energy. Some of this energy is in turn transferred to the electrons, which then get excited to an energetic conducting level, no longer occupying all the available energy states up to the Fermi level and thus giving rise to the bandgap that characterizes semiconductors. This process is called thermal generation.The reverse process can also occur, that is an energetic conducting electron can collide with the latice ions, thus losing its extra energy and decaying to a lower vacancy level. This process is called thermal recombination. In general for solar cells under equilibrium thermal recombination and generation is not an affecting recombination mechanism because usually the generation rate is equal to the recombination rate giving a net zero rate. Nevertheless this rates are taken into account when calculating the net generation-recombination rates given by the other mechanisms.

B.1.4 Shockley-Read-Hall Recombination

One of the most dramatic effects that impurities and defects have on crystals is the formation of intermediate energy levels on the band gap. These energy levels make the defects act as recombination centers to where conducting ehp decay and possibly recombine through a process called Shockley-Read-Hall recombination, for they were the first ones to develop the theory that allows to understand this mechanism.

When an electron decays from the conduction band into an energy level created by a defect (denoted by E_t), two situations may happen: 1) The electron stays for a period of time in the E_t energy level and then it is emitted back to the conduction band. In this case the impurity is called a trap. 2) A hole is also captured into E_t and the electron-hole pair recombines. Then the impurity is called a recombination center. Similar processes can also happen for a hole. Besides this two events, it can also happen in an impurity that a generation process takes place . For this to happen it is necessary that a hole decays from E_t to the valence band and that then an electron be emitted from E_t to the conduction band . In this case the defect is called a generation center. In most cases, defects that act as recombination centers also act as generation centers, so they are called generation-recombination centers (G-R centers).

In the famous 1952 paper Shockley and Read developed a formula for the net rate of recombination in the traps present in a semiconductor, [31]. They found the following relation for it:

$$U_{SRH} = \frac{C_n C_p (pn - p_1 n_1)}{C_n(n + n_1) + C_p(p + p_1)}.$$ (38)

where C_n and C_p are recombination constants dependent on the defects, they represent the probability per unit time that electrons/holes decay in a defect state in case they have available empty states . p and n are the density of conducting holes and electrons and the product $p_1 n_1$ is equal to the square of the intrinsic charge density n_i^2. In appendix (1) it is presented a brief outlook to the derivation of formula (43) as well as a better explanation of the meaning of the constants C_n and C_p.

In order to have a nonzero net recombination rate it is necessary that the electron and holes densities have deviations above their thermal equilibrium values n_0 and p_0, that is that some external source generates electron hole pairs. So if there is a deviation of electrons and holes $\triangle n$ and $\triangle p$ respectively, then the carrier densities are:

$$n = n_0 + \triangle n, \qquad p = p_0 + \triangle p. \tag{39}$$

In many cases, when the badgap is narrow as in Si, there is very little trapping in the defect states and they act mostly as generation-recombination centers, in this cases $\triangle n \approx \triangle p$. Using equation (43) it is found that the SHR lifetime is given by:

$$\tau_{SRH} \equiv = \frac{\triangle n}{U_{SRH}} = \frac{\tau_p(n_0 + n_1 + \triangle n) + \tau_n(p_0 + p_1 + \triangle p)}{n_0 + p_0 + \triangle n} \tag{40}$$

where $\tau_n = 1/C_n$ represents the decaying lifetime for electrons in case all traps have available holes, which would be the case for highly P doped semiconductor [31]. So it is seen in formula (45) that besides the nature and density of the defects, the SHR lifetime depends in general also on the injected density charge carriers $\triangle n$. This is a quantity that can be varied depending on the particular measurement technique used, therefore in order to interpret correctly the information gained from a measurement it is necessary to understand well the particular measurement technique. Nevertheless there are two injection regimes in which the SHR lifetimes are independent of $\triangle n$, this are the low and high injection regimes. In the low injection regime the injected minority carrier density is small compared to the majority carrier density. So if it is a P type semiconductor $\triangle n = \triangle p \ll p_0$ and $p_0 \gg n_o$, then it is seen that equation (45) approximates as:

$$\tau_{SRH} \approx \tau_p(n_1/p_0) + \tau_n(1 + p1/p_0) \tag{41}$$

Furthermore if the defects energy levels are not too near the conduction or valence band the lifetime takes the simple form $\tau_{SRH} \approx \tau_n$.

Now in the high level injection regime $\triangle p \gg p_0, n_0, p_1, n_1$ in this case (45) approximates as:

$$\tau_{SRH} \approx \tau_p + \tau_n \tag{42}$$

In general when measuring lifetimes there are no standard values used for the injection levels, rather this depend on the requirements of the different measurement techniques.

B.1.5 SHR Surface recombination

In general recombination through defects is a phenomenon present over all the length of the semiconductor, but the nature of the defects present in the interfaces is different from the ones in the bulk of the material. Therefore there is no reason to think that the cross sections and energy levels of the defects present in one of these two regions of a semiconductor are equal. Since the surface is assumed to be a very thin layer of material we think of its defects as being distributed over a 2 dimensional and not in a 3 Dimensional array. For this reason the recombination at the surface is best characterized by a recombination flux which tells us the number off carriers that are recombining at the surface per unit time per unit area. So if we assume that the surface has a very small thickness δx the recombination flux in terms of the surface recombination rate (U_s) would be $U_s \delta x$. With this we define the surface recombination velocity (s_r) by $U_s \delta x = s_r \triangle n$, so that it would represent the velocity at which charges are being driven to the surface to recombine. In other words is as we had a leakage current of minority carriers escaping at the surface [33]. Using a similar analysis as the one used for deriving these quantities in the bulk in equation 43), it is found that the net SHR surface recombination velocity is given by [30], [33] :

$$s_r = \frac{s_n s_p (p_{os} + n_{os} + \triangle n_s)}{s_n (n_{0s} + n_{1s} + \triangle n_s) + s_p (p_{0s} + p_{1s} + \triangle p_s)}. \tag{43}$$

where the quantities s_n and s_p are quantities analogous to C_n and C_p, thus they represent the average probability that an electron or hole at the surface respectively decays into some defect state in case they all have available empty states (see appendix B.2). In general when considering surface recombination between two regions with different dopings or materials , care must be taken with respect to the position of the surface, for not always do the surfaces between the two regions coincide with the edge of the depletion region, as it is sometimes assumed. As a matter of fact surface recombination is a more complicated phenomenon than bulk recombination because besides the density and energy of the interface defect states it also depends on the particular state of the surface ([32]). In general measuring the surface lifetime is not an easy task for most of the measuring techniques don't differentiate between surface and bulk recombination. Nevertheless there are some special techniques that could help to separate the recombination in these two places, for instance in reference [30] it is pointed out that in reference [35] the surface recombination lifetime can be obtained from the following relation

$$\tau_s = \frac{1}{\beta^2 D_n}. \tag{44}$$

where D_n is the electron diffusion constant and β can be obtained by somehow solving the following equation:

$$\tan(\frac{\beta t}{2} = \frac{s_r}{\beta D_n} \tag{45}$$

where t is the sample thickness.

B.1.6 Auger Recombination

Auger recombination is an intrinsic process that occurs in semiconductors when a conducting electron collides with another one, giving up some of its extra energy and then decaying to a lower energetic level by recombining with an available hole. The now highly energetic electron will in turn transfer some of its energy to the lattice, thus converting it into heat. Since Auger recombination involves three different charge carriers, its recombination rate is proportional to the square of the carrier density. Therefore the general expression for the Auger recombination lifetime is [30]:

$$\tau_{Aug} = \frac{1}{C_{p,Aug}(p_0^2 + 2p_0 \triangle n + \triangle n^2) + C_{n,Aug}(n_0^2 + 2n_0 \triangle n + \triangle n^2)} \tag{46}$$

where $C_{p,Aug}$ and $C_{n,Aug}$ are the Auger holes and electrons recombination coefficients respectively. As it can be seen from equation 46 Auger recombination is a doping concentration dependent process whose effect on the efficiency of the semiconductors is more important on highly doped ones. Unlike radiative recombination where the emission of a photon conserves energy but not momentum, the collision of two electrons conserves both energy and momentum therefore Auger recombination is a process that is frequent in indirect bandgap semiconductors, thus being one of the most important recombination mechanism in very pure materails such as Si and Ge.

B.1.7 Effective lifetime

As we have seen, recombination is a process that is present in every semiconductor material and is carried out by more than one mechanism. For this reason the total recombination rate is the sum of the contributions of each one of the mechanisms exposed in the former sections. As we saw which mechanism is more dominant in each region depends mainly on the nature and purity of the semiconductor. Since the minority carriers lifetimes is in general inversely proportional to the recombination rates (equation 24) we can define an effective recombination lifetime (τ_{eff}) which gives the average time that a conducting charge would take to decay be means of any of the recombination mechanisms.

$$\frac{1}{\tau_{eff}} = \left(\frac{1}{\tau_{rad}} + \frac{1}{\tau_{Auger}} + \frac{1}{\tau_{SHR}} \right) + \frac{1}{\tau_{surface}} \tag{47}$$

So as we saw the first three terms inside the parenthesis are due to the recombination in the bulk of the material, so it is common to associate this terms as bulk recombination lifetime τ_{bulk}^{-1} while the last term is the recombination in the surface, this might be measured using certains techniques like saturation current measurements (section 3.2.4) [36].

Most of the commonly used lifetime measurement techniques don't differentiate the actual recombination mechanism but actually give as result the effective lifetime.

Nevertheless there are special techniques that allow to obtain measurements of separate recombination mechanisms.

B.2 Shockley Read Hall recombination rate

In the following appendix it will be presented a rough sketch of the original derivation of the Shockley-Read-Hall recombination rate formula made by Shockley and Read [31]. For doing this they first calculated the average probability that electrons with energy E and average random velocity v_e falls into a empty trap with cross-section σ_n. This probability denoted $c_n(E)$ would be

$$c_n(E) = \sigma_n v_e \tag{48}$$

Then by assuming thermal equilibrium Fermi Dirac statistics can be used in order to find the occupation probabilities . So if a certain state has energy E and Fermi level F the probability that it is occupied is:

$$f = \frac{1}{1 + e^{(E-F)/kT}} \tag{49}$$

with k the Boltzmann constant and T the average temperature.
The probability that an electron decays into a trap is proportional to the probability that there is a hole in the trap times the number of traps present. Thus if we denote by f_{pt} the probability that a trap be occupied by a hole, N_t the densities of traps and $N(E)dE$ the density of electrons states in the range dE, it is found that the capture rate of electrons into the trap is:

$$dU_{cn} = f_{pt} N_t c_n(E) f(E) N(E) dE. \tag{50}$$

By the other hand for electrons to be emitted the traps should have occupied electronic states and the conduction band should have empty ones, that is, there should be holes in the conduction band. Thus if f_t is the occupation probability of electrons in the traps and f_p the holes occupation probability in the conduction band (with $f = 1 - f_p$) the emission rate can be expressed as:

$$dU_{en} = f_t N_t e_n(E) f_p(E) N(E) dE \tag{51}$$

where e_n is a emission rate constant and the occupation probability F_t is described by its own quasi Fermi level F_t. Under thermal equilibrium the quasi Fermi levels of the electrons and traps should be equal and the net rate of capturing and emission into the traps must be zero. Therefore by equating equations (48) and (51) the following relation is found:

$$e_n/c_n = e^{(E_t - E)/kT} \tag{52}$$

Thus using this result and again equations (48) and (51), it is found after a small mathematical manipulation that the net rate of electron capturing into the trap U_{nn} (absorption minus emission) can be expressed as:

$$U_{nn} = [1 - e^{(F_t - F_n)/kT}]f_{pt}N_t \times \int_{E_c}^{\infty} f(E)N(E)c_n(E)dE, \qquad (53)$$

where the integrated quantity represents a non normalized average over c_n. But when a semiconductor is moderately doped the electron Fermi level is not too high, thus it follows that for most of the electrons in the conduction band $E - F \gg kT$ This implies that:

$$\frac{1}{1 + e^{(E-F)/kT}} \approx e^{(F-E)/kT}$$

so the Boltzmann statistics can be used instead of the Fermi Dirac. This just reflects the fact that the electronic states in the conduction band is continuous rather than discrete.

$$\langle c_n \rangle = \frac{\int_{E_c}^{\infty} e^{(E_c-E)/kT}N(E)c_n(E)dE}{\int_{E_c}^{\infty} e^{(E_c-E)/kT}N(E)dE} \equiv \frac{\int_{E_c}^{\infty} e^{(E_c-E)/kT}N(E)c_n(E)dE}{N_c} \qquad (54)$$

where we have defined N_c, the effective density of states. Using this we can define $C_n = N_t\langle c_n \rangle$, which represents the probability per unit time that an electron in the conduction band gets trapped in any of the empty traps given in the density N_t. Also we write the density of electrons in the conduction band as $n = N_c e^{(F_n - E_c)/kT}$ and with this we rewrite the net rate of absorption equations (53) as:

$$\begin{aligned} U_{nn} &= [1 - e^{(F_t - F_n)/kT}]f_{pt}nC_n = [f_{pt}n - f_{pt}N_c e^{(F_n - E_c)/kT}e^{(F_t - F_n)/kT}]C_n \quad (55) \\ &= [f_{pt}n - f_{pt}N_c e^{(F_t - E_c)/kT}]C_n = [f_{pt}n - f_t N_c e^{(E_t - E_c)/kT}]C_n \end{aligned}$$

$$(56)$$

where in the last step we used $f_{pt} = 1 - f_t = f_t e^{(E_t - F_t)/kT}$. Now we define from the last term in the last equality $n_1 = N_c e^{(E_t - E_c)/kT}$ which is just the number of electrons in the conduction band for a Fermi level at E_t.

So with this we have that the net rate of electron absorption in the traps is :

$$U_{nn} = C_N[f_{pt}n - f_t n_1] \qquad (57)$$

Similarly the net rate of holes capture in the traps is found to be:

$$U_{np} = C_p[f_t n - f_{pt} p_1] \qquad (58)$$

Now let's find the net rate of recombination in the traps for the case of steady rate of generation of electron-hole pairs U, which is the common case for semiconductors under constant illumination. Since electrons and holes are being generated at the same rate, their rate of decayment into the traps should be equal. Thus equating equations (57) and (58) we find that:

$$C_N[(1 - f_t)n - f_t n_1] = C_p[f_t n - (1 - f_t)p_1], \qquad (59)$$

Both f_{pt} and f_t can be found from this equation by replacing and solving. Then after replacing their values into equations (57) or (58) it is found that the recombination rate in the traps is:

$$U = \frac{C_n C_p (pn - p_1 n_1)}{C_n(n + n_1) + C_p(p + p_1)}. \tag{60}$$

In in this equation we have the term $p_1 n_1$ which is equal to the square of the intrinsic charge carrier concentration:

$$p_1 n_1 = N_c N_p e E_v - E_c/kT = N_c N_v e - E_G/kT = n_i^2. \tag{61}$$

B.3 Metal-N type semiconductor interface.

Similarly to what happens in a PN junction, when a metal-semiconductor interface is formed, the Fermi Levels of the two materials equate by exchanging some electric charges until the chemical potentials difference is zero. If we have a N doped semiconductor joined together with a metallic material such that the work function of the metal Φ_m is bigger than the work function of the semiconductor Φ_n, electrons will flow to the metal until enough charge is accumulated so to create a field that contrarest the flux. This creates a potential barrier as illustrated in figure 36a

(a) Lowly doped semiconductor

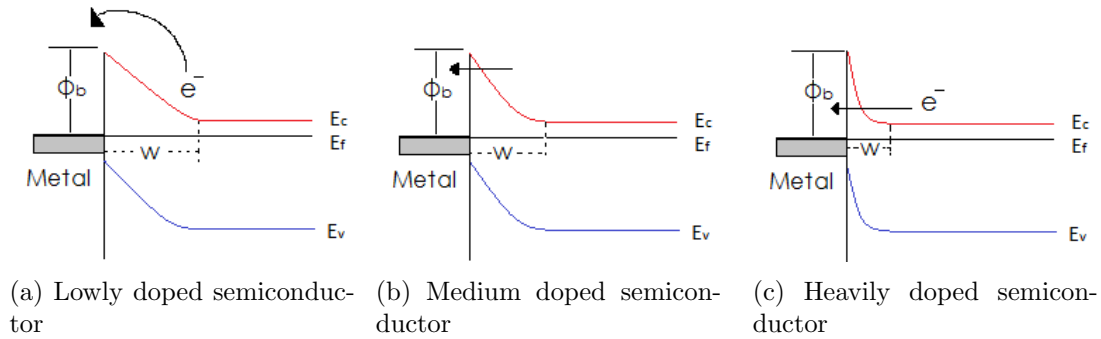(b) Medium doped semiconductor

(c) Heavily doped semiconductor

Figure 36: The different conducting regimes in a metal semiconductor interface

Just as in a PN diode the conduction through the junction depends on the height of this barrier, thus in order to have a good conducting contact (called Ohmic contact) a very low barrier is desirable. In the early days when Schottky proposed his metal-semiconductor interface theory, it was thought that the height of the barrier depended only on the metal's work function and therefore by choosing a metal with appropriate work function it could be easy to create a very low resistance interface. But soon it was found out that for most of the popular semiconductor materials the barrier height is independent of the metals work function because of a Fermi level pinning effect, which even today is not completely understood [7].
Given this it was realized that the only possible way to control the junction conduction was through the semiconductor doping level. In general the barrier height Φ_B is independent of the semiconductor's doping concentration, but as we saw on equation

3 the depletion width decrease with increasing doping concentration. If the barrier height and the depletion width are large the only way that electrons have to go from the semiconductor to the metal is by thermal excitation (formerly called thermionic emission), figure 36a . Nevertheless when the depletion zone is narrow enough the electrons can overcome the barrier by tunneling thus being able to create a fair amount of current. Therefore by increasing the doping concentration in the semiconductor conduction will be enhanced by means of both tunnel effect and thermionic emission, this in turns decreases the voltage drop across the junction, giving as result a current-voltage characteristics propper of an Ohmic contact. In figure 36 it can be seen three conducting regimes that happen in the metal semiconductor interface according to the doping level. In figure 36a the semiconductor is lightly doped, thus the depletion width is large so all the electrons that go from the semiconductor to the metal do it by thermionic emission. In figure 36b the semiconductor is intermediately doped, so the depletion width is not so large, thus some electrons can tunnel through the junction while others still jump to the metal by thermionic emission. In 36c the semiconductor is heavily, so the depletion width is very narrow allowing all the electrons passing from the semiconductor to the metal to tunnel through the junction. Next we will see what is the necessary condition for each one of this regimes to happen and what are the respective J-V characteristics

The current density in a metal-semiconductor interface in which the depletion width is wide enough so that no Quantum tunneling happens and only Thermionic emission is possible is given by:

$$J = AT^2 e^{q\phi_b/K_BT}(e^{qV_a/K_BT} - 1) \tag{62}$$

where $A = 4\pi m * q(k_BT)^2/h^3$ is the Richardson constant for thermionic emission and V_a is the applied voltage.This equation is derived by using the classical Richardsons law of emission taking into account that since electrons have also a wave behavior some of them can be reflected at the boundary even though they have enough energy to surpassed it [12].

Now the Quantum tunneling current. Suppose we have an electron coming from the semiconductor to the metal, the probability that it crosses the junction interface is given by the square of the transmission coefficient $T(E)$. The rate at which the electrons hit such interface per unit area would be given by $f_n(\mathbf{k})v_v(\mathbf{k})d^3\mathbf{k}/(2\pi)^3$, where f_n is the Fermi distribution function for the electrons in the N-type semiconductor (see equation 51) and v_v is the average speed perpendicular to the surface [9] . So we have that the current density from the metal to the semiconductor is given by:

$$2e \int_{z^+} f_n(\mathbf{k}) \left[1 - f_m(\mathbf{k})\right] |T(\mathbf{k})|^2 \frac{d^3\mathbf{k}}{(2\pi)^3} \tag{63}$$

where the term $[1 - f_m(\mathbf{k})]$ accounts for the availability of holes in the metal and we have set the interface at $z = 0$ with the semiconductor in the $+$ side . Similarly there is a current from the metal to the semiconductor which would be:

$$-2e \int_{z^-} f_m(\mathbf{k}) \left[1 - f_n(\mathbf{k})\right] |T(\mathbf{k})|^2 \frac{d^3\mathbf{k}}{(2\pi)^3} \tag{64}$$

So adding both currents the net total current would be:

$$J = -2e \int_{z^-} [f_n(\mathbf{k}) - f_m(\mathbf{k})] \, |T(\mathbf{k})|^2 \frac{d^3\mathbf{k}}{(2\pi)^3} \tag{65}$$

Thus in order to find these tunneling current it is necessary to find an expression for the transmission coefficient. This in principle can be done by finding the wave function $\Psi(z)$ from solving $Scrödinger's$ equation with the appropriate Hamiltonian and boundary conditions. Then the square of the transmission coefficient would be given by the square of the square function in the region $z < 0$ divided by a normalization constant I_0^2:

$$|T(\mathbf{k})|^2 = \frac{\Psi(z)^2}{I_0^2} \qquad z < 0 \tag{66}$$

Suppose that the depletion region has a width d, then potential in this zone is obtained by simply solving the Poisson's equation with N_d as the total charge (just as it is usually done for the PN diode). So if the contact is under an applied bias V_b the resulting energy potential is:

$$\varphi(z) = \frac{e^2 N_d}{2\epsilon}(x - d_s)^2 + e(V_a - E_{f_N}) \qquad 0 \le z \le d \tag{67}$$

Where E_{f_N} is the electrons Fermi level in the semiconductor. With this this the Hamiltonian of the system is :

$$
\begin{aligned}
\hat{H} &= -\frac{\hbar^2}{2m_n*}\frac{d^2}{dz^2}, & z \ge d \\
\hat{H} &= -\frac{\hbar^2}{2m_n*}\frac{d^2}{dz^2} + \varphi(z), & 0 < z < d \\
\hat{H} &= -\frac{\hbar^2}{2m_m*}\frac{d^2}{dz^2} + e(V_a - E_{f_N}), & z \le 0
\end{aligned}
\tag{68}
$$

where m_m* and m_n* are the electron's effective masses in the metal and semiconductor respectively. One way to solve the $Scrödinger's$ equation for this Hamiltonian is to use the WKB approximation in which the wave function $phi(z)$ is expressed as a exponential function. For example in this case the wave function in the region $z < d$ would have the form [8]:

$$\psi = I_0 \, T e^{ik_{mz}(z-d)}, \qquad z \le 0$$

One of the usual procedures for solving $Scrödinger's$ equation is postulating a solution for the wave function and plug it in the equation with the correct boundary conditions so to find the eigenfunctions and the energy eigenvalues. But as in everything in semiconductor physics there is no exact analytical solution for the eigenvectors in this case.F.A Padovani and R.Stratton expanded the transmission coefficient

in Taylor series for the energy around the electron's Fermi level of the semiconductor [10]. They only picked out the first two terms and from this they arrived at the following expression for the current density

$$J = -\frac{Ae^{-b_1}}{(c_1 k_B T)^2} \frac{\pi c_1 k_B T}{\sin(\pi c_1 k_B T)} \left[1 - e^{-c_1 V_a}\right] \tag{69}$$

where b_1 and $c1$ are the parameters of the first two terms of the Taylor expantion which after evaluation for junctions such that $e\phi_b >> E_{fn}$ are found to be:

$$b_1 = \frac{(e\phi_b - E)}{E_{00}} \qquad\qquad z \geq d \tag{70}$$

$$c_1 = \frac{\log\left[4\frac{\phi_b - E}{E_{fn}}\right]}{2E_{00}}, \qquad 0 < z < d \tag{71}$$

where E_{00} is given by :

$$E_{00} = q\hbar \left(\frac{N_D}{2m^*\epsilon}\right)^{1/2}$$

In this expression the doping concentration N_D appears because it was present in the junction potential and width (equations 3 and 67).

The third coefficient in the Taylor expantion is $g_1 = 1/4E_{00}E_{fn}$. This term was not taken into account when arriving at equation 69. This means that this equation is only valid when the two first terms in the Taylor expansion of the transmission coefficient are bigger than the third and subsequent ones.In reference [10] and [11] they show that this is equivalent to the following condition on the temperature T of the sample:

$$K_b T < \left[2(E_{00}E_{fn})^{-1/2} + 2(E_{00})\log(4e\phi_B/E_{fn})\right]^{-1} \tag{72}$$

So since phi_B and E_{fn} and are constants of the metal-semiconductor interface at the end what matters in inequality 72 is the relation $K_B T/E_{00}$. In reality what happens is that when 72 is not satisfied the current from the semiconductor to the metal due to Quantum tunneling is negligible, thus in general the quantity $K_B T/E_{00}$ tells us how important is the thermionic emission current with respect to the Quantum tunneling. Since it is difficult to control the temperature of the system the relation $K_B T/E_{00}$ can only be modified by means of the semiconductor doping level , which means that N_D will determine the conducting characteristics of the contact. As already said this is illustrated in figure 36 where three doping situations are illustrated. The case that $k_B T/E_{00} \gg 1$ is called the Thermionic Emission regime (**TE**), which correspond to lightly doped semiconductor. When $k_B T/E_{00} \sin 1$ it is called the thermionic-field emission regime (TFE) and this corresponds to medium doped semiconductors. In this case electrons to the metal by both jumping over the potential barrier and through tunneling. In the case that $k_B T/E_{00} \ll 1$ the E_{00} term

is dominant so the conduction is done mostly by tunneling. This happens when the semiconductor is highly doped. Now that we have expressions for the current density due to Quantum tuneling and thermionic emission the conduction through the junction can be evaluated. Theoretically the resistance in the contact is characterized by the specific interfacial resistivity ρ_i defined as

$$\rho_i = \left. \frac{V}{J} \right|_{V=0} \tag{73}$$

This quantity is a mainly theoretical quantity which is not possible to measure because the resistivity in a metal semiconductor interface is not only caused by the interface it self but will have also some contributions from both regions in each side of the interface. But nevertheless it gives us some insight in the nature of the resistance in the interface. By applying equation (73) to equation (62) one obtains the following ex presion for ρ_i in the thermionic emission regime [7]:

$$\rho_i(TE) = \rho_1 e^{q\phi_B/k_b T}, \qquad\qquad \text{for} k_b T/E_{00} \gg 1 \tag{74}$$

where $\rho = k/(qAT)$.
For the Thermionic field emission regime Padovani developed an expression of the following form [10]:

$$\rho_i(TFE) = C_1 \rho_1 e^{q\phi_B/E_0} \qquad\qquad \text{for } k_b T/E_{00} \sim 1 \tag{75}$$

where $E_0 = E_{00} \coth(E_{00/k_b T})$ and C_1 is a function of T, N_D and ϕ_B. This equation is valid when $E_0 < 2/3(\phi_B + E_{fn})$.
For the FE region one uses equation (69) and gets an expression of the form:

$$\rho_i(FE) = C_2 \rho_1 e^{q\phi_B/E_{oo}}, \qquad\qquad \text{for } k_b T/E_{00} \ll 1 \tag{76}$$

where again C_2 depends on T, N_D and ϕ_B. Thus we see in equations 75 and 77 that the resistance in the metal-semiconductor interface for the **TFE** and **FE** decrease with semiconductor doping, because they have the following dependence on N_d:

$$exp\left(\frac{\phi_B}{\sqrt{N_d}\coth\left(E_{00}/k_B T\right)}\right) \qquad\qquad \text{for the } \textbf{TFE} \text{ regime,}$$

$$exp\left(\frac{\phi_B}{K_b T}\right) \qquad\qquad \text{for the } \textbf{FE} \text{ regime.}$$

which are decreasing functions of N_d. Figure (37) illustrates the expected dependence of the resistance on the doping concentration for the three different regimes (taken from reference [13]).

Looking at equations (75) and (77) and Figure (37) it is clear that in order to have a good conduction in an N-type semiconductor-metal interface the semiconductor ought to be highly doped.
As mentioned before the measurement of the resistance in the contact is not an easy
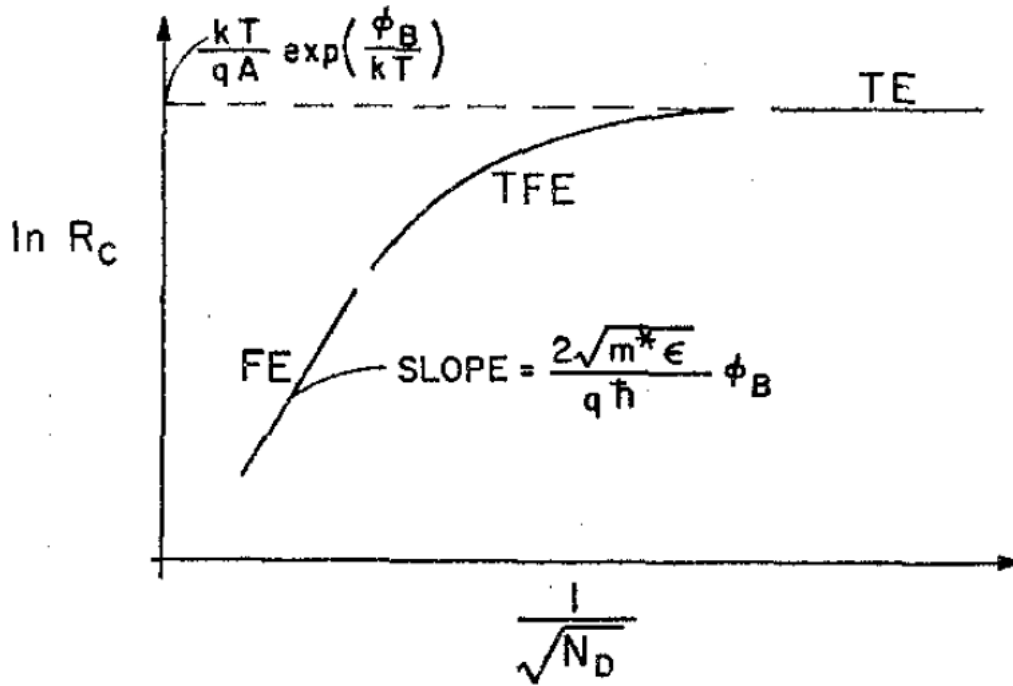
Figure 37: Expected theoretical dependence of ρ_i on N_d. Taken from [13]

task because when doing it is not always clear which part of the current was lost due to the resistance in the metal-semiconductor interface and which was lost due to recombination and leakage currents in the semiconductor. Nevertheless several methods for doing so have been developed, they can vary in complexity depending on the level of accuracy desired. The most basic one is the two terminals methods in which a current is forced to pass betweentwo metal terminals which have a semiconductor in between. Then the total resistance of the structure is measured and then the contact resistance is found by subtracting the semiconductor spreading resistance from the total measured resistance. This method fails in that determination of the semiconductors spreading resistance comes out with a great uncertainty that usually gives place to a great error to the contact resistance[7]. Some other more accurate methods include multiple terminals methods which by playing with the geometry of the configuration of the terminals the innaccuracies due to the measuring of complementary resistances in the system are possible to reduce.

In addition to the doping level of the semiconductor the other factor that affects conduction through the metal contacts is the contact area. This is so because in semiconductors we have current densities flowing around, so that the total current that passes through a metal contact of area A is $J \times A$. The maximum power output that can pass through a contact is given by $AJ_{mp}V_{mp} =$, where J_{mp} and V_{mp} are the current density and Voltage at the maximum power point [4]. Therefore in general

the higher the metal contacts area is, the better the charge transport will be. But as mentioned before this might be a problem when designing the solar cell, because in general the wafer regions lying under contacts will be shadowed and no light absorption will occur there. Therefore the dimensions and the geometry of the contacts is one of the parameters that is important to optimize.

One method to optimize the width of the metal busbar is to calculate the power loss due to the resistive losses in the busbar and also the power loss due to the shadowing cause by it. These two quantities depend on the area and thus its thickness. Then by adding them up and differentiating with respect to the thickness one finds the value that gives the minimum power loss. This happens when both power loss mechanisms are equal and is given by:

$$W_B = A\sqrt{\frac{R_{msb}}{3}\frac{J_{mp}}{V_{mp}}} \tag{77}$$

where W_B is the optimal busbar width and R_{msb} is metal semiconductor sheet resistance in the bussbar [4] .

References

[1] Global Market outlook for photovoltaics 2013-2017. European photovoltaics industry association.

[2] John David Jackson, Classical Electrodynamics Third Edition

[3] William Shockley and Hans J. Queisser, "Detailed Balance Limit of Efficiency of p-n Junction Solar Cells", Journal of Applied Physics, Volume 32 (March 1961), pp. 510-519;

[4] Martin A . Green. Solar Cells, operating principles technology and system applications, Prentice Hall 1982.

[5] Solid state physics, Guiseppe Grosso, Guisepe Pastori Parravacini, Academic Press 2001

[6] Solid state physics, Guiseppe Grosso, Guisepe Pastori Parravacini, Academic Press 2001 grosso cap 13.

[7] Semiconductor Material and Devices Characterization. Third Edition, by Dieter K. Schroder. Cap 3

[8] J. W. Conley, C. B. Duke, G. D. Mahan, and J. J. Tiemann, Electron Tunneling in Metal-Semiconductor Barriers, Phys. Rev. 150, 466 (1966).

[9] Theory of Electron Tunneling in Semiconductor Junctions Fredkin, D. R.; Wannier, G. H. Physical Review, vol. 128, Issue 5, pp. 2054-2061

[10] F.A Padovani and R.Stratton, FIELD AND THERMIONIC-FIELD EMISSION IN SCHOTTKY BARRIERS Solid-State Electronics Pergamon Press 1966. Vol. 9, pp. 695-701.

[11] E. L. MURPHY and R. H. GOOD, JR., Phys. Rev. 3. M. M. ATALLA and R. W. SOSHEA, Scientific Report 102, 1464 (1956).

[12] 14. E.H. Rhoderick and R.H. Williams, Metal-Semiconductor Contacts, 2nd ed., Clarendon, Oxford, 1988.

[13] A. Y. C. YU, ELECTRON TUNNELING AND CONTACT RESISTANCE OF METAL-SILICON CONTACT BARRIERS*, Solid-State Electronics Pergamon Press 1970. Vol. 13, pp. 239-247.

[14] EDVRD BLINT KUTHI, Crystalline silicon solar cells with selective emitter and the self-doping contact

[15] Crystalline silicon solar cells with selective emitter and the self-doping contact EDVRD BLINT KUTHI

[16] Simple integral screenprinting process for selective emitter polycrystalline silicon solar cells, J. Szlufcik, H. E. Elgamel, M. Ghannam, J. Nijs, and R. Mertens Citation: Appl. Phys. Lett. 59, 1583 (1991);

[17] A. Rohatgi1 , M. Hilali1, D. L. Meier2, A. Ebong1, C. Honsberg1 , A. F. Carrol3, and P. Hacke2, SELF-ALGINED SELF-DOPING SELECTIVE EMITTER FOR SCREEN-PRINTED SILICON SOLAR CELLS.

[18] G. Hahn , STATUS OF SELECTIVE EMITTER TECHNOLOGY ,Preprint 25th EU PVSEC / WCPEC-5 Valencia 2010

[19] HIGH EFFICIENCY SELECTIVE EMITTER ENABLED THROUGH PATTERNED ION IMPLANTATION, Russell Low1, Atul Gupta1, Nicholas Bateman1, Deepak Ramappa1, Paul Sullivan1, Wesley Skinner1, James Mullin1.

[20] J.M. Serra, R. Gamboa and A.M. Vallra, A study on selective emitter formation through an oxide mask for silicon solar cells.

[21] H. Antoniadis, F. Jiang, W. Shan, Y. Liu, All screen printed mass produced silicon ink selective emitter solar cells, Proc. 35th IEEE PVSC, Honolulu 2010

[22] Helg Haverkamp, Amir Dastgheib-Shirazi , Bernd Raabe , Felix Book , Giso Hahn 1,2,MINIMIZING THE ELECTRICAL LOSSES ON THE FRONT SIDE: DEVELOPMENT OF A SELECTIVE EMITTER PROCESS FROM A SINGLE DIFFUSION

[23] Fabrication engineering at the micro and nanoscale / Stephen A. Campbell, New York : Oxford University Press ISBN: 9781613441151, 161344115x

[24] M. H. Rein. Wet chemical wafer cleaning of muliticrystalline silicon. Master?s thesis. Department of Mathematical Science and Technology, University of Lifesciences, 2001.

[25] R.B. Fair, "Concentration profiles of diffused dopants in silicon, in F.F.Y. Wang, Ed. Impurity Doping Process in Silicon, North Holland, New York, 1981

[26] Optimiisation of SINx:H anti-reflection coatings for silicon solar cells J. Hofstetter, C. del Cañizo, S. Ponce-Alcantara, A. Luque Instituto de Energia Solar - Universidad Politecnica de Madrid

[27] Chetan Singh Solanki, Solar Photovoltaics : Fundamentals, Technologies and Applications

[28] M. Mller, P.P. Altermattb, K. Schlegela, G. Fischera Evaluating The Quality Of Selective Emitter Structures By Imaging The Emitter Saturation Current Density, SiliconPV: April 03-05, 2012, Leuven, Belgium

[29] pveducation.org

[30] D.K. Schroder, "Semiconductor Material and Device Characterization",Chapter 7 ,Wiley-IEEE Press; 3 edition ISBN-13: 978-0471739067 —

[31] D.K. Schroder, Carrier Lifetimes in Silicon, IEEE TRANSACTIONS ON ELECTRON DEVICES, VOL. 44, NO. 1, JANUARY 1997

[32] T. Otaredian, ?The influence of the surface and oxide charge on the surface recombination process,? Solid-State Electron., vol. 36, pp. 905915, June 1993.

[33] The Physics of Solar Cell, Jenny Nelson, Imperial college Press 2003

[34] Claude Cohen-Tannoudji, Bernard Diu, Franck Lalo, Quantum Mechanics Vol 2. Wiley, 1977

[35] Analysis of the interaction of a laser pulse with a silicon wafer: Determination of bulk lifetime and surface recombination velocity Keung L. Luke1 and Li Jen Cheng, J. Appl. Phys. 61, 2282 (1987);

[36] Chih Hsin Wang,Minority-Carrier Lifetime and Surface Recombination Velocity Measurement by Frequency-Domain Photoluminescence IEEE TRANSACTIONS ON ELECTRON DEVICES. VOL. 38. NO. 9, SEPTEMBER 1991

[37] Laser doping for microelectronics and microtechnology ,Original Research Article Applied Surface Science, Volume 247, Issue 14, 15 July 2005, Pages 537-544 Thierry Sarnet, Gurwan Kerrien, Nourdin Yaakoubi, Alain Bosseboeuf,

[38] J.M. Fairfield,G.H. Schwuttke, Silicon diodes made by laser irradiation,Solid-State Electronics

Volume 11, Issue 12, December 1968, Pages 1175-1176

[39] R. F. Wood,Modeling of nonequilibrium melting and solidification in laser-irradiated materials Physical Review B, VOLUME 34, NUMBER 4.

[40] Back-contacted back-junction silicon solar cells Krister Mangersnes THESIS University of Oslo. 2010

[41] Laser induced defects in laser doped solar cells Z. Hameiri et al., Progress in Photovoltaics Research and Applications 19, 391 (2011) dd

[42] Properties of Silicon, EMIS Datareview Series No. 4 (INSPEC, London, 1988).

[43] Toshiyuki Sameshima and Setsuo Usui Analysis of Dopant Diffusion in Molten Silicon Induced by a Pulsed Excimer Laser Jpn. J. Appl. Phys. 26 (1987) pp. L1208-L1210

[44] R. F. Wood, Modeling of nonequilibrium melting and solidification in laser-irradiated materials PHYSICAL REVIEW B 8 VOLUME 34, NUMBER 4 15 AUGUST 1986

[45] R. F. Wood, Macroscopic theory of pulsed-laser annealing. I.Thermal transport and melting PHYSICAL REVIEW B VOLUME 23, NUMBER 6 15 MARCH 1981

[46] R. F. Wood, LASER PROCESSING OF SEMICONDUCTOR MATERIALS 1, Ann. Rev. Mater. Sci. 1982. 12: 323-50

[47] R. T. Young and R. F. Wood,LASER PROCESSING OF SEMICONDUCTOR MATERIALS Ann. Rev. Mater. Sci. 1982. 12: 323-50

[48] Jellison GE, Modine FA. Optical absorption of silicon between 1.6 and 4.7 eV at elevated temperatures. Applied Physics Letters 1982; 41: 180-182.

[49] Young RT, Narayan J, Wood RF. Electrical and structural characteristics of laser-induced epitaxial layers in silicon. Applied Physics Letters 1979; 35: 447-449.

[50] P.M. MOONEY 4) (a) , R.T. YOUNG (b), J. KARINS (a), Y.H. LEE . Defects in Laser Damaged Silicon Observed by DLTS. phys. stat. sol. (a) 48, K31 (1978)

[51] Characterization of a diode double-end pumped Nd:YVO4 laser for high-bit-rate free-space and intersatellite communications

[52] Gould, R. Gordon (1959). "The LASER, Light Amplification by Stimulated Emission of Radiation". In Franken, P.A. and Sands, R.H. (Eds.). The Ann Arbor Conference on Optical Pumping, the University of Michigan, 15 June through 18 June 1959. p. 128.

[53] 3. A. Safiei, H. Windgassen, K. Wolter, H. Kurz. Emitter Profile Tailoring to Contact Homogeneous High Sheet Resistance Emitter. Energy Procedia, Volume 27, 2012, Pages 432-437.

[54] UNDERSTANDING AND DEVELOPMENT OF MANUFACTURABLE SCREENPRINTED CONTACTS ON HIGH SHEET-RESISTANCE EMITTERS FOR LOW-COST SILICON SOLAR CELLS, page 119. Mohamed M. Hilali. PHD thesis Georgia Institute of Technology August 2005

[55] M. Mllera*, P.P. Altermattb, K. Schlegela, G. Fischera, Evaluating The Quality Of Selective Emitter Structures By Imaging The Emitter Saturation Current Density, Energy Procedia 27 (2012) 293 299

[56] http://www.pvlighthouse.com